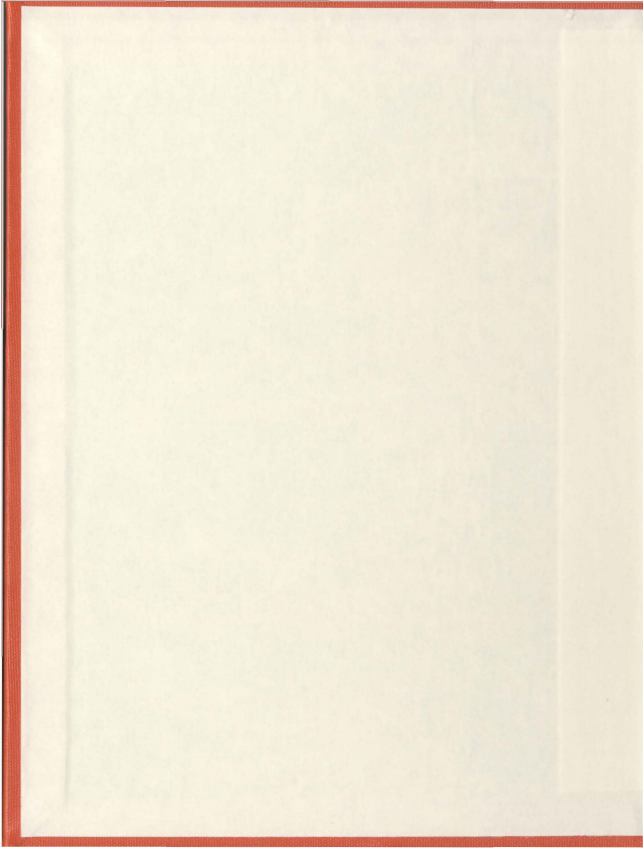


A WAVELET PACKET TRANSFORM BASED ON-LINE
TECHNIQUE FOR THE PROTECTION OF THREE-PHASE
INTERIOR PERMANENT MAGNET MOTORS

MD. ABDESH SHAFIEL KAFIEY KHAN



A Wavelet Packet Transform Based On-line Technique for the Protection of Three-Phase Interior Permanent Magnet Motors



By

© Md. Abdesh Shafiq Kafiey Khan

A thesis submitted to the School of Graduate
Studies in partial fulfillment of the
Requirements for the degree of
Master of Engineering

Faculty of Engineering and Applied Science
Memorial University of Newfoundland

St. John's

Newfoundland

Canada

May 2006

Abstract

Interior permanent magnet (IPM) synchronous motors are attractive for a variety of applications because of their high electromagnetic torque per permanent-magnet volume, high efficiency, low noise and low cost with a high power factor. However, interior permanent magnet motors are subject to time-to-time transients primarily due to faults and switches of loads. As a result, it is very important to understand the IPM motor's response to any potential fault condition in order to prevent fault-induced damage to the motors or to the connected loads. There have been many proposed techniques to carry out the protection of interior permanent magnet motors. These techniques include the harmonic content analysis of line currents using the fast Fourier transform (FFT), dq modeling of IPM motors relative to the faults, and pattern recognition of fault currents using the artificial intelligence techniques such as expert systems (ES), artificial neural networks (ANN), fuzzy logic systems (FLS), genetic algorithm (GA) and support vector machine (SVM). However, output signals of the running machine often contain non-stationary components and the FFT-based methods are not suitable for the non-stationary signal analysis. Moreover, there have been few efforts in the experimental implementation of dq modeling based protection of interior permanent magnet motors. Furthermore, pattern recognition techniques require a large number of data files for off-line training and have computational complexity, which may affect the reliability and speed of operation of these protection techniques. In this work, a wavelet packet transform based algorithm for the protection of the interior permanent magnet motor is developed, implemented and tested on-line on two types of interior permanent magnet motors using the DS1102 digital signal processor board. In the proposed algorithm, a signature analysis method is used for extracting the features of fault currents. For this purpose, three-phase line currents of different faulted and normal unfaulted conditions are acquired through the three-channel A/D converters of the DS1102 digital signal processor board, and then these are decomposed off-line up to the second level of resolution of the

wavelet packet transform. The second level high frequency details (dd^2) only show the distinctive features between faulted and normal unfaulted (healthy) currents. So, the proposed wavelet packet transform based algorithm is dependent upon the identification of high frequency components or coefficients in the second level high pass filter output. The output of cascaded filter banks associated with the selected mother wavelet and number of levels of resolution produce details and approximations of the original signal, which are related to high frequency and low frequency components, respectively. An experimental setup is developed for collecting line currents of different faulted and normal (unfaulted) conditions in order to select the optimum mother wavelet and optimal number of levels of resolution in addition to off-line testings of the proposed algorithm. It is found that the mother wavelet 'db3' of the Daubechies family and the second level of resolution are adequate enough to discriminate fault currents from the normal unfaulted currents. The off-line testing of the proposed algorithm is performed in the MATLAB environment on the collected data from both types of interior permanent magnet motors. An experimental setup for detecting disturbances incorporating also the protection circuit is developed to accommodate on-line testings on both types of IPM motors. In all the tests carried out, the proposed algorithm identified disturbances properly and initiated a trip signal almost at the instant or within one cycle of the fault occurrence. The on-line testing results are consistent with those obtained from off-line testings. The real-time testing of the proposed algorithm is also extended on the inverter-fed interior permanent magnet motor to demonstrate the universality of the proposed wavelet packet transform (WPT)-based protection algorithm for either the line-fed or inverter-fed three-phase interior permanent magnet motors.

Acknowledgements

I would like to express my most sincere gratitude and thanks to my supervisor Dr. M. Azizur Rahman for his guidance, advice and encouragements throughout this program. I would also like to thank him for the financial support he provided me during my Masters degree program. I wish to thank the School of Graduate Studies for providing me with the research assistantship and fellowship to pursue my graduate study at the Memorial University of Newfoundland. I also wish to thank Dr. M.A. Rahman and Faculty of Engineering for providing me with the necessary laboratory space, equipments and technical assistances in order to conduct the research project successfully. My special thanks goes to Dr. T.S. Radwan for helping me to work on the DS1102 digital signal processor board.

I express my sincere appreciation to my parents Dr. Md. Abdul Kuddus Khan and Mrs. Samsun Nahar Khan, my sister Mrs. Mehjabin Tusqin Khan, uncle Dr. Golam Mostafa, as well as other family members for their encouragements and support. I would like to thank my student colleagues Saleh Saleh, Casey Butt, Jahangir Khan for their help and useful suggestions.

DEDICATED TO:

My parents ***Dr. Md. Abdul Kuddus Khan*** and ***Mrs. Samsun Nahar Khan***

Contents

Abstract	ii
Acknowledgements	iv
List of Figures	x
List of Symbols	xxii
List of Acronyms	xiv
List of Tables	xvii
1 Introduction	1
1.1 Permanent Magnet Motors.....	1
1.2 Structure of PMSMs.....	2
1.3 Literature Review on the Electrical Machine Condition Monitoring and Fault Diagnostics.....	5
1.3.1 Application of Artificial Intelligence.....	6
1.3.2 Application of Advanced Signal Processing.....	10
1.3.3 Application of Wavelet Transform.....	14
1.3.4 Application of Miscellaneous Techniques.....	18
1.4 Problem Identification and Objective of the Thesis.....	20
1.5 Outline of the Thesis.....	22

2	Application of General Techniques for the Detection of Disturbances in the Interior Permanent Magnet (IPM) Motors	24
2.1	Discrete Fourier transform (DFT).....	25
2.1.1	Implementing the DFT Algorithm for the Interior Permanent Magnet (IPM) Motor Protection.....	26
2.2	Power Spectral Density (PSD).....	30
2.2.1	Non-parametric methods.....	31
2.2.2	Parametric methods.....	33
2.2.3	Subspace methods.....	35
2.3	Short-time Fourier transform.....	37
2.4	Artificial Neural Network (ANN).....	40
2.4.1	Implementing the Artificial Neural Network for the Interior Permanent Magnet Motor Protection.....	43
3	Wavelets and Wavelet Transforms	47
3.1	Wavelets and Scaling Functions.....	49
3.1.1	Orthogonal Wavelets.....	52
3.1.2	Non-orthogonal Wavelets.....	55
3.2	Wavelet Transforms.....	57
3.2.1	Continuous Wavelet transform.....	57
3.2.2	Discrete Wavelet transform.....	60
3.2.3	Wavelet Packet transform.....	62
3.3	Multiresolution analysis.....	65
3.3.1	Quadrature Mirror Filter Banks.....	66
3.4	Selection of the Mother Wavelet.....	67
3.4.1	Best-basis Selection.....	68
3.4.2	Minimum Description Length (MDL) Criterion....	70

4	Data Acquisition and the Mother Wavelet	72
4.1	Experimental setup for acquiring the Normal and Fault currents data.....	73
4.2	Selection of Mother Wavelet and number of Levels of resolution.....	75
4.2.1	Selecting Mother Wavelet.....	76
4.2.2	Selecting number of Levels of resolution.....	78
4.3	Proposed Disturbance Detector and Classifier.....	80
4.4	Off-line Testing of the WPT based Algorithm.....	89
5	On-line Testing of the WPT based Algorithm	100
5.1	Experimental setup for On-line Testings.....	101
5.2	Real-time Implementation of the Proposed Algorithm.....	101
5.3	On-line Test Results.....	104
5.3.1	Fault Currents.....	105
5.3.1.1	Line to ground (L-G) fault.....	105
5.3.1.2	Line-to-line (L-L) fault.....	110
5.3.1.3	Loss of supply (single phasing) fault.....	110
5.3.2	Normal (unfaulted) conditions.....	110
5.4	Extending the Real-time Testing.....	123
5.4.1	Experimental Setup for the Inverter-fed IPM Motor...	123
5.4.2	On-line Test Results of the Inverter-fed IPM Motor...	125
5.4.2.1	Fault currents.....	125
5.4.2.2	Normal (unfaulted) conditions.....	126

6	Conclusions and Future Work	132
6.1	Summary.....	132
6.2	Contributions.....	136
6.3	Conclusions.....	136
6.4	Future Works.....	137
Appendix A	Line-to-Ground Fault	139
Appendix B	Line-to-Line Fault	147
Appendix C	Loss of Supply (Single Phasing) Fault	155
References		163

List of Figures

1.1	Cross section of the interior type PM motor.....	3
1.2	Cross section of the surface mounted type PM motor.....	3
1.3	Cross section of the inset type PM motor.....	3
2.1	FFT of the phase-a stator current of the 1hp IPM motor: (a) normal healthy operation, (b) stator winding line-a to ground (L-G) fault.....	27
2.2	FFT of the phase-a stator current of the 1hp IPM motor: (a) loss of phase-a supply, (b) stator winding line-a to line-b (L-L) short circuit fault.....	27
2.3	FFT of the phase-a stator current of the 1hp IPM motor: (a) normal unfaulted full load operation, (b) loss of three-phase supply fault.....	28
2.4	FFT of the phase-a stator current of the 5hp IPM motor: (a) normal healthy operation, (b) stator winding line-a to ground (L-G) fault.....	28
2.5	FFT of the phase-a stator current of the 5 hp IPM motor: (a) loss of phase-a supply, (b) stator winding line-a to line-b (L-L) short circuit fault.....	29
2.6	The <i>periodogram</i> PSD estimates of the phase-a stator current of the 1hp IPM motor: (a) normal healthy operation, (b) stator winding line-a to ground (L-G) fault.....	31
2.7	The <i>Welch</i> PSD estimates of the phase-a stator current of the 1hp IPM motor: (a) normal healthy operation, (b) loss of phase-a supply.....	32
2.8	The <i>multitaper</i> PSD estimates of the phase-a stator current of the 1hp IPM motor: (a) normal healthy operation, (b) stator winding line-a to line-b (L-L) fault.....	32

2.9	The <i>Yule-Walker</i> PSD estimates of the phase-a stator current of the 5hp IPM motor: (a) normal healthy operation, (b) stator winding line-a to ground (L-G) fault.....	34
2.10	The <i>Burg</i> PSD estimates of the phase-a stator current of the 5hp IPM motor: (a) normal healthy operation, (b) loss of phase-a supply.....	34
2.11	The <i>multiple signal classification</i> (MUSIC) pseudospectrum PSD estimates of the phase-a stator current of the 1hp IPM motor: (a) normal healthy operation, (b) stator winding line-a to ground (L-G) fault.....	35
2.12	The <i>eigenvector</i> pseudospectrum PSD estimates of the phase-a stator current of the 1hp IPM motor: (a) normal healthy operation, (b) stator winding line-a to ground (L-G) fault.....	36
2.13	STFT tiling.....	37
2.14	STFT block diagram.....	37
2.15	STFT based spectrogram of the phase-a stator current during the healthy operation of the 1hp IPM motor.....	38
2.16	STFT based spectrogram of the phase-a stator current of the 1hp IPM motor for the case of stator winding line-a to ground (L-G) fault.....	38
2.17	STFT based spectrogram of the phase-a stator current of the 1hp IPM motor for the case of loss of phase-a supply.....	39
2.18	STFT based spectrogram of the phase-a stator current of the 1hp IPM motor for the case of stator winding line-a to line-b (L-L) short circuit fault.....	39
2.19	General structure of a multi-layer feed forward neural network	44
2.20	ANN based detector response and phase-a stator current of the 1hp IPM motor: (a) normal unfaulted condition, (b) normal starting condition.....	45
2.21	ANN based detector response and phase-a stator current of the 1hp IPM motor: (a) stator winding line-a to ground (L-G) fault, (b) loss of phase-a supply fault.....	45
3.1	The <i>Daubechies</i> (' <i>db3</i> ') wavelet: (a) the scaling function, (b) the wavelet function.....	54

3.2	The <i>Coiflet</i> (' <i>coif1</i> ') wavelet: (a) the scaling function, (b) the wavelet function.....	54
3.3	The <i>Spline biorthogonal</i> (' <i>bior2.6</i> ') wavelet: (a) the wavelet and its scaling function for the decomposition, (b) the wavelet and its scaling function for the reconstruction.....	55
3.4	The non-orthogonal <i>Morlet</i> (' <i>morl</i> ') wavelet function (does not have scale function).....	56
3.5	The non-orthogonal <i>Mexican Hat</i> (' <i>mexh</i> ') wavelet function (does not have scale function).....	56
3.6	Stretching and squeezing the Mexican Hat wavelet (dilation).....	59
3.7	Moving the Mexican Hat wavelet (translation).....	59
3.8	The two-level decomposition of a discrete signal by the discrete wavelet transform (DWT).....	62
3.9	The two-level decomposition of a discrete signal by the wavelet packet transform (WPT).....	64
4.1	Experimental setup for the data acquisition.....	74
4.2	The 555-timer circuit connection ($R1=100\text{ k}\Omega$, $C1=1\text{ }\mu\text{F}$, $R2=10\text{ k}\Omega$, $C2=0.01\text{ }\mu\text{F}$, and $T=1.1R1C1=0.1\text{ sec}$).....	75
4.3	The entropy values of each subspace of the wavelet packet tree up to the third level of resolution for the case of normal full load current of the 1hp IPM motor.....	79
4.4	The entropy values of each subspace of the wavelet packet tree up to the third level of resolution for the case of loss of supply fault (single phasing) current of the 1hp IPM motor.....	79
4.5	The time location diagram of the wavelet packet coefficients for the case of normal unloaded current of the 1hp IPM motor: (a) first level high frequency details (d^1), (b) second level high frequency details (dd^2).....	82

4.6	The time location diagram of the wavelet packet coefficients for the case of line-to-line (L-L) fault current of the 1hp IPM motor: (a) first level high frequency details (d^1), (b) second level high frequency details (dd^2).....	83
4.7	The time location diagram of the wavelet packet coefficients for the case of normal (unfaulted) full load current of the 1hp IPM motor: (a) first level high frequency details (d^1), (b) second level high frequency details (dd^2).....	84
4.8	The time location diagram of the wavelet packet coefficients for the case of normal unloaded current of the 5hp IPM motor: (a) first level high frequency details (d^1), (b) second level high frequency details (dd^2).....	85
4.9	The time location diagram of the wavelet packet coefficients for the case of line to ground (L-G) fault current of the 5hp IPM motor: (a) first level high frequency details (d^1), (b) second level high frequency details dd^2).....	86
4.10	The time location diagram of the wavelet packet coefficients for the case of loss of supply (single phasing) fault current of the 5hp IPM motor: (a) first level high frequency details (d^1), (b) second level high (b) frequency details (dd^2).....	87
4.11	The flow chart of the proposed WPT algorithm.....	88
4.12	The WPT based detector response and the three-phase stator currents for the case of normal (unfaulted) unloaded condition of the 1hp interior permanent magnet	91
4.13	The WPT based detector response and the three-phase stator currents for the case of normal (unfaulted) loaded condition of the 1hp interior permanent magnet	92
4.14	The WPT based detector response and the three-phase stator currents for the case of line to ground (L-G) fault of the 1hp interior permanent magnet motor.....	93
4.15	The WPT based detector response and the three-phase stator currents for the case of line-to-line (L-L) fault of the 1hp interior permanent magnet motor.....	94

4.16	The WPT based detector response and the three-phase stator currents for the case of loss of supply (single phasing) fault of the 1hp interior permanent magnet motor.....	95
4.17	The WPT based detector response and the three-phase stator currents for the case of normal (unfaulted) unloaded current of the 5hp interior permanent magnet motor.....	96
4.18	The WPT based detector response and the three-phase stator currents for the case of loss of supply (single phasing) fault of the 5hp interior permanent magnet motor.....	97
4.19	The WPT based detector response and the three-phase stator currents for the case of line to ground (L-G) fault of the 5hp interior permanent magnet motor.....	98
4.20	The WPT based detector response and the three-phase stator currents for the case of line-to-line (L-L) fault of the 5hp interior permanent magnet motor.....	99
5.1	Experimental setup for on-line testings on the three-phase interior permanent magnet motor.....	102
5.2	Flowchart of on-line implementation of the wavelet packet transform (WPT) based algorithm using the DS1102 digital signal processor board.....	103
5.3	Loaded line to ground (L-G) fault on phase-a of the 1hp IPM motor: (a) the WPT response and phase-a stator current, (b) phase-c and phase-b stator currents. (Scales: trip signal: 5v/div., phase-a: 4.172 A/div., phase-b: 4.66 A/div., and phase-c: 4.82 A/div.).....	106
5.4	Unloaded line to ground (L-G) fault on phase-a of the 1hp IPM motor: (a) the WPT response and phase-a stator current, (b) phase-c and phase-b stator currents. (Scales: Trip signal: 5v/div., phase-a: 4.172 A/div., phase-b: 4.66 A/div., and phase-c: 4.82 A/div.).....	107

5.5	Loaded line to ground (L-G) fault on phase-a of the 5hp IPM motor: (a) the WPT response and phase-a stator current, (b) phase-c and phase-b stator currents. (Scales: Trip signal: 5v/div., phase-a: 4.172 A/div., phase-b: 4.66 A/div., and phase-c: 4.82 A/div.).....	108
5.6	Unloaded line to ground (L-G) fault on phase-a of the 5hp IPM motor: (a) the WPT response and phase-a stator current, (b) phase-c and phase-b stator currents. (Scales: Trip signal: 5v/div., phase-a: 4.172 A/div., phase-b: 4.66 A/div., and phase-c: 4.82 A/div.).....	109
5.7	Unloaded line-to-line (L-L) fault between phase-a and phase-b of the 1hp IPM motor: (a) the WPT response and phase-a stator current, (b) phase-c and phase-b stator currents. (Scales: Trip signal: 5v/div., phase-a: 4.172 A/div., phase-b: 4.66 A/div., and phase-c: 4.82 A/div.)...	111
5.8	Loaded line-to-line (L-L) fault between phase-a and phase-b of the 1hp IPM motor: (a) the WPT response and phase-a stator current, (b) phase-c and phase-b stator currents. (Scales: Trip signal: 5v/div., phase-a: 4.172 A/div., phase-b: 4.66 A/div., and phase-c: 4.82 A/div.).....	112
5.9	Unloaded line-to-line (L-L) fault between phase-a and phase-b of the 5hp IPM motor: (a) the WPT response and phase-a stator current, (c) phase-c and phase-b stator currents. (Scales: Trip signal: 5v/div., phase-a: 4.172 A/div., phase-b: 4.66 A/div., and phase-c: 4.82 A/div.)....	113
5.10	Loaded line-to-line (L-L) fault between phase-a and phase-b of the 5hp IPM motor: (a) the WPT response and phase-a stator current, (b) phase-c and phase-b stator currents. (Scales: Trip signal: 5v/div., phase-a: 4.172 A/div., phase-b: 4.66 A/div., and phase-c: 4.82 A/div.).....	114
5.11	Unloaded loss of supply fault in phase-a of the 1hp IPM motor: (a) the WPT response and phase-a stator current, (b) phase-c and phase-b stator currents. (Scales: Trip signal: 5v/div., phase-a: 4.172 A/div., phase-b: 4.66 A/div., and phase-c: 4.82 A/div.).....	115

5.12	Loaded loss of supply fault in phase-a of the 1hp IPM motor: (a) the WPT response and phase-a stator current, (b) phase-c and phase-b stator currents. (Scales: Trip signal: 5v/div., phase-a: 4.172 A/div., phase-b: 4.66 A/div., and phase-c: 4.82 A/div.).....	116
5.13	Unloaded loss of supply fault in phase-a of the 5hp IPM motor: (a) the WPT response and phase-a stator current, (b) phase-c and phase-b stator currents. (Scales: Trip signal: 5v/div., phase-a: 4.172 A/div., phase-b: 4.66 A/div., and phase-c: 4.82 A/div.).....	117
5.14	Loaded loss of supply fault in phase-a of the 5hp IPM motor: (a) the WPT response and phase-a stator current, (b) phase-c and phase-b stator currents. (Scales: Trip signal: 5v/div., phase-a: 4.172 A/div., phase-b: 4.66 A/div., and phase-c: 4.82 A/div.).....	118
5.15	Unloaded normal (unfaulted) current condition of the 1hp IPM motor: (a) the phase-a stator current and WPT response of no trip signal, (b) phase-b and phase-c stator currents. (Scales: Trip signal: 5v/div., phase-a: 1.93 A/div., phase-b: 1.87 A/div., and phase-c: 1.67 A/div.).....	119
5.16	Loaded normal (unfaulted) current condition of the 1hp IPM motor: (a) the phase-a stator current and WPT response of no trip signal, (b) phase-b and phase-c stator currents. (Scales: Trip signal: 5v/div., phase-a: 1.93 A/div., phase-b: 1.87 A/div., and phase-c: 1.67 A/div.).....	120
5.17	Unloaded normal (unfaulted) current condition of the 5hp IPM motor: (a) the phase-a stator current and WPT response of no trip signal, (b) phase-b and phase-c stator currents. (Scales: Trip signal: 5v/div., phase-a: 4.172 A/div., phase-b: 4.66 A/div., and phase-c: 4.82 A/div.).....	121
5.18	Loaded normal (unfaulted) current condition of the 5hp IPM motor: the phase-a stator current and WPT response of no trip signal, (b) phase-b and phase-c stator currents. (Scales: Trip signal: 5v/div., phase-a: 4.172 A/div., phase-b: 4.66 A/div., and phase-c: 4.82 A/div.).....	122

5.19	Experimental setup for on-line testing of the WPT-algorithm on the inverter-fed interior permanent magnet motor.....	124
5.20	Unloaded line to ground (L-G) fault on phase-a of the inverter-fed 1hp IPM motor: (a) the phase-a stator current and WPT response, (c) phase-b and phase-c stator currents. (Scales: Trip signal: 5v/div., phase-a: 4.172 A/div., phase-b: 4.66 A/div., and phase-c: 4.82 A/div.)...	127
5.21	Unloaded line-to-line (L-L) fault between phase-b and phase-c of the inverter-fed 1hp IPM motor: (a) the phase-a stator current and WPT response, (b) phase-b and phase-c stator currents. (Scales: Trip signal: 5v/div., phase-a: 4.172 A/div., phase-b: 4.66 A/div., and phase-c: 4.82 A/div.).....	128
5.22	Unloaded single phasing fault on phase-a of the inverter-fed 1hp IPM motor: (a) the phase-a stator current and WPT response, (b) phase-b and phase-c stator currents. (Scales: Trip signal: 5v/div., phase-a: 4.172 A/div., phase-b: 4.66 A/div., and phase-c: 4.82 A/div.).....	129
5.23	Unloaded normal (unfaulted) current condition of the inverter-fed 1hp IPM motor: (a) the phase-a stator current and WPT response of no trip signal, (b) phase-b and phase-c stator currents. (Scales: Trip signal: 5v/div., phase-a: 4.172 A/div., phase-b: 4.66 A/div., and phase-c: 4.82 A/div.).....	130
A.1	Unloaded line to ground (L-G) fault on phase-b of the 1hp IPM motor: (a) the WPT response and phase-b stator current, (b) phase-c and phase-a stator currents. (Scales: Trip signal: 5v/div., phase-a: 4.172 A/div., phase-b: 4.66 A/div., and phase-c: 4.82 A/div.).....	139
A.2	Unloaded line to ground (L-G) fault on phase-c of the 1hp IPM motor: (a) the WPT response and phase-c stator current, (b) phase-b and phase-a stator currents. (Scales: Trip signal: 5v/div., phase-a: 4.172 A/div., phase-b: 4.66 A/div., and phase-c: 4.82 A/div.).....	140

A.3	Loaded line to ground (L-G) fault on phase-b of the 1hp IPM motor: (a) the WPT response and phase-a stator current, (b) phase-c and phase-b stator currents. (Scales: Trip signal: 5v/div., phase-a: 4.172 A/div., phase-b: 4.66 A/div., and phase-c: 4.82 A/div.).....	141
A.4	Loaded line to ground (L-G) fault on phase-c of the 1hp IPM motor: (a) the WPT response and phase-a stator current, (b) phase-c and phase-b stator currents. (Scales: Trip signal: 5v/div., phase-a: 4.172 A/div., phase-b: 4.66 A/div., and phase-c: 4.82 A/div.).....	142
A.5	Unloaded line to ground (L-G) fault on phase-b of the 5hp IPM motor: (a) the WPT response and phase-a stator current, (b) phase-c and phase-b stator currents. (Scales: Trip signal: 5v/div., phase-a: 4.172 A/div., phase-b: 4.66 A/div., and phase-c: 4.82 A/div.).....	143
A.6	Unloaded line to ground (L-G) fault on phase-c of the 5hp IPM motor: (a) the WPT response and phase-a stator current, (b) phase-c and phase-b stator currents. (Scales: Trip signal: 5v/div., phase-a: 4.172 A/div., phase-b: 4.66 A/div., and phase-c: 4.82 A/div.).....	144
A.7	Loaded line to ground (L-G) fault on phase-b of the 5hp IPM motor: (a) the WPT response and phase-a stator current, (b) phase-c and phase-b stator currents. (Scales: Trip signal: 5v/div., phase-a: 4.172 A/div., phase-b: 4.66 A/div., and phase-c: 4.82 A/div.).....	145
A.8	Loaded line to ground (L-G) fault on phase-c of the 5hp IPM motor: (a) the WPT response and phase-a stator current, (b) phase-c and phase-b stator currents. (Scales: Trip signal: 5v/div., phase-a: 4.172 A/div., phase-b: 4.66 A/div., and phase-c: 4.82 A/div.).....	146
B.1	Unloaded line-to-line (L-L) fault between phase-b and phase-c of the 1hp IPM motor: (a) the WPT response and phase-a stator current, (b) phase-c and phase-b stator currents. (Scales: Trip signal: 5v/div., phase-a: 4.172 A/div., phase-b: 4.66 A/div., and phase-c: 4.82 A/div.).....	147

B.2	Unloaded line-to-line (L-L) fault between phase-a and phase-c of the 1hp IPM motor: (a) the WPT response and phase-a stator current, (b) phase-c and phase-b stator currents. (Scales: Trip signal: 5v/div., phase-a: 4.172 A/div., phase-b: 4.66 A/div., and phase-c: 4.82 A/div.).....	148
B.3	Loaded line-to-line (L-L) fault between phase-b and phase-c of the 1hp IPM motor: (a) the WPT response and phase-a stator current, (b) phase-c and phase-b stator currents. (Scales: Trip signal: 5v/div., phase-a: 4.172 A/div., phase-b: 4.66 A/div., and phase-c: 4.82 A/div.).....	149
B.4	Loaded line-to-line (L-L) fault between phase-a and phase-c of the 1hp IPM motor: (a) the WPT response and phase-a stator current, (b) phase-c and phase-b stator currents. (Scales: Trip signal: 5v/div., phase-a: 4.172 A/div., phase-b: 4.66 A/div., and phase-c: 4.82 A/div.).....	150
B.5	Unloaded line-to-line (L-L) fault between phase-b and phase-c of the 5hp IPM motor: (a) the WPT response and phase-a stator current, (b) phase-c and phase-b stator currents. (Scales: Trip signal: 5v/div., phase-a: 4.172 A/div., phase-b: 4.66 A/div., and phase-c: 4.82 A/div.).....	151
B.6	Unloaded line-to-line (L-L) fault between phase-a and phase-c of the 5hp IPM motor: (a) the WPT response and phase-a stator current, (b) phase-c and phase-b stator currents. (Scales: Trip signal: 5v/div., phase-a: 4.172 A/div., phase-b: 4.66 A/div., and phase-c: 4.82 A/div.).....	152
B.7	Loaded line-to-line (L-L) fault between phase-b and phase-c of the 5hp IPM motor: (a) the WPT response and phase-a stator current, (b) phase-c and phase-b stator currents. (Scales: Trip signal: 5v/div., phase-a: 4.172 A/div., phase-b: 4.66 A/div., and phase-c: 4.82 A/div.).....	153
B.8	Loaded line-to-line (L-L) fault between phase-a and phase-c of the 5hp IPM motor: (a) the WPT response and phase-a stator current, (b) phase-c and phase-b stator currents. (Scales: Trip signal: 5v/div., phase-a: 4.172 A/div., phase-b: 4.66 A/div., and phase-c: 4.82 A/div.).....	154

C.1	Unloaded single phasing fault on phase-b of the 1hp IPM motor: (a) the WPT response and phase-a stator current, (b) phase-c and phase-b stator currents. (Scales: Trip signal: 5v/div., phase-a: 4.172 A/div., phase-b: 4.66 A/div., and phase-c: 4.82 A/div.).....	155
C.2	Unloaded single phasing fault on phase-c of the 1hp IPM motor: (a) the WPT response and phase-a stator current, (b) phase-c and phase-b stator currents. (Scales: Trip signal: 5v/div., phase-a: 4.172 A/div., phase-b: 4.66 A/div., and phase-c: 4.82 A/div.).....	156
C.3	Loaded single phasing fault on phase-b of the 1hp IPM motor: (a) the WPT response and phase-a stator current, (b) phase-c and phase-b stator currents. (Scales: Trip signal: 5v/div., phase-a: 4.172 A/div., phase-b: 4.66 A/div., and phase-c: 4.82 A/div.).....	157
C.4	Loaded single phasing fault on phase-c of the 1hp IPM motor: (a) the WPT response and phase-a stator current, (b) phase-c and phase-b stator currents. (Scales: Trip signal: 5v/div., phase-a: 4.172 A/div., phase-b: 4.66 A/div., and phase-c: 4.82 A/div.).....	158
C.5	Unloaded single phasing fault on phase-b of the 5hp IPM motor: (a) the WPT response and phase-a stator current, (b) phase-c and phase-b stator currents. (Scales: Trip signal: 5v/div., phase-a: 4.172 A/div., phase-b: 4.66 A/div., and phase-c: 4.82 A/div.).....	159
C.6	Unloaded single phasing fault on phase-c of the 5hp IPM motor: (a) the WPT response and phase-a stator current, (b) phase-c and phase-b stator currents. (Scales: Trip signal: 5v/div., phase-a: 4.172 A/div., phase-b: 4.66 A/div., and phase-c: 4.82 A/div.).....	160
C.7	Loaded single phasing fault on phase-b of the 5hp IPM motor: (a) the WPT response and phase-a stator current, (b) phase-c and phase-b stator currents. (Scales: Trip signal: 5v/div., phase-a: 4.172 A/div., phase-b: 4.66 A/div., and phase-c: 4.82 A/div.).....	161

C.8 Loaded single phasing fault on phase-c of the 5hp IPM motor: (a) the WPT response and phase-a stator current, (b) phase-c and phase-b stator currents. (Scales: Trip signal: 5v/div., phase-a: 4.172 A/div., phase-b: 4.66 A/div., and phase-c: 4.82 A/div.)..... 162

List of Symbols

$\psi(t)$	Wavelet function
$\hat{\psi}(t)$	Dual wavelet function
$\hat{\psi}(f)$	Fourier transform of the wavelet function
$\phi(t)$	Scaling function
$\hat{\phi}(t)$	Dual scaling function
\mathfrak{R}	Real continuous number system
a	Dilation parameter
b	Translation parameter
$g[n]$	Impulse response of the low pass filter or scaling filter
$h[n]$	Impulse response of the high pass filter or wavelet filter
J	Total number of levels of resolution
j	Number of levels of resolution
I_a, I_b, I_c	Phase-a, phase-b and phase-c line currents
$x[n]$	Discrete sequence of the continuous signal $x(t)$
$\tilde{x}[n]$	Discrete periodic sequence of the continuous signal $x(t)$
$X[k]$	Discrete Fourier transform co-efficients of $x[n]$
$\tilde{X}[k]$	Discrete Fourier series co-efficients of $\tilde{x}[n]$
ω	Frequency in rad./sample
$S(\omega)$	Power spectrum of the discrete signal
$R(\omega)$	Correlation sequence
$P(\omega)$	Power spectral density of the discrete signal

B_k^h	Bias of the k -th hidden layer
B_j^o	Bias of the j -th output layer
W_j^o	Weight of the j -th output layer
W_k^h	Weight of the k -th hidden layer
f^h	Transfer function of the hidden layer
f^o	Transfer function of the output layer
δ_k^h	Error terms of the k -th hidden layer
δ_j^o	Error terms of the j -th output layer
η	Learning rate
\mathbb{N}	Set of positive integers

List of Acronyms

DSP	Digital signal processor
PM	Permanent magnet
PMSM	Permanent magnet synchronous motor
IPMSM	Interior permanent magnet synchronous motor
Nd-B-Fe	Neodymium-boron-iron
Sm-Co	Samarium-cobalt
MW	Mega watt
MMF	Magneto motive force
AI	Artificial intelligence
ES	Expert system
ANN	Artificial neural network
FFNN	Feed forward neural network
FLS	Fuzzy logic system
GA	Genetic algorithm
SVM	Support vector machine
SVC	Support vector classifier
DFT	Discrete Fourier transform
DFS	Discrete Fourier series
FFT	Fast Fourier transform
STFT	Short-time Fourier transform
HOS	Higher order spectrum
WT	Wavelet transform
CWT	Continuous wavelet transform
DWT	Discrete wavelet transform

UDWT	Undecimated discrete wavelet transform
WPT	Wavelet packet transform
WPD	Wavelet packet decomposition
WNN	Wavelet neural network
PD	Partial discharge
WVD	Wigner-Ville distribution
CWD	Choi-Williams distribution
CSD	Cone-shaped distribution
TFR	Time-frequency region
A/D	Analog to digital
D/A	Digital to analog
ANFIS	Adaptive neuro-fuzzy inference system
C-ANFIS	Clustering adaptive neuro-fuzzy inference system
HIF	High impedance fault
PWM	Pulse width modulation
IGBT	Insulated gate bipolar transistor
HVDC	High voltage direct current
SVD	Singular value decomposition
APD	Amplitude probability density
PSD	Power spectral density
TSA	Time synchronous averaging
MUSIC	Multiple signal classification
ROOT-MUSIC	Root multiple signal classification
MCSA	Motor current spectral analysis
RT	Real-time
CPU	Central processing unit
FIR	Finite impulse response
IIR	Infinite impulse response
MRA	Multiresolution analysis

THD	Total harmonic distortion
RMS	Root mean square
MDL	Minimum description length
MTM	Multi taper method
AR	Auto-regressive
EV	Eigen-vector
QMF	Quadrature mirror filter
CT	Current transformer
ISA	Industry standard architecture
PC/AT	Personal computer/advanced technology
ASCII	American standard code for information interchange
L-G	Line to ground
L-L	Line-to-line

List of Tables

4.1 The two level MDL index evaluations of the phase-a stator current of the 1hp interior permanent magnet motor: (a) normal unfaulted condition, (b) line-to-line (L-L) fault.....	77
4.2 The two level MDL index evaluations of the phase-a stator current of the 5hp interior permanent magnet motor: (a) normal unfaulted condition, (b) line-to-line (L-L) fault.....	77

Chapter 1

Introduction

1.1 Permanent Magnet Motors

The development of the permanent magnet (PM) motor is directly related to the recent achievement in high-energy permanent magnet like neodymium-boron-iron (Nd-B-Fe), samarium-cobalt (Sm-Co), etc. The fast digital signal processor (DSP) board with built-in interface provisions and artificial intelligence algorithms provide advanced starting and control means for a PM motor drive. Permanent magnets have been used for both the dc and ac motors. In the case of dc motors, PM dc motors are separately excited dc motors with the permanent magnets as the field excitation source. The PM dc motor is widely used in industry for control purposes. The permanent magnet ac motors are usually considered as synchronous motors according to the operational point of view. Permanent magnet ac synchronous motors are commonly known as permanent magnet synchronous motor (PMSM). It is also simply called as PM motor [3].

The use of permanent magnets in construction of electrical machines brings the following benefits [1]:

- No electrical energy is required for the field excitation system, and thus there are no excitation losses which means substantial increase in the efficiency,
- Higher torque and/or output power per volume than when using electromagnetic excitation,

- Better dynamic performance than motors with electromagnetic excitation,
- Simplification of construction and maintenance,
- Reduction of prices for some types of machines.

PM motors are used in a broad power range from mili-watts (mWs) to hundreds of kilo-watts (kWs). There are also attempts to apply PM materials in large motors rated at 1.5 MW. Thus, PM motors cover a wide variety of application fields, from stepping motors for wristwatches, through industrial drives for machine tools to large PM synchronous motors for ship propulsion (navy frigates, cruise ships, medium size cargo vessels and ice breakers). Recently PM motors are widely used in air compressors and hybrid electric vehicles [2]. The car industry uses a large quantity of PM dc commutator motors. The number of auxiliary dc PM commutator motors can vary from a few in an inexpensive car to about one hundred in a luxury car [1].

1.2 Structure of PMSMs

The stator of a PMSM is essentially of the same structure as that of an induction motor or a synchronous motor. The rotating magneto motive force (MMF) in the air gap produced by the three phase stator windings has approximate sinusoidal distribution. Depending on the position of magnets in the rotor, the permanent magnet synchronous motors can be broadly classified into three categories: (a) interior type, where the permanent magnets are buried inside the rotor core; (b) surface mounted type, where the permanent magnets are mounted on the surface of the rotor; (c) inset type, where the permanent magnets are fully or partially inset into the rotor core [4]. The cross section of interior, surface mounted, and inset type PM synchronous motors are shown in figures 1.1, 1.2 and 1.3, respectively.

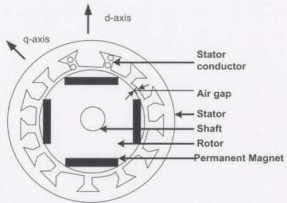


Figure 1.1: Cross section of the interior type PM motor

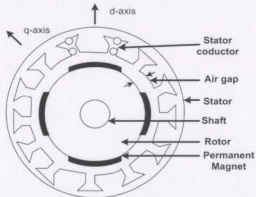


Figure 1.2: Cross section of the surface mounted type PM motor

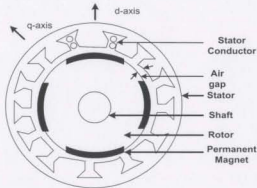


Figure 1.3: Cross section of the inset type PM motor

Depending on the orientation of the magnets, the PM motors can be classified into three types: (a) radial type, (b) circumferential type, and (c) axial type. The orientations of the magnets of PM motors in figures 1.1-1.3 are radial. The PM motors can also be classified according to the rotor cage winding. In the case of the cage type motor, the squirrel cage winding provides the starting torque so that the motor can start itself at rated supply voltage and frequency. However, a proper control strategy is needed in the case of PM motor without the rotor cage winding in order to run the motor from standstill to synchronous speed.

Among the various types of PM motors discussed above, the interior type PM (IPM) motor with radial magnetization is the most economical to manufacture. Moreover, as the permanent magnets are buried within the rotor core, it provides a smooth rotor surface and reduced air gap. As a result, this type of motor can be used for high speed with quiet operation and better dynamic performance, which are the major requirements for high performance drive systems. The interior permanent magnet synchronous motor (IPMSM) saves up to 50% of the energy for split type air conditioners. Use of IPMSM for air-conditioner compressor pumps up to 3.7 kW has been the industrial standard of the Japanese air conditioner manufactures like Daiken, Mitsubishi, Hitachi, Toshiba and Carrier [3].

Faults in either the machine or inverter create special challenges in any of PM synchronous machines because of the presence of spinning rotor magnets that cannot be turned off at will. It is very important to understand the response of the PM synchronous motors to any potential fault condition in order to prevent fault-induced damage to either the machine, the inverter, or to the connected load [5]. The interior permanent magnet synchronous motor has been used as a working model in this thesis in order to develop a protection scheme against some potential disturbances of the motor. Intensive research has been conducted to develop and implement reliable techniques for fault diagnosis in electrical machines. Most of the modern techniques are based on the application of advanced signal processing, which includes fast Fourier transform, wavelet transform and other high level frequency spectrum analysis techniques. Other approaches such as

model-referenced method, artificial intelligence that includes neural networks, fuzzy logic, neuro-fuzzy and neuro-wavelet have been reported in the literature. Either stator current or vibration of the motor is used as decision making variable in non-invasive fault diagnosis techniques. In the following section, a brief review of the condition monitoring and protection techniques for electrical machine disturbances has been given.

1.3 Literature Review on the Electrical Machine Condition Monitoring and Fault Diagnostics

It is becoming increasingly important to use comprehensive monitoring schemes for the continuous assessment of the operating conditions of electrical machines. By using condition monitoring, it is possible to provide adequate warning of imminent/incipient failures, and in addition to diagnosing present maintenance needs, it is also possible to schedule future preventive maintenance and repair work. This can result in minimum downtime and optimum maintenance schedules. Diagnosis allows the machine operator to have the necessary spare parts before the machine is stripped down, thereby reducing outage times. If diagnosis is integrated into the maintenance policy, the usual maintenance at specified intervals can be replaced by a condition-centered maintenance. This can also eliminate unnecessary maintenance [6]. The techniques used for failure prognosis in electrical machine can be broadly classified into three categories such as: (a) application of artificial intelligence, (b) application of advanced digital signal processing, (c) application of wavelet transform. The artificial intelligence (AI) techniques illustrate the application of expert systems (ES), artificial neural networks (ANN), fuzzy logic systems (FLS), genetic algorithm (GA), and support vector machine (SVM). The advanced digital signal processing techniques illustrate the application of discrete Fourier transform (DFT), fast Fourier transform (FFT), short-time Fourier transform (STFT), and higher-order spectrum (HOS) analysis such as: bi-spectrum, tri-spectrum, etc. The wavelet transforms analysis illustrated the application of continuous wavelet transform (CWT), discrete wavelet transform (DWT), modulus maxima of discrete wavelet transform coefficients, wavelet packet transform (WPT), and wavelet-neural (WN)

network based techniques. Besides those above mentioned techniques, techniques such as: partial discharge (PD), stator temperature measurement, measurement of negative sequence impedance using power system decomposition, and mathematical model based condition monitoring are documented in the literatures. A brief review of various forms of condition monitoring and diagnostic techniques discussed above for induction machines and permanent magnet synchronous machines are given in the following subsections.

1.3.1 Application of Artificial Intelligence

Artificial intelligence (AI) is basically the study of system mental facilities through the use of computational models. It has produced a number of tools since its emergence as a discipline in mid 1950s. The tools are of great practical significance in engineering to solve various complex problems normally requiring human intelligence [7]. Recently, significant efforts have been made on the use of artificial intelligence tools to develop condition monitoring and fault diagnostic for motor and motor drives.

Filippetti et. al., [8] have outlined a diagnostic method based on the knowledge representation of induction machine suitable to be inserted, after operative rearrangements, in an expert system (ES). The knowledge utilized two instantaneous line currents, two instantaneous line voltages and rotor speed as input data. The proposed scheme include some combinations of 'IF-THEN-ELSE' rules, factual statements, frames, objects, procedures, and cases in order to realize an expert system for induction machine diagnostics. Leith et. al., [9] have presented an on-line real-time expert system for diagnosing faults in induction motors. The knowledge base comprising of a failure tree, an observation tree, and a case tree used off-line for realizing the real-time expert system. It is to be noted that expert systems used in the above mentioned references require details of the fundamentals of operation of the machine, theoretical and practical studies of fault mechanisms, and case histories of fault analyses. As a result, the method is vulnerable to uncertainty and not quite suitable from computational point of view.

Chow et. al., [10] have used a generic three layer feed-forward neural network for real-time condition monitoring of induction motors. They have investigated turn-to-turn insulation failure and motor bearing failure at constant load torque. Based upon the dynamic behavior of the induction motor, the stator current and rotor speed have been correlated to equivalent number of turns and damping coefficient of the motor, respectively. It has been assumed that turn-to-turn insulation failure is related to the change of equivalent number of turns of the motor. In addition, the damping coefficient is also assumed to carry information about motor bearing fault. A training data set of input variables of stator currents and rotor speeds with output target variables of percentage of equivalent number of turns and damping coefficients utilizing the expert knowledge of machine behavior are used for the off-line training of the neural network. Finally, the network is implemented in real-time with digital signal processor board using C compiler. The network showed better response for higher number of hidden nodes. The work is focused mainly only on the changes in certain machine parameters for two specific faults. However, the method is not quite accurate for the dynamic nature of machine parameters, and it requires large number of training data set to overcome the interaction effect of input variables. Schoen et. al., [11] have used artificial neural networks to learn the spectral characteristics of the induction motor operating on-line. The learned spectrum contained many harmonics for faulted and normal (unfaulted) operating conditions. A frequency selective filter based on the expert system is employed to reduce the number of harmonics to a manageable number that were continuously monitoring. After a sufficient training period, the network formed a cluster that represents valid operating conditions of the motor. The network initiated a potential failure signal when a new cluster was formed. It is to be noted that the network has to be trained for more and varied operating conditions in order to increase the acceptable classification techniques. Chow, Sharpe, et. al., [12-13] have proposed general design considerations of feed-forward artificial neural networks for performing motor fault detection. A brief review of feed-forward nets and the back propagation-training algorithm along with its pseudo codes has been presented in reference [12]. Design considerations such as

network performance, network implementation, size of training data set, assignment of training parameter values, stopping criteria, and finally, a fuzzy logic based criterion to optimize network structure has been illustrated in reference [13].

Lasurt, et. al., [14] have implemented a novel fuzzy logic based artificial intelligence procedure for the condition monitoring and fault diagnosis of induction motors. The proposed technique utilized the higher order statistical (HOS) analysis method as the preprocessing procedure on the machine vibration signal. The combination of data reduction, parameterization and fuzzy logic procedures are then applied to the HOS signatures to enable diagnosis of machine fault. Another fuzzy logic approach for fault detection and diagnosis of induction motor is presented in reference [15]. The motor condition is described here using linguistic variables. Fuzzy subsets and the corresponding member functions are generated using stator current amplitudes. A knowledge base, comprising rule and databases are built to support the fuzzy inference. The diagnosis accuracy of the fuzzy inference is quite satisfactory. However, fourteen 'IF-THEN-ELSE' rules are used in the knowledge base of the fuzzy inference based on stator current amplitudes to diagnose two types of faults. As a result, more rules will have to be added in the knowledge base for diagnosing greater number of disturbances, and it will be more complicated as well. Moreover, it is not feasible to compare stator currents when the motor is fed from inverter due to the presence of harmonics produced by the converter.

Goode, et. al., [16-18] have reported a hybrid fuzzy/neural fault detector that utilized the learning capabilities of the neural network to detect an incipient fault in motor. The heuristic knowledge about the motor and the fault detection process has been extracted from the hybrid structure through the use of fuzzy rules and fuzzy membership functions. Zhongming, et. al., [19] have presented the multiple adaptive neuro-fuzzy inference system, where wavelet packet decomposition coefficients are used as input set for fault diagnosis in induction motors. The diagnosis scheme includes data acquisition, pre-processing and detection stages. At the data acquisition stage, the analog signal of the stator current from current transducer is measured and transmitted to the data acquisition

board, where the signal is low-pass filtered to eliminate high order harmonics, and then digitized by an A/D converter. After the noise and dc offsets have been filtered out, the signal is fed to the preprocessing unit, where it is transformed into time-frequency domain using wavelet packet decomposition. The wavelet packet feature coefficients together with the slip speed of the induction motor are used in the detection algorithm. The fuzzy logic is used for transferring the range of values of the input feature coefficients into corresponding universe of discourse and converting the input values into suitable linguistic values, which may be viewed as labels of fuzzy sets. Multiple adaptive neuro-fuzzy inference system (ANFIS) units are used in the implementation of the fault detection system. The underlying idea based on which this system is implemented is that the corresponding feature coefficients for each of such fault modes are different, and as such the training data sets used for each type of fault would be different. However, the training of multi-layer perception neural network is a time-consuming task, and the performance of the neural network depends on the quality of samples.

Park, et. al., [20] have presented a clustering adaptive neuro-fuzzy inference system (C-ANFIS) based fault diagnosis for voltage-fed pulse width modulated (PWM) induction motor drive systems. The diagnosis technique consists of data acquisition part, d-q transformation part, feature extraction part, and detection part. The technique utilized the periodic mean values of d-q phase current as input pattern for the C-ANFIS. A data clustering technique based on scatter partition has been used in this work to effectively reduce the number of fuzzy rules and learning time.

Pöyhönen, et. al., [21] have reported the use of support vector classification technique for fault diagnosis of an electrical machine. The support vector machine (SVM) is a relatively new soft computing method based on statistical learning theory presented by Vapnik [22]. Numerical magnetic field analysis is used to provide virtual measurement data from healthy and faulty operations of an electrical machine. Power spectra estimates of the stator current of the motor are calculated with Welch's method, and then SVC is applied to distinguish healthy spectrum from faulty spectra. In [23], the same authors have extended the 2-class SVM classifiers of reference [21] to a multi-class

classification structure with a majority voting approach. Also, the influence of noise is studied here. It is to be noted that noise degraded the performance of the classifier to a significant low percentage. However, the approach can create problems if two separate classes get equal amount of votes. In addition, it did not take into account the possible redundancy from pair-wise classifiers' outputs.

1.3.2 Application of Advanced Signal Processing

Signal processing based techniques have been widely used for detection and diagnosis of faults in electrical machines for the last fifteen years. These techniques have traditionally been applied, separately, in time and frequency domains. A time-domain analysis focuses principally on statistical characteristics such as peak level, standard deviation, kurtosis, skewness, and crest factor of the measurements of vibration, acoustic noise, temperature, and stator currents. A frequency domain approach uses Fourier methods to transform the time-domain signal in the frequency-domain, where further analysis is carried out, conventionally using signal amplitude and power spectra. It should be noted that use of either domain implicitly excludes the direct use of information present in the other domain [24].

Yang, et. al., [24] have reported four approaches based on bi-spectral and wavelet analysis of vibration signals as signal processing techniques for application in the diagnosis of a number of induction motor rolling element bearing faults. The vibration analysis methods are based on the bi-spectrum, bi-spectrum diagonal slice, summed bi-spectrum as well as wavelets. Singular value decomposition (SVD) is applied to extract the most significant features from the vibration signatures, and the features are used as inputs to an artificial neural network trained to identify the bearing faults. Roux, et. al., [25] have presented two condition monitoring techniques, which are based on harmonic spectrum analysis of the stator voltage and current as well as magnet strength estimation from d-q axis voltage and current of the rotor synchronous reference frame, in order to detect rotor faults in surface mounted type permanent magnet synchronous motor. The type of faults that have been investigated are: (a) static and dynamic eccentricity, (b)

broken magnet, and (c) rotor misalignments. The magnet strength estimation technique was found to be suitable only for the detection of broken magnet fault. On the other hand, harmonic spectrum analysis method based on the fast Fourier transform (FFT) was able to differentiate all faults except the static eccentricity from the normal case. Therefore, the harmonics of the negative sequence component of the stator current were used for the detection of static eccentricity case, and it was able to differentiate successfully the static eccentricity from the normal case. However, the signal processing capabilities of the proposed condition-monitoring techniques are limited with the control of the motor and it can result in monitoring only one fault harmonic. In addition, the main disadvantage of fast Fourier transform (FFT) based harmonic spectrum analysis is the impact of side lobe leakage due to windowing of finite data sets.

Again, Pöyhönen, et. al., [26] have used the electromagnetic model of an induction motor and a slip-ring generator for predicting the performance of different faults implemented in their structure. The Welch's method of power spectra estimation is applied on the virtual data provided by the numerical magnetic field analysis of the machine model to get a reliable indication of the fault. The virtual measurement data included stator line currents, circulating currents between parallel stator branches and forces between the stator and rotor. Dalpiaz, et. al., [27] have reported different vibration analysis techniques for condition monitoring and diagnostics in automatic machines. Common vibration processing techniques such as amplitude probability density (APD), power spectral density (PSD), and time synchronous averaging (TSA) are illustrated at first with the help of number of statistical parameters. Then, the wavelet transform is applied since the vibrations of this kind of machine are highly non-stationary. Finally, an inverse filtering approach is used to recover the actual output link motion from the casing vibration for enabling condition monitoring and diagnostics to be carried out through the analysis of the mechanism motion.

Roux, et. al., [28] have investigated the effects of the speed-controller bandwidth on the detection of rotor faults in the surface mounted type permanent magnet synchronous motor. The mechanism by which fault harmonics show up in the stator currents and rotor

speed has been discussed at the beginning. It is shown that the rotor speed has a proportional effect on the harmonics of stator voltages and currents. It has also been shown that the same harmonic for varying load torque shows up in the stator currents and voltages as in the rotor fault case. Again, these harmonics increase with increased speed controller bandwidth. Finally, the harmonic content of the electromagnetic torque is used for distinguishing the rotor fault from the varying load torque by increasing the speed-controller bandwidth on-line. The fast Fourier transform (FFT) based harmonic spectrum analysis is used to identify these fault harmonics. However, the faults studied in this work manifest themselves as short transients superimposed on the stator currents. Analysis of these short transients requires information in both time and frequency. But the fundamental limitation of the FFT is the inability to provide time localization of a signal.

A method based on the analysis of the short-time Fourier transform (STFT) of the torque-producing component of the field-oriented stator currents is described in reference [29] for detecting faults in the six-pole surface mounted type permanent magnet synchronous motor. Rather than analyzing the three phase stator currents independently of each other, the field oriented currents i_d and i_q have been used in this analysis. The analysis has the advantage that the fundamental electrical frequency is absent in i_d and i_q . Consequently, rotor speed has little effect on the spectrum of these currents, allowing for invariance in the algorithm to rotor speed. Thresholding on the energy in the STFT has been used to detect a fault in the motor, and linear discriminant analysis has been used to classify between the fault types. However, the basis function for the short time Fourier transforms based analysis is always stationary. As a result, the method is limited due to the constraint on the window size. In addition, no experimental results were provided to validate the performance of the algorithm. Arthur, et. al., [30] have described a novel predictive frequency method for detecting, and unambiguously diagnosing the type and magnitude of induction machine fault conditions from the single sensor measurement of the radial electromagnetic machine vibration. The detection mechanism is based on the hypothesis that the induction machine can be considered as a simple system, and that the action of the fault conditions are to alter the output of the system in a characteristic and

predictable fashion. It has been assumed that the effect of induction machine fault conditions is to create a disturbance in the air-gap flux density, and the magnitude of the air-gap flux frequency components are directly proportional to the magnitude of the fault conditions. Therefore, the air-gap flux density and the electromagnetic vibration are used as the system input and output, respectively. The nature of the system transfer function is assumed to be quadratically nonlinear. Higher order spectra (HOS) measures of order 3 and more have been used for predicting frequencies of the induction motor vibration containing information about the motor condition. However, the method is not valid for permanent magnet synchronous machine due to the absence of rotor slots and slip frequencies, which have been used for predicting the frequency components of air-gap flux density in the induction motor. Benbouzid, et. al., [31] have addressed the application of advanced signal processing techniques such as high-resolution spectral analysis for the detection and localization of the incipient faults in induction motors. This technique is based on an eigenanalysis of the autocorrelation matrix, which allowed keeping only the principal spectral components of the signal and decreasing noise influence. Authors have used two well-known eigenanalysis-based frequency estimators such as multiple signal classification (MUSIC) and ROOT-multiple signal classification (ROOT-MUSIC) in this work.

Schoen, et. al., [32] have addressed the application of motor current spectral analysis (MCSA) for the detection of rolling-element bearing damage in induction machines. In this work, authors have used the stator currents for the first time in detecting bearing faults by correlating the relationship between vibration and current frequencies caused by incipient bearing failures. Yazici, et. al., [33] have reported an adaptive statistical time–frequency method for the detection of broken bars and bearing faults in induction motors using stator current. The method consists of four stages: preprocessing, training, testing, and post processing. In the preprocessing stage, analog current data were low-pass filtered in order to prevent aliasing in the frequency domain. Next, the time–frequency spectrums of the digitized data were computed and fed into the training stage. In the training stage, fault frequencies were estimated and a window of frequency

components around the estimated fault frequencies were selected to form a feature vector. Next, feature vectors were segmented into homogenous sections along the time axis in time–frequency space. Segmentation was performed by a statistical method, which divided the time–frequency spectrum into statistically homogenous regions along the time axis. However, the method has complex interactions of machine operating conditions and variables. Lindh, et. al., [34] have presented a method for discriminating stator current signals from two classes, motors in normal condition and ones with a bearing failure. At first, a feature providing discriminative information was developed using the optimal energy of the Gabor filter response of the selected bandwidth and frequency. Finally, second-order statistics based discrimination was used for classification. However, the method was able to detect a bearing fault only if the internal radial clearance of the bearing was adequate.

1.3.3 Application of Wavelet Transform

Most of the widely used processing techniques, analyzing vibrations or stator currents in the amplitude or frequency domains, are based on the assumption of stationary and periodic signals. Thus these are not fully suitable for detecting short-duration dynamic phenomena, whose time localization and identification are also difficult. Therefore, the application of advanced signal processing techniques is required, including signal modeling techniques, filtering techniques and time-frequency distribution techniques. Among the latter, the wavelet transform algorithm is one of the most recent mathematical tools adopted for processing transient signals [27].

A failure prognosis system based on undecimated discrete wavelet transform (UDWT) of the torque-producing components of the field oriented stator currents was developed for surface mounted type permanent magnet ac (PMAC) drives in reference [35]. Thresholding on the energy of the UDWT of the normal unfaulted and faulted currents was used to detect a fault in the machine, and linear discriminant analysis was used to classify the fault types. A collection of observed data was used to train the detection and classification components of the algorithm. However, the algorithms in this

work were used offline, and additional CPU speed and memory capacity would be required for enabling an existing motor controller to run close to real-time. Zanardelli, et. al., [36] have compared three wavelet based methods for the prognosis of failures in electrical machines. A framework for the development of a fault detection and classification algorithm based on the coefficients calculated from the discrete wavelet transform of the fault currents and using clustering has been described. In the first technique, authors have used an *if-then-else* set of rules directly on results from the wavelet decomposition of the current through a machine to identify and distinguish between faults. The second technique focused on mapping the wavelet decomposition of the current into a multi-dimensional space, clustering the resultant vectors, and using several variants of the nearest neighbor rule. In the third technique, a set of trained weighting coefficients were applied to the wavelet decomposition of the current through a machine and the linear discriminant analysis was used as the criterion to distinguish between faults. Authors have used a real-time Linux (RT-Linux) based operating system for the on-line implementation of the experimental setup.

Kim, et. al., [37] have developed a model-based fault diagnosis system including recurrent dynamic neural networks and multi-resolution signal processing for predicting the transient response and for extracting the feature of non-stationary signal, respectively in induction motors. The transient motor predictor model was used to generate the stationary type residuals. Then, the residuals are processed by the wavelet packet transform based decomposition algorithm to generate two decoupled fault indicators.

A new wavelet based methodology for extracting a narrow-band vibration spectrum that contains the required features of the critical frequencies has been reported in reference [38] in order to diagnose induction motor faults operating at different rotating speeds. As a result, the spectral components of the critical frequencies were effectively extracted and analyzed. The gaussian-enveloped oscillation type mother wavelet was used in the analysis. The matching of the wavelet basis functions with the associated signals was obtained by appropriately selecting the parameters of basis functions.

An on-line fault detection approach based on the continuous wavelet transform of vibration signals for detecting the bearing fault of induction motors has been reported in reference [39]. The approximated Morlet wavelet was used to develop an infinite impulse response (IIR) causal filter by keeping the error at an acceptable level. Using this filter, the continuous wavelet transform (CWT) of the fault current was computed. The rapid computation of the CWT, together with autocorrelation enhancement, was developed for the detailed on-line analysis of the vibration signals. However, due to the use of IIR filter, the algorithm has less computational advantages than other condition monitoring techniques, and it is highly exposed to problems of finite-length arithmetic, such as noise generated by calculations and limit cycles.

Saleh, et. al., [40] have presented a new technique based on the multiresolution analysis (MRA) of the fault currents for detecting and diagnosing various disturbances occurring in three-phase induction motors. Stator currents of different faulted and normal unfaulted conditions were collected in order to be processed by the wavelet packet transform (WPT). The application of the WPT has shown that all fault conditions have non-zero second level high frequency sub-band coefficients, while normal and starting currents have zero values for the same coefficients. The algorithm is implemented in the MATLAB environment using the Daubechies 'db4' mother wavelet for both the first and second levels of resolution of the wavelet packet transform. However, the proposed algorithm was not validated through the experimental results. Douglas, et. al., [41] have developed a new algorithm based on the signature analysis of starting currents of the induction motors operating under different transients. At the beginning the measured line currents were transformed into a single rotating current vector and the vector transformed again into the time domain was applied as an input to the proposed algorithm. The algorithm estimated the frequency, amplitude, and phase of a single sinusoid embedded in the non-stationary waveform. The discrete wavelet transform (DWT) using the Daubechies 'db8' mother wavelet was then applied to the residual current vector for discriminating a healthy motor from the damaged motor. However, the algorithm was able to detect only the passive faults rather than the incipient failures in induction motors.

Toliyat, et. al., [42] have presented the wavelet packet transform as the diagnostic tool for detecting defects in railroad track. Authors have used the Perseval theorem in order to calculate the energy of the DWT coefficients of different signals obtained from the magnetic coil and Hall effect sensors on the railroad track. The experimental results showed the deviation of energy of the DWT coefficients in the faulty state from the healthy state. Yen, et. al., [43] have formulated a systematic method for selecting the best wavelet-packet-based features that exploit class specific differences among interesting signals. In the method the signal is first decomposed via the wavelet packet transform (WPT) to extract the time-frequency-dependent information. A simple statistical processing technique based on the discriminant analysis is then applied to identify a set of robust features that provides the most discrimination among the classes of vibration data. Finally, a neural network classifier is trained by this reduced feature set. Several feature components containing little discriminant information were discarded with the help of statistical-based feature selection criterion. Zhengjia, et. al., [44] have used the wavelet packet transform in tandem with some signal processing methods such as autoregressive spectrum, energy monitoring, fractal dimension, etc. for condition monitoring and fault diagnosis of turbo generators. The proposed method successfully diagnosed the weak defects and looseness faults in ball bearings of inside the bearing terminal of 50MW turbine generator.

A systematic method for analyzing different power system disturbances in the wavelet domain is described in reference [45]. The disturbance detection and localization was performed using a threshold obtained from the DWT coefficients of different signals at the certain level of resolution. The proposed classification process was started with the mapping of distortion events data into the wavelet domain using the discrete wavelet transform. The energy distribution of the distortion events at different resolution levels was computed by Perseval theorem to generate a set of translation invariant features with small dimensionality. Consequently, the total harmonic distortion (THD) and root mean square (RMS) values of distorted signals were also calculated using DWT coefficients of different levels of resolution. Finally, a new disturbance monitoring system based on

RMS variations of different signals was used for classifying different power system disturbances.

1.3.4 Application of Miscellaneous Techniques

A closed-form solution is used in references [5,46] for predicting the steady-state response of interior permanent magnet (IPM) synchronous motors to symmetrical and asymmetrical short circuit faults and single-phase open-circuit fault including the effects of q-axis magnetic saturation. The faults were analyzed using dynamic simulation techniques and the experimental results were presented for validating the simulations. In addition to presenting the new model, authors have investigated two alternative post-fault inverter control strategies. Jeong, et. al., [47] have illustrated different control strategies that could provide fault tolerance to the major sensor faults, which might occur in an interior permanent magnet motor based electric vehicle propulsion drive system. Failures of a position sensor, a dc-link voltage sensor, and current sensors were included in the study assuming no multiple faults. In each possible sensor fault, a corresponding method of detection or diagnosis was formulated. For the case of position sensor fault, a sensor less rotor position estimation scheme was used to provide post-fault control. The combination of saliency-based and model-based position estimation algorithms were utilized to estimate the rotor position at all operating speeds. For the case of dc-link voltage sensor failure, the principle of power balance was adopted to detect sensor malfunction and its effect to the stability of current control was also discussed. In the case of current sensor failure, sequences of simple tests were devised to detect the sensor failure. The missing current information was obtained using a state observer to estimate the unknown quantities and the analysis was done introducing a sensor gain matrix.

Jack, et. al., [48] have presented a comparative study of permanent magnet and switched reluctance motors for high-performance fault-tolerant applications. A switched reluctance motor has better fault-tolerant capabilities than that of permanent magnet synchronous motor because of internal rotor structural differences. In this work, a surface mounted type permanent magnet synchronous motor was designed to enhance its fault-

tolerance capabilities. It has been shown that the permanent magnet motor offered a greater torque density than the switched reluctance motor after the inclusion of fault-tolerance characteristics. Trutt, et. al., [49] have used the positive and negative sequence components of stator voltages and currents of the polyphase induction motor during the steady-state condition for determining a library of parameters, which are the function of motor design, operating speeds, internal deterioration, and imperfections in the measurement system. The fault detection was performed by looking into the deviations in the positive or negative sequence components of stator voltages or currents of the healthy induction motor. However, the on-line implementation of the proposed technique in mining or other industrial situation would require an initial training period with the healthy motor to build a library of parameters as a function of motor speed assuming that the speed variation over the sample time would be within an acceptable limit.

Arkan, et. al., [50] have illustrated a power decomposition technique, which involved the transformation of stator voltages and currents from balanced 3-phase to 2-dimensional orthogonal co-ordinate axis for detecting and diagnosing faults in three-phase induction motors. The magnitude and phase of the negative sequence current calculated from the reactive component of the negative sequence impedance of the induction motor was used to indicate the unbalanced state of the motor. However, the proposed technique could detect only the presence rather than the location of the faults. Rosu, et. al., [51] have presented a hysteresis model based on the classical Preisach-type finite element time stepping analysis for describing the demagnetization characteristic of the permanent magnet in the three-phase star-connected, six-pole, 1.5 MW PMSM under a failure condition. It has been shown that the demagnetization of the permanent magnets occurred after the line-to-line fault with a slight reduction of the no-load voltage.

1.4 Problem Identification and Objective of the Thesis

On the basis of the literature review, it could be asserted that most of the fault diagnosis and detection techniques have been developed and implemented for the protection of either induction motors or surface mounted type permanent magnet motors. Interior permanent magnet (IPM) synchronous machines, with magnets buried inside the rotor, offer some important opportunities for minimizing short circuit faults by making degrees of design freedom available that do not exist in other types of PM machines. More specifically, the presence of reluctance torque attributed to the magnetic saliency of the IPM machine's rotor provides machine designers with freedom to adjust the relative contributions of the reluctance and magnet-based torque components in a way that cannot be matched in conventional surface PM machines [46]. Researchers in references [5, 46-47] have tried to develop a fault diagnosis and condition monitoring technique for the protection of the interior permanent magnet (IPM) motors and drives in the case of symmetrical and asymmetrical (including open circuit) short circuit faults in the stator side of the motor. For this purpose, the usual dq model for an IPM motor was modified and implemented experimentally for predicting the steady-state response of interior permanent magnet (IPM) synchronous motor to the symmetrical and asymmetrical short circuit faults. Finally a control strategy, which involved the transition from the asymmetric faults to the three-phase symmetric short circuit fault, was proposed because of the severe machine fault response associated with the asymmetric faults in the IPM motor [46]. The transition of control strategies following a fault were implemented successfully in reference [47] for the case of variable speed IPMSM drive fed from pulse width modulated voltage source inverter. Mechanical faults such as position sensor failure, dc link voltage source failure and current sensor failure were considered in the implementation of this condition monitoring technique. However, in case of the line-start interior permanent magnet (IPM) motor, it is not feasible to have the post-fault control strategies following the electrical or mechanical faults. Therefore, a fault detection and protection scheme is needed for the case of line-start interior permanent magnet (IPM) motor that will disconnect the motor from the supply soon after a fault happens.

There have been many fault detection and condition monitoring techniques for carrying out the protection of electrical machines. The artificial neural network (ANN) with fuzzy logic and expert knowledge, motor current signature analysis based on the spectrum measurement of stator currents or voltages, and finally time-frequency analysis based on the short time Fourier transform or wavelet transforms are widely used from the last decade. The wavelet transform is a relatively new technique in the diagnosis and protection of electrical machines. It replaces other condition monitoring techniques because of its better frequency resolution and time localization property. It does not require any learning from the experimental data of steady-state condition of the motor. In addition, desirable basis functions can be chosen in wavelet transform according to the nature of the signal in contrast to the fixed sinusoidal basis in conventional Fourier transform analysis.

A novel condition monitoring technique based on the wavelet packet transform has been developed in this thesis for the detection and diagnosis of electrical faults in interior permanent magnet (IPM) motors fed from the three-phase power supply. Faults considered are the loss of single-phase supply and stator winding line faults (line to ground or line to line short circuit). The three-phase stator currents from the sensors mounted in series with the supply have been used as the medium of fault detection and protection technique. The protection has been achieved through the use of three triac switches connected in series with the supply in order to disconnect the motor from the supply immediately after a fault happens. The effective and efficient implementation of the wavelet packet transform based algorithm requires a proper selection of a mother wavelet. The normalized Shannon entropy based criterion and the minimum description length (MDL) data criterion for perfect reconstruction have been used to determine the optimum number of levels of resolution and the optimum mother wavelet, respectively [52]. The proposed algorithm has been developed and tested on-line on two types of interior permanent magnet motors. It provided satisfactory results in terms of speed, accuracy, computational burden, memory size and reliability. In addition, the algorithm has been implemented in real-time using Texas Instrument TMS320C31 32 bit floating

point digital signal processor with the help of object-oriented programming written in Turbo C. It also has been tested on a pulse width modulated (PWM) inverter fed interior permanent magnet (IPM) motor in order to generalize the proposed algorithm for the interior permanent magnet motors.

1.5 Outline of the Thesis

Chapter 2 describes the application of commonly used condition monitoring and fault diagnosis techniques for the three-phase interior permanent magnet motors. Four diagnosis tools including the discrete Fourier transform (DFT), power spectral density (PSD), short time Fourier transform (STFT) and artificial neural network (ANN) are discussed and implemented off-line for the protection of the interior permanent magnet motors. Chapter 3 illustrates the concept of wavelet and filter banks with the detail description of continuous, discrete and wavelet packet transforms. The chapter is concluded with the description of the normalized Shannon entropy based criterion and the minimum description length (MDL) data criterion for selecting the optimum number of levels of resolution and the optimum mother wavelet, respectively. In chapter 4, an experimental setup is developed using the DS1102 digital signal processor board for acquiring the data in case of faulted and normal unfaulted conditions of IPM motors. Signature analysis based feature extraction of the fault currents using the continuous wavelet transform of these collected data is done for formulating the proposed algorithm. The proposed algorithm is tested off-line in the Matlab environment. Both Shannon entropy and minimum description length data criterion are applied in this section to determine the optimal number of levels of resolutions and optimum mother wavelet for both the off-line and on-line testings of the proposed algorithm. In chapter 5, a step-by-step real-time implementation of the proposed algorithm is given for the protection of the IPM synchronous motors. The complete protection scheme is successfully implemented in real-time using a DS1102 DSP board on a prototype 1 hp and a 5 hp interior permanent magnet motors. The detailed hardware and softwares required for the real-time implementation are provided in this chapter. The on-line test results of different

disturbances in both the line-fed and inverter fed 1 hp and 5 hp interior permanent magnet motors are provided in this chapter. Finally, in chapter 6, the summary and conclusion of the thesis is presented along with the future scope of this work. The pertinent references and appendices are listed.

Chapter 2

Application of General Techniques for the Detection of Disturbances in the Interior Permanent Magnet (IPM) Motors

This chapter presents an overview of the application of commonly used condition monitoring and fault diagnosis techniques for the protection of three-phase interior permanent magnet motors. Four general techniques to detect and diagnose faults in IPM motors have been discussed and implemented in this chapter. At the beginning the discrete Fourier transform (DFT) is implemented using the fast Fourier transform (FFT) based algorithm to determine the magnitude of the fundamental fault frequency for differentiating normal conditions from the abnormal conditions. Then the measurement of power spectral density (PSD) of stator current frequencies during the normal unfaulted and faulted conditions are used to detect faults in three-phase interior permanent magnet (IPM) motors. A short-time Fourier transform (STFT) based algorithm is implemented after the PSD measurement based technique for detecting faults in both the time and frequency domains. Finally a modern pattern recognition technique is implemented off-line in the MATLAB environment using the three-layer feed forward artificial neural network with the back propagation algorithm for detecting and protecting various disturbances occurring in a laboratory 1hp interior permanent magnet motor.

2.1 Discrete Fourier transform (DFT)

The DFT is a sequence rather than a function of a continuous variable, and it corresponds to samples, equally spaced in frequencies of the Fourier transform of the discrete signal. In addition to its theoretical importance as a Fourier representation of sequences, the DFT plays a central role in the implementation of a variety of digital signal-processing algorithms. This is because efficient algorithms exist for the computation of the DFT. The interpretation of DFT begins by considering the Fourier series representation of periodic sequences. The discrete Fourier series (DFS) coefficients $\tilde{X}[k]$ of the periodic sequence $\tilde{x}[n]$ are itself a periodic sequence with period N [53]. Thus, the DFT of the discrete sequence $x[n]$, $X[k]$ is related to DFS coefficients $\tilde{X}[k]$ by

$$\begin{aligned} X[k] &= \tilde{X}[k], & 0 \leq k \leq N-1 \\ &= 0, & \text{otherwise} \end{aligned} \quad (2.1)$$

and

$$\tilde{X}[k] = X[(k \bmod N)] = X[(k)_N] \quad (2.2)$$

Generally, the DFT analysis and synthesis equations are written as follows:

$$\text{Analysis equation: } X[k] = \sum_{n=0}^{N-1} x[n] W_N^{kn}, \quad 0 \leq k \leq N-1 \quad (2.3)$$

$$\text{Synthesis equation: } x[n] = 1/N \sum_{k=0}^{N-1} X[k] W_N^{-kn}, \quad 0 \leq n \leq N-1 \quad (2.4)$$

$$\text{Here, } W_N = e^{-j(2\pi/N)} \quad (2.5)$$

In case of non-periodic signals (like currents with transient components for the protection purposes), the windowed DFT is normally used. If the signal is sampled with sampling interval of Δt , such that there are $N/\Delta t$ samples per cycle, then the DFT basis function coefficients can be represented as [54]

$$S_k = \frac{2}{N} \sum_{n=1}^{N-1} x[n] \sin\left(\frac{2\pi kn}{N}\right) \quad (2.6)$$

$$C_k = \frac{2}{N} \sum_{n=1}^{N-1} x[n] \cos\left(\frac{2\pi kn}{N}\right) \quad (2.7)$$

The Fourier harmonic coefficients can be expressed as,

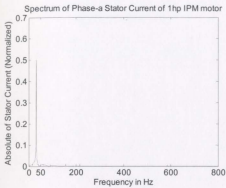
$$F_k = \sqrt{S_k^2 + C_k^2} \quad (2.8)$$

Where F_k is the k th harmonic Fourier coefficient, where $k=1,2,\dots,N$ and $x[n]$ is the sampled sequence of the continuous signal $x[t]$.

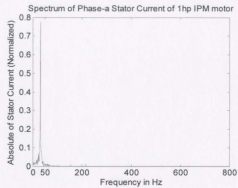
2.1.1 Implementing the DFT Algorithm for the Interior Permanent Magnet (IPM) Motor Protection

It has been shown in reference [55] that the number of frequency components in stator currents could be changed for the stator or rotor faults in the PM motors. However, it was shown that the best frequency components to monitor for detecting rotor faults were the frequency of the rotor speed and its integer multiple. These were denoted as fault frequencies. The lowest fault frequency was the synchronous frequency divided by the number of pole pairs. These fault frequencies usually appear in the stator currents due to the air-gap flux disturbances caused by faults.

In the present work, three types of electrical faults such as the loss of supply, stator-winding line to ground fault, and stator winding line-to-line short circuit fault are considered and detected for the protection of three-phase interior permanent magnet (IPM) motors. It has been assumed that these faults create unbalance in the air gap electromagnetic flux density. As a result, according to reference [55] different fault frequencies will appear in stator currents and these can be used for detecting and diagnosing different types of faults occurring in three-phase interior permanent magnet (IPM) motors. The discrete Fourier transform (DFT) using the fast Fourier transform (FFT) based algorithm [56] is implemented in this section to determine the spectrum of stator currents for the faulted and normal unfaulted conditions.

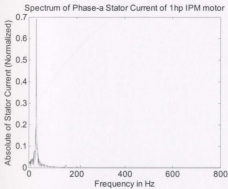


(a)

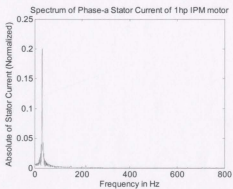


(b)

Figure 2.1: FFT of the phase-a stator current of the 1hp IPM motor: (a) normal healthy operation, (b) stator winding line-a to ground (L-G) fault.

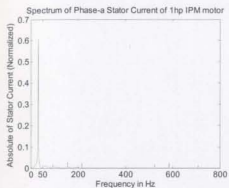


(a)

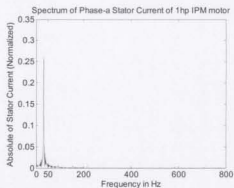


(b)

Figure 2.2: FFT of the phase-a stator current of the 1hp IPM motor: (a) loss of phase-a supply, (b) stator winding line-a to line-b (L-L) short circuit fault.

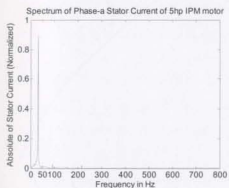


(a)

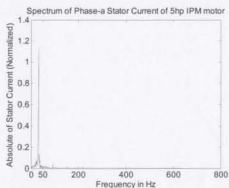


(b)

Figure 2.3: FFT of the phase-a stator current of the 1hp IPM motor: (a) normal unfaulted full load operation, (b) loss of three-phase supply fault.



(a)



(b)

Figure 2.4: FFT of the phase-a stator current of the 5hp IPM motor: (a) normal healthy operation, (b) stator winding line-a to ground (L-G) fault.

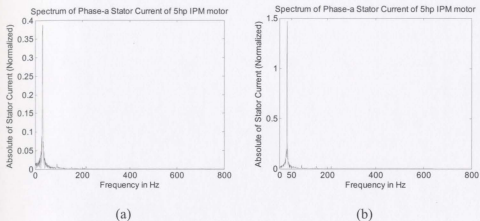


Figure 2.5: FFT of the phase-a stator current of the 5 hp IPM motor: (a) loss of phase-a supply, (b) stator winding line-a to line-b (L-L) short circuit fault.

Figures 2.1-2.3 show the FFT based spectra of the phase-a stator current for different disturbances in the laboratory 1-hp interior permanent magnet motor. The lowest fault frequency of the 4-pole interior permanent magnet motor according to reference [55] is 30 Hz and it is evident from Figs 2.1-2.3 that this lowest fault frequency dominated other frequencies. However, the amplitude of this fundamental harmonic varied between the faulted and normal unfaulted (healthy) conditions and also within disturbances.

The normalized magnitude of the fundamental fault frequency (30 Hz) varied between 0.5 and 0.6 for the case of no-load and full load unfaulted operating conditions of the 1-hp IPM motor. However, it showed the peak values of greater than 0.69 and less than 0.3 for cases of disturbance. Figures 2.4-2.5 describe the FFT based spectra of the fault current of the 5hp (4-pole) interior permanent magnet (IPM) motor. Here the lowest fault frequency also dominated other frequencies. In addition, the magnitude of this fundamental harmonic varied within disturbances. It showed the peak values of greater than 0.9 and less than 0.4 in case of disturbances. The fundamental harmonic has the peak value equal to 0.9 for the case of healthy operating condition of the 5hp IPM motor.

Depending on the results obtained it could be asserted that the FFT based spectrum analysis technique of fault currents is capable of detecting and classifying possible disturbances in IPM motors. However, the FFT based technique is not suitable for the analysis of non-stationary signals, and it cannot localize faults in the time domain. In addition, faults studied in this work are short transients superimposed on stator currents. So, analysis of these transients would require information in both the time and frequency domains.

2.2 Power Spectral Density (PSD)

The power spectral density is the estimation of the distribution of the power over frequencies contained in a signal, based on a finite set of data. The power spectrum of a stationary random process $x[n]$ is mathematically related to the correlation sequence by the discrete-time Fourier transforms [56]. In terms of normalized frequency, this is given as:

$$S_{xx}(\omega) = \sum_{m=-\infty}^{\infty} R_{xx}(m)e^{-j\omega m} \quad (2.9)$$

The correlation sequence can be derived from the power spectrum by use of the inverse discrete-time Fourier transform:

$$R_{xx}(m) = \int_{-\pi}^{\pi} \frac{S_{xx}(\omega)e^{j\omega m}}{2\pi} d\omega \quad (2.10)$$

The power spectral density (PSD) of the stationary random signal $x[n]$ is defined as:

$$P_{xx}(\omega) = S_{xx}(\omega) / 2\pi \quad (2.11)$$

There have been many algorithms for the estimation of power spectral density (PSD) of a finite length signal. These can be categorized as follows [56]:

- 1) Non-parametric methods
- 2) Parametric methods
- 3) Sub-space methods

2.2.1 Non-parametric methods

In non-parametric methods, the estimate of the power spectral density (PSD) is made directly from the signal itself. Techniques such as the *periodogram*, *Welch*, and *multitaper* are classified as the non-parametric methods of PSD estimation. The estimate of the PSD from the magnitude squared FFT of the discrete signal is known as the *periodogram* [56]. In *Welch's* method of PSD estimation [56], the discrete-time input signal is first divided into segments and the PSD is calculated from each segment separately; and finally, averaging the PSD estimation yields the overall PSD of the input signal. It tends to decrease the variance of the estimate relative to the single *periodogram* estimate of the entire data record. The *multitaper method* (MTM) [56] uses a bank of optimal finite impulse response (FIR) filters, which are derived from a set of sequences known as the *discrete prolate spheroidal* sequences, in the PSD estimation of the input signal. In addition, it uses a time-bandwidth parameter for balancing between the variance and resolution.

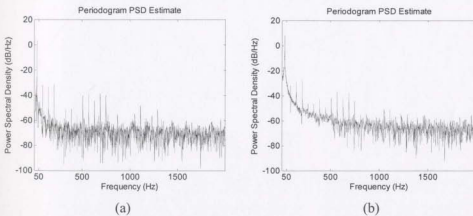


Figure 2.6: The *periodogram* PSD estimates of the phase-a stator current of the 1hp IPM motor: (a) normal healthy operation, (b) stator winding line-a to ground (L-G) fault.

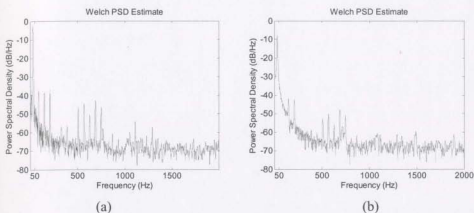


Figure 2.7: The *Welch* PSD estimates of the phase-a stator current of the 1hp IPM motor: (a) normal healthy operation, (b) loss of phase-a supply.

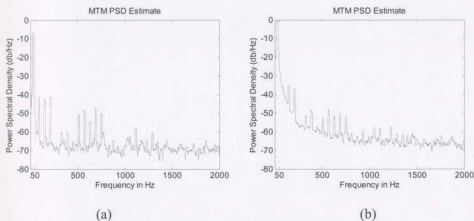


Figure 2.8: The *multitaper* PSD estimates of the phase-a stator current of the 1hp IPM motor: (a) normal healthy operation, (b) stator winding line-a to line-b (L-L) fault.

Figures 2.6(a)-2.6(b) show the *periodogram* PSD estimate of the phase-a stator current of the 1hp IPM motor for the normal unfaulted and faulted conditions. The lowest fault frequency of the 4-pole IPM motor has the highest power distribution than that of other harmonics. It is also to be noted that the PSD of the lowest fault frequency varied between the faulted and normal unfaulted conditions. However, the effects of spectral leakage and resolution are the limitations of *periodogram* method of PSD estimation. A

non-rectangular window can be used to overcome the spectral leakage, which will result in the net reduction of the resolution.

Figures 2.7(a)-2.7(b) show the *Welch* PSD estimate of the phase-a stator current of the 1hp IPM motor for the normal unfaulted and faulted conditions. Here, the variance is reduced by averaging of PSD estimates of each segment. However, the combined use of short data records and non-rectangular window can result in the reduced resolution of the estimator. Figures 2.8(a)-2.8(b) show the *multitaper* PSD estimate of the phase-a stator current of the 1hp IPM motor for the normal unfaulted and faulted conditions. Here, PSD peaks are resolvable due to the addition of time-bandwidth parameter. However, the method is more computationally extensive than the *Welch's* method because of the time required for computing the *discrete prolate spheroidal sequences*. Although the above-mentioned non-parametric methods can differentiate a faulted condition from the normal unfaulted condition, these cannot provide any pertinent information of the input signal in the time domain.

2.2.2 Parametric methods

In parametric method, the signal, whose PSD one needs to estimate, is assumed to be the output of a linear system driven by white noise. These include the *Yule-Walker* [56] auto-regressive (AR) and *Burg* [56] methods. These methods estimate the PSD of the input signal by estimating the parameter coefficients of the linear system that hypothetically generates the signal. They tend to produce better results than the classical non-parametric methods in case of short data records. The most common linear system includes an all pole filter with all of its zeroes at the origin in the z-plane. The output of such a filter for the white noise input is known as the auto-regressive (AR) process. Therefore, these methods are sometimes referred to as the AR methods for the purpose of spectral estimation [56].

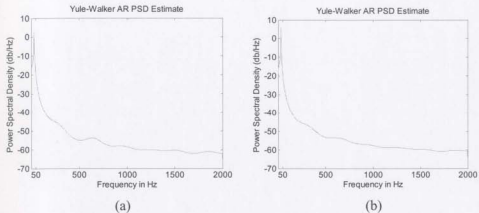


Figure 2.9: The *Yule-Walker* PSD estimates of the phase-a stator current of the 5hp IPM motor: (a) normal healthy operation, (b) stator winding line-a to ground (L-G) fault.

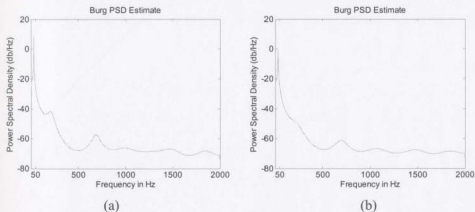


Figure 2.10: The *Burg* PSD estimates of the phase-a stator current of the 5hp IPM motor: (a) normal healthy operation, (b) loss of phase-a supply.

Figures 2.9(a)-2.9(b) show the *Yule-Walker* autoregressive PSD estimates of the phase-a stator current of the 5hp IPM motor for the normal unfaulted and faulted conditions. The distribution of power for the lowest fault frequency varied between these two conditions. The *Yule-Walker* AR spectrum is smoother than the *periodogram*, because of the simple underlying all-pole model. The *Burg* PSD estimate of the phase-a

stator current of the 5hp IPM motor for the normal unfaulted and faulted conditions are shown in Figs 2.10(a)-2.10(b). The *Burg* method was able to differentiate between the normal unfaulted and faulted conditions. However, the accuracy of the *Burg* method is lower for the high-order models, long data records, and high signal-to-noise ratios. The PSD estimate computed by the *Burg* method is also susceptible to the frequency shifts (relative to the true frequency) resulting from the initial phase of noisy sinusoidal signals [56]. These parametric methods can provide the resolvable PSD peaks at certain frequencies. However, these methods are not able to provide any pertinent information in the time-axis.

2.2.3 Subspace methods

Subspace methods, also known as high-resolution methods or super-resolution methods, generate frequency component estimates of a signal based on the eigen-analysis or eigen-decomposition of the correlation matrix. These include the multiple signal classification (MUSIC) [56] or eigenvector (EV) [57] methods. These methods are best suited for the line spectra, i.e. spectra of sinusoidal signals. These are effective in the detection of sinusoids, which are buried in noise, especially when the signal to noise ratios are low [56-57].

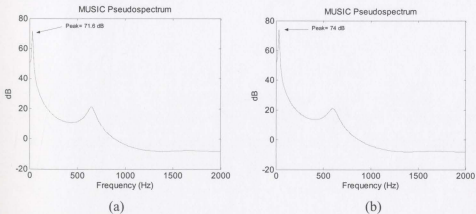


Figure 2.11: The *multiple signal classification* (MUSIC) pseudospectrum PSD estimates of the phase-a stator current of the 1hp IPM motor: (a) normal healthy operation, (b) stator winding line-a to ground (L-G) fault.

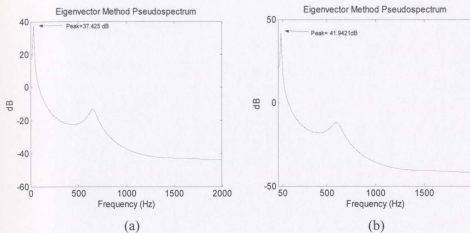


Figure 2.12: The *eigenvector* pseudospectrum PSD estimates of the phase-a stator current of the 1hp IPM motor: (a) normal healthy operation, (b) stator winding line-a to ground (L-G) fault.

Figures 2.11(a)-2.11(b) show the PSD estimates of the phase-a stator current using the *multiple signal classification* (MUSIC) pseudospectrum method for the case of normal unfaulted and faulted conditions. The peak PSD estimate of the lowest fault frequency is equal to 71.5682 dB for the case of healthy operation of the motor. However, it is equal to 74 dB during the line-a to ground fault. The effects of spectral leakage and resolution are also absent in this method. The *eigenvector* pseudospectrum based PSD estimates of the stator current is shown in Figs 2.12(a)-2.12(b). The peak power spectral density (PSD) of the lowest fault frequency during the healthy operation is found to be different from that of the abnormal condition. So, the method is able to differentiate between faulted and normal unfaulted conditions. However, the inability to localize a fault signal in the time-axis is the fundamental limitation of the above-described subspace methods.

2.3 Short-time Fourier transform (STFT)

The short time Fourier transform (STFT) is an extension of the fast Fourier transform (FFT), allowing for the analysis of non-stationary signals. Here, the signal is broken up into small parts, and each part is analyzed using the FFT [29]. The results of the STFT are intuitive and easy to correlate with the original signal. Tiling for the STFT is shown in Figure 2.13.

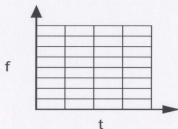


Figure 2.13: STFT tiling [29].

The tiling for the STFT as shown in the figure 2.13 is uniform. The tiling shows how the spectrum of a signal changes with time in the STFT. In the implementation of the STFT, a design tradeoff is normally made between the time and frequency resolution. This is due to the uncertainty principle, which limits the lower bound of the time-bandwidth product [29]. A block diagram showing the implementation of the STFT algorithm is given in figure 2.14.

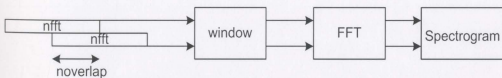


Figure 2.14: STFT block diagram [29].

where $nfft$ is the length of the DFT, $noverlap$ is the number of overlap samples, and $window$ is a weighting vector applied to the FFT input. The spectrogram is the graphical way to display the output of the STFT.

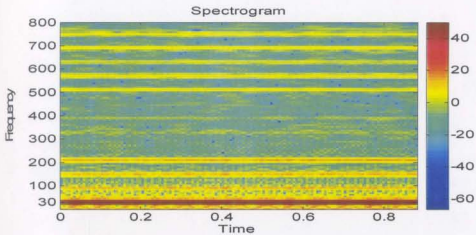


Figure 2.15: STFT based spectrogram of the phase-a stator current during the healthy operation of the 1hp IPM motor.

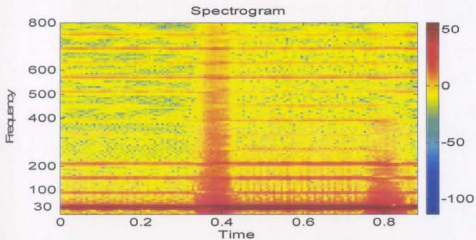


Figure 2.16: STFT based spectrogram of the phase-a stator current of the 1hp IPM motor for the case of stator winding line-a to ground (L-G) fault.

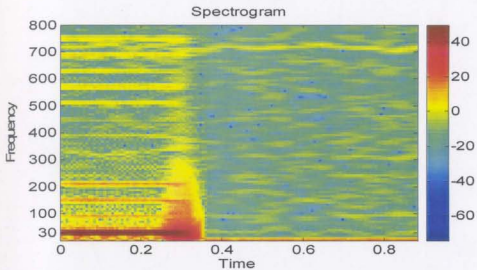


Figure 2.17: STFT based spectrogram of the phase-a stator current of the 1hp IPM motor for the case of loss of phase-a supply.

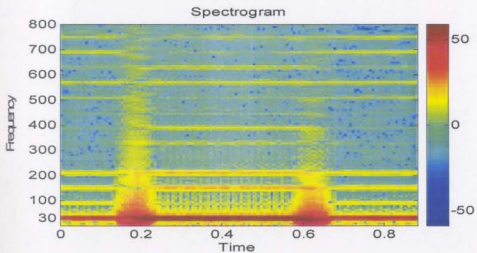


Figure 2.18: STFT based spectrogram of the phase-a stator current of the 1hp IPM motor for the case of stator winding line-a to line-b (L-L) short circuit fault.

The STFT based spectrogram of the stator current of the 1hp IPM motor for the case of normal unfaulted and faulted conditions are shown in Figs. 2.15-2.18. In the detailed analysis, a 512-point FFT [56] with 475 overlap samples between the data segments is used to compute the frequencies of the discrete signal. A 500-point Kaiser window [56] is applied in each data segment. The analysis generated 257 frequency points in 141 time-axis values. It is to be noted that the concentration of the energy of the lowest fault frequency (30 Hz) of the 4-pole 1hp IPM motor is uniform over the entire time axis of the spectrogram for the case of healthy operating condition of the motor. However, the concentration of energy of the frequency band ranging from 30 Hz to 210 Hz is different than that of the healthy motor during the inception and clearing of the fault over the time-axis.

Based on the analysis performed, it could be asserted that the STFT based algorithm can detect the faults in the IPM motor in both the time and frequency domains. However, as the length of the window is fixed in each of the data segment of the discrete signal, so the STFT based analysis is not able to provide good energy resolution concentrated around a point. In addition, the frequency analysis is performed with the help of the sinusoidal basis functions.

2.4 Artificial Neural Network (ANN)

Recently, the emerging technology of the artificial neural networks has been successfully implemented in many different areas such as the fault detection, control and signal processing. The first use of the artificial neural networks can be dated back to the 1940's. Several different neural network paradigms have been developed over the past few decades. Some of the major paradigms are the multilayer feed forward net, Kohonen net, Hamming net, Hopfield net, adaptive resonance theory net, etc. Each paradigm has its own internal network structure, properties and training algorithms. Some paradigms are more suitable to solve certain types of problems, while other paradigms are more appropriate for others. Of the different paradigms, the feed forward net is probably the most popular, and it constitutes more than eighty percent of the current artificial neural

network applications [12]. There have been many research works on the application and design of neural networks for the fault detection in electrical motor [10], [12-13], [16-19], [80]. In most of the works, the problem has been formulated as the pattern recognition of fault currents.

In implementing the ANN technique, the case has to be stated at the beginning. This includes the formulation of the inputs and outputs to the neural network. Then the network has to be trained for these inputs and the desired outputs. The network is trained to give input-output patterns when there is an input propagating from the input layer to the hidden (processing) layer, and finally to the output layer. In each processing unit the net sum is calculated first and then the sum is passed through the corresponding transfer function with appropriate bias for that unit to obtain the output of that unit. Thus for a given pattern $X_p = (X_{p1}, X_{p2}, \dots, X_{pN})^t$, the net-input value of the j th hidden-layer unit is given as [58]:

$$sum_{pj}^h = \sum_{i=1}^N W_{ji}^h X_{pi} + B_j^h \quad (2.12)$$

where the subscript p and superscript h stand for the pattern and the hidden layer respectively, W_{ji}^h 's are weights associated with connections between the input layer and hidden layer, and B_j^h 's are biases associated with the hidden-layer neurons. And the output of the j th hidden layer is found just by applying the transfer function on the net-input as given below:

$$I_{pj} = f^h (sum_{pj}^h) \quad (2.13)$$

Similarly, the net-input value of the k th output-layer unit can be calculated as:

$$sum_{pk}^o = \sum_{j=1}^L W_{kj}^o I_{pj} + B_k^o \quad (2.14)$$

where the superscript o stands for the output layer, W_{kj}^o 's are weights associated with connections between hidden layer and output layer, and B_k^o 's are biases associated with

the hidden-layer neurons. The expression for the output O_{pk} of the k th output-layer unit is given as:

$$O_{pk} = f^0(\text{sum}_{pk}^o) \quad (2.15)$$

The output O_{pk} is then compared with the desired or target output T_{pk} , and depending on the error between the obtained output and desired output, the weight of each connection and the bias of each processing unit are updated. To update the weights and biases, delta rule is applied and the cost function is defined as [58]

$$E_p = \frac{1}{2} \sum_k (T_{pk} - O_{pk})^2 \quad (2.16)$$

The main objective of the ANN training is to minimize the cost function. Steepest descent method is normally used for this purpose, where the changes in weights are proportional to the negative slope of the cost function i.e. $\Delta_p W_{kj}^o \propto -(\delta E_p / \delta W_{kj}^o)$. After some deductions and manipulations, the changes in weights and biases are found to be

$$\Delta_p W_{kj}^o = \eta \delta_{pk}^o I_{pj} \quad (2.17)$$

$$\Delta_p W_{ji}^h = \eta \delta_{pj}^h X_{pi} \quad (2.18)$$

$$\Delta_p B_k^o = \eta \delta_{pk}^o \quad (2.19)$$

$$\Delta_p B_j^h = \eta \delta_{pj}^h \quad (2.20)$$

where δ_{pk}^o and δ_{pj}^h are called the error terms for the output layer and hidden layer, respectively and these are calculated as shown below

$$\delta_{pk}^o = (T_{pk} - O_{pk}) f'^o(\text{sum}_{pk}^o) \quad (2.21)$$

$$\delta_{pj}^h = f'^h(\text{sum}_{pj}^h) \sum_k \delta_{pk}^o W_{kj}^o \quad (2.22)$$

and η is the learning rate, which is chosen by trial and error. The learning rate η is an important factor. Too small a value of η slows the learning process i.e. a large number of iterations are required; on the other hand, too big a value of η although speeds up the learning process might cause instability. A simple method helps speeding up the learning process to some extent and yet avoiding the danger of instability is to introduce a

momentum factor α in the delta rule. The hidden layer weight change equation can be written according to the modified delta rule as:

$$\Delta W_{ji}^h(n) = \alpha W_{ji}^h(n-1) + \eta \delta_{pj}^h X_{pi} \quad (2.23)$$

Although the above procedure is described for one hidden layer, this can be extended for multiple hidden layers. At first, the above procedure is done for all available training patterns and then the whole process is done repeatedly until a tolerance error is reached to a specified minimum value. The total average error is define as [58]:

$$E_{global} = \frac{1}{P} \sum_{p=1}^P E_p^2 \quad (2.24)$$

where P is the total number of available training patterns.

2.4.1 Implementing the Artificial Neural Network (ANN) for the Interior Permanent Magnet (IPM) Motor Protection

The first step in developing the ANN based protection for the IPM motors is to select a suitable network structure. There have been many network topologies reported in different literatures on the application of neural networks for detecting and diagnosing disturbances in electrical machines. It has been mentioned earlier that the multi-layer feed forward neural network structure constitutes more than eighty percent of the current neural network applications. Therefore, a three-layer feed forward network has been chosen in this work for implementing the ANN based protection of the IPM motors. The network has three neurons in the hidden layer and one neuron in the output layer. The numbers of neurons in the hidden layer have been selected by trial and error that had better stability and high converge rate. The Nguyen-Widrow initialization algorithm [56] has been to initialize the weights and biases of each neuron in the hidden and output layers. The algorithm chose the initial values in the hidden and output layers in order to distribute the active region of each neuron evenly across the layer's input space. The most common activation function *log-sigmoid* [81] is used in both the hidden and output layers in order to define the output of the neurons in terms of the activity level at its input. The general structure of a multi-layer feed forward neural network is shown in the figure 2.19.

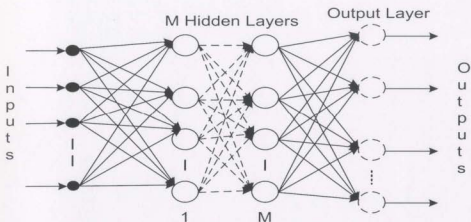


Figure 2.19: General structure of a multi-layer feed forward neural network (FFNN)

The network has been trained off-line in a supervised manner with the back propagation function *traingdm* [81], which updates the weight and bias values of the hidden and output layers according to the gradient descent with momentum. In implementing the fault detection algorithm for the IPM motor using ANN, the three-phase stator currents are used as the input to the network. The discrete data of the normal unfaulted and faulted conditions are used to train the neural network so that it can recognize and differentiate the normal conditions from the abnormal conditions. To generate the realizable training patterns for the ANN based protection, samples of the summation of the squared three-phase stator currents are compared with a predefined threshold to convert it a binary value of either 1 or 0, depending on whether the value is greater or smaller than the threshold, respectively. In this way each training pattern became a different combination of 1 and 0. It is expected that the starting current and fault currents data would not have the same training pattern. The elements of the target vector for the case of normal unfaulted (both no load and full load) and starting current samples were chosen equal to binary '0'. On the other hand, the elements of the target vector were equal to binary '1' for the case of fault current samples. After training the

network with one set of training pattern, which includes the samples of the normal unfaulted and faulted currents, and starting currents, the network is tested off-line in the MATLAB environment with the different set of testing pattern. The following figures show the off-line test results of the ANN based protection algorithm on the 1hp interior permanent magnet motor.

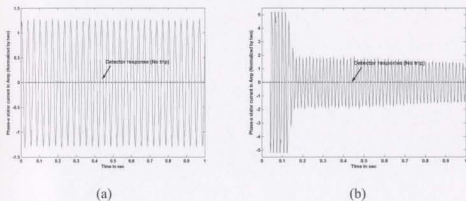


Figure 2.20: ANN based detector response and phase-a stator current of the 1hp IPM motor: (a) normal unfaulted condition, (b) normal starting condition.

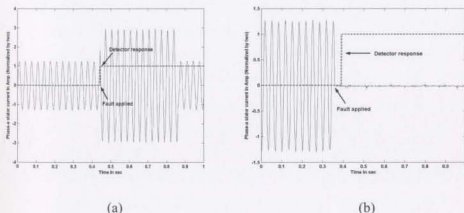


Figure 2.21: ANN based detector response and phase-a stator current of the 1hp IPM motor: (a) stator winding line-a to ground (L-G) fault, (b) loss of phase-a supply fault.

Figures 2.20(a)-2.20(b) show the ANN based detector response and phase-a stator current of the 1hp IPM motor for the case of normal (unfaulted) and starting conditions. The artificial neural network (ANN) based detection algorithm identified these as the normal conditions and did not generate any trip signal. The phase-a stator current with the associated trip signal for the case of stator winding line-a to ground (L-G) fault and loss of phase-a supply fault are shown in Figs. 2.21(a)-2.21(b). The algorithm identified both disturbances properly and initiated a trip signal at the almost instant of the faults. However, the technique needs a lot of data files to train the network. In addition the number of hidden layers must be increased to improve the accuracy. Therefore, more memory is also needed to accommodate the weights and biases for the new layers, and as a result, many trials are required to determine the learning rate, so as to improve the functionality of the ANN based detection algorithm.

In the general fault detection techniques as implemented in this chapter including the application of the DFT, the application of the STFT, and PSD measurements of line currents, the fault current signals are transformed into discrete harmonics. But the WPT based protection algorithm transforms the fault current signals into frequency bandwidths utilizing the filter bank structure of the wavelet packet tree, which can cover all significant harmonics. In the artificial neural network based detection technique, the network is trained off-line, and it takes approximately one hour to reach an overall mean square error of 0.001. In addition, many trials are used to determine an optimum number of hidden layers, and the memory requirements of the on-line implementation of the neural network based fault detection technique are high. The WPT based technique does not require time consuming off-line training or preprocessing of input data. The real-time implementation of the protection algorithm involves two filtering operations and one down sampling operation. So, the memory requirements for the on-line implementation are small. It is to be noted that the computational complexity of the real-time implementation of the DFT, STFT, or PSD measurements based techniques is also high.

Chapter 3

Wavelets and Wavelet Transforms

Condition monitoring and fault diagnostics are necessary for ensuring the safe running of machines. Signal analysis is one of the most important methods used for condition monitoring and fault diagnostics, whose aim is to find a simple and effective transform to the original signals. Therefore, the important information contained in signals can be shown, and the dominant features of signals can be extracted for fault diagnostics. Hitherto, many signal analysis methods have been used for fault diagnostics, among which the fast Fourier transform (FFT) is one of the most widely used and well-established methods. Unfortunately, the FFT-based methods are not suitable for non-stationary signal analysis and are not able to reveal the inherent information of non-stationary and non-periodic signals. However, various kinds of factors, such as the change of the environment and the faults from the machine itself, often make the output signals of the running machine contain non-stationary and non-periodic components. Usually, these non-stationary components contain enough information about machine faults. Therefore, it is important to analyze the non-stationary signals [59]. Because of the limitations of the FFT analysis, it is necessary to find supplementary methods for the non-stationary signal analysis.

Time–frequency analysis such as the Wigner–Ville distribution (WVD) [60] and the short time Fourier transform (STFT) [29] are the most popular methods for the analysis

of non-stationary signals. These methods perform a mapping of the one-dimensional discrete signal $x[n]$ into the two-dimensional function of time and frequency. And as such these are able to provide true time–frequency representations for the continuous signal $x[t]$. But each of the time–frequency analysis method has suffered some problems. It is no doubt that the WVD has good concentration in the time–frequency plane. However, even support areas of the signal do not overlap each other, interference terms can appear on the time–frequency plane. This can mislead the signal analysis. In order to overcome these disadvantages, many improved methods such as Choi–Williams distribution (CWD), cone-shaped distribution (CSD) [60], etc. have been proposed. Without exception, however, the elimination of one shortcoming always leads to the loss of other merits. For example, the reduction of interference terms will bring the loss of time–frequency concentrations. The problem with the STFT is that it provides the constant resolution for all frequencies, since it uses the same window for the analysis of the entire signal. This means that if one wants to obtain a good frequency resolution using the wide windows, one may not be able to obtain good time resolution (narrow window), which is desired for the analysis of high-frequency components. Therefore, the STFT is suitable for the quasistationary signal analysis (stationary at the scale of the window but not the real stationary signals). However, there exist no orthogonal bases for the STFT. Therefore, it is difficult to find a fast and effective algorithm to calculate the STFT of the non-stationary and non-periodic signals [60].

The wavelet transform (WT) has been found to be particularly useful for analyzing signals which can best be described as the aperiodic, noisy, intermittent, transient and so on. Its ability to examine the signal simultaneously in the time and frequency domains in a distinctly different way from the traditional short time Fourier transform (STFT) has spawned a number of sophisticated wavelet-based methods for the signal manipulation and interrogation. Wavelet transform analysis has now been applied in the investigation of a multiple of diverse physical phenomena, from climate analysis to the analysis of financial indices, from heart monitoring to the condition monitoring of rotating machinery, from seismic signal denoising to the denoising of astronomical images, from

crack surface characterization to the characterization of turbulent intermittency, from video image compression to the compression of medical signal records, and so on [61]. This chapter provides a detailed description of the wavelets, scaling functions and the different types of wavelet transforms. Also, the multiresolution analysis and the concept of quadrature mirror filter banks are introduced in this chapter. Finally, it describes methods for selecting the optimal mother wavelet and optimal number of levels of resolution.

3.1 Wavelets and Scaling Functions

In order to perform the wavelet transform one needs a *wavelet*, which as the name suggest, is a little wave in the sense of having short duration with finite energy and fast decaying behavior in time. In addition, wavelets have an oscillating feature that comes along with the location in time and frequency. These basic features of any wavelet make wavelets highly adequate for signal representation [62]. In order to be classified as a wavelet, a function must satisfy certain mathematical criteria. These are as follows [61]:

1). A wavelet must have finite energy:

$$E = \int_{-\infty}^{\infty} |\psi(t)|^2 dt < \infty \quad (3.1)$$

where E is the energy of the wavelet function equal to the integral of its squared magnitude, and the vertical brackets $| \quad |$ represent the modulus operator, which gives the magnitude of the wavelet function $\psi(t)$. If $\psi(t)$ is a complex function, its magnitude must be found using the real and complex parts.

2). If $\hat{\psi}(f)$ is the Fourier transform of $\psi(t)$, i.e.

$$\hat{\psi}(f) = \int_{-\infty}^{\infty} \psi(t) e^{-i(2\pi f)t} dt \quad (3.2)$$

then the following condition must be hold:

$$C_g = \int_0^{\infty} \frac{|\hat{\psi}(f)|^2}{f} df < \infty \quad (3.3)$$

This implies that the wavelet function should not have any zero frequency components i.e. $\hat{\psi}(0) = 0$ or it must have a zero mean. Equation (3.3) is known as the *admissibility condition* and C_g is called the *admissibility constant*. The value of C_g depends on the chosen wavelet and is equal to π for the Mexican hat wavelet given in equation (3.4) as:

$$\psi(t) = (1 - t^2)e^{-t^2/2} \quad (3.4)$$

3). An additional criterion that must be hold for the complex wavelets is that the Fourier transform must be real and vanished for the negative frequencies.

Some wavelet functions of the orthogonal type have a companion function called the scaling function $\phi(t)$ and it is responsible for generating all basis functions needed to represent any signal, i.e. to either decompose or reconstruct any signal. The scaling function has the following properties [63]:

- a. Compact support, which indicates that the value of the scaling function is zero outside the interval of support $[t_0, t_1]$ of the mother wavelet i.e. $\phi(t) = 0$ for $t \notin [t_0, t_1]$.
- b. Averaging, which guarantees an average value of the scaling function to be 1 over the region of support i.e. $\int_{t_0}^{t_1} \phi(t) dt = 1$. (3.5)
- c. Orthogonality, which ensures the orthogonal property of all translations of the scaling function $\phi(t)$, i.e. $\phi(t - m_1)$ is orthogonal to $\phi(t - m_2)$ where $m_1, m_2 \in \mathbb{N}$. Here \mathbb{N} is the set of positive integers.
- d. Regularity, which guarantees that the constant and linear functions can be regenerated by $\phi(t)$ and its translations.

The term "Mother" of the mother wavelet implies that the functions with different region of support used in the transformation process are derived from the one main

function. The region of support is defined as an interval $[t_0, t_s]$ of the smallest length, outside of which the mother wavelet $\psi(t)$ vanishes identically.

A basis of a vector space V is a set of linearly independent vectors, such that any vector λ in V space can be written as the linear combination of these basis vectors. There may be more than one basis for a vector space. However, all of them have the same number of vectors, and this number is known as the dimension of the vector space. For example in the five-dimensional space, any vector λ in the vector space V can be written as [63]:

$$\lambda = \sum_{k=1}^5 c_{\lambda}^k b_k \quad (3.6)$$

where c_{λ}^k are corresponding coefficients and b_k are basis vectors of the vector space V . This concept, given in terms of vectors, can easily be generalized to functions by replacing the basis vectors b_k with the basis functions $\phi_k(t)$, and the vector λ with the function $f(t)$. These basis functions may be polynomials or any other type of functions. In case of the Fourier transform these basis functions are the complex exponentials. The expression of any function $f(t)$ in the space vector V using the basis functions can be stated as [63]:

$$f(t) = \sum_k c_f^k \phi_k(t) \quad (3.7)$$

The scaling function (if it exists) of the mother wavelet should have the capability of generating polynomials of degree p such that $p \leq m$. Here m is the number of vanishing moments of the wavelet function. The level of resolutions refers to translations of the mother wavelet frequency bands. Such translations will produce another wavelet, which is the shifted scaled copy of the mother wavelet in the previous level of resolution. The new generated wavelet is known as the "Daughter Wavelet". At each level, where a daughter wavelet can be generated, the scaling function related to the mother wavelet generates the basis functions in that level. This property is given as [64]:

$$\phi_{j,k}(t) = 2^{-j/2} \phi(2^j t - k); j, k \in Z \quad (3.8)$$

where j is the number of levels of resolution and k is the dimension of the function space at level j . The relation between the generated wavelet at level j , and the mother wavelet is given as [64]:

$$\psi_{j,k}(t) = 2^{-j/2} \psi(2^{-j}t - k); j, k \in Z \quad (3.9)$$

Wavelets can be classified into two main types: orthogonal and non-orthogonal. The following subsections give brief explanation of main properties of each type.

3.1.1 Orthogonal Wavelets

A mother wavelet with the scaling function, which is capable of generating the orthogonal basis function at the each level of resolution, is termed as the orthogonal wavelet. In orthogonal wavelets, the wavelet functions are orthogonal to the basis functions. These basis functions are created through translations and dilations or expansions of the mother wavelet in time and frequency domains, respectively. There have been several orthogonal wavelets families including the *Daubechies family* ('dbN'), *Coiflets family* ('coifN'), *Symlets family* ('symN'), *Meyer family* ('meyr') and the *biorthogonal spline* ('biorN.M') family [65]. Here N and M denotes the order of a wavelet family in the decomposition and reconstruction of a discrete signal, respectively. The orthogonal wavelets have to meet the orthogonality or orthonormality condition, which is given as [61]:

$$\int_{-\infty}^{\infty} \psi_{m,n}(t) \psi_{m',n'}(t) dt = 1 \quad \text{if } m = m' \text{ and } n = n' \quad (3.10)$$

$$= 0 \quad \text{otherwise}$$

such that the product of the each wavelet function with others (i.e. those who are translated and/or dilated versions of each other) in the same dyadic system are zero. This means that the information stored in a wavelet-transformed coefficient $T_{m,n}$ is not repeated elsewhere and allows for the complete regeneration of the original signal without redundancy [61].

The most common properties of orthogonal wavelets are given as [65]:

1. Compact support width.
2. Highest number of vanishing moments for a given support width.
3. Perfect reconstruction and symmetry.
4. FIR approximations of the wavelet and scaling filters.
5. Fast algorithm exists for the computation of each coefficient of the wavelet transforms.

The *Daubechies* family of the orthogonal wavelets has been extensively used in image processing, denoising and reconstruction of a blurred signal, detection and classification of disturbances in power systems and rotating machineries, and many other applications. The phase response of the *Daubechies* wavelets and their scaling filters are non linear and they have problems at the edges of signals (the start and end points of signals). These problems are tried to overcome in references [66-67] by the zero padding, wrap-around or reflection. However, all of these options impose a particular choice, which degraded the wavelet decomposition at the edges of the signal. Figure 3.1 shows the *Daubechies* ('*db3*') wavelet and its scaling function. The *Coiflet* ('*coif1*') wavelet and its scaling function are shown in Fig. 3.2.

In certain applications it is necessary to have the real and symmetric wavelets. One way to get the symmetric wavelets is to construct two sets of biorthogonal wavelets: the wavelet function $\psi_{m,n}$ and its dual $\hat{\psi}_{m',n'}$. One set is used to decompose the signal and the other one is used for reconstruction. Biorthogonal wavelets satisfy the biorthogonality condition as:

$$\int_{-\infty}^{\infty} \psi_{m,n}(t) \hat{\psi}_{m',n'}(t) dt = 1 \quad \text{if } m = m' \text{ and } n = n' \quad (3.11)$$

$$= 0 \quad \text{otherwise}$$

Using biorthogonal wavelets allows one to have perfectly symmetric and antisymmetric wavelets. Further, they allow certain desirable properties to be incorporated separately within the decomposition wavelet and the reconstruction wavelet. The wavelet function

$\psi_{m,n}(t)$ and its dual $\hat{\psi}_{m,n}(t)$ can have different number of vanishing moments. If $\psi_{m,n}(t)$ has more vanishing moments than $\hat{\psi}_{m,n}(t)$, then decomposition using the wavelet function $\psi_{m,n}(t)$ suppresses higher order polynomials and aids data compression. Reconstruction with the dual wavelet $\hat{\psi}_{m,n}(t)$ with fewer vanishing moments leads to a smoother reconstruction [61]. Figure 3.3 shows the *spline biorthogonal* ('bior2.6') wavelet and its scaling function.

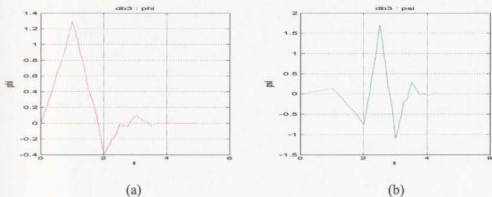


Figure 3.1: The *Daubechies* ('db3') wavelet: (a) the scaling function, (b) the wavelet function.

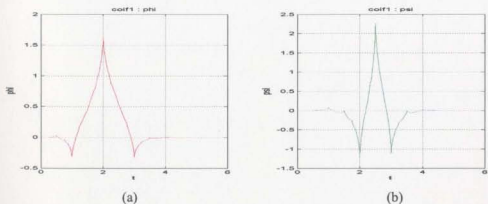


Figure 3.2: The *Coiflet* ('coif1') wavelet: (a) the scaling function, (b) the wavelet function.

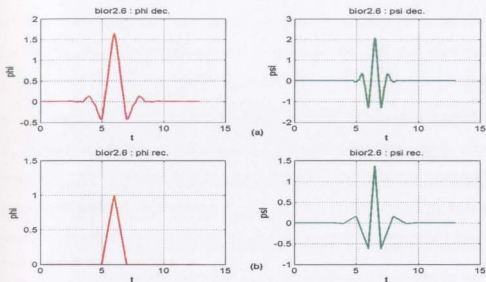


Figure 3.3: The *Spline biorthogonal* ('*bior2.6*') wavelet: (a) the wavelet and its scaling function for the decomposition, (b) the wavelet and its scaling function for the reconstruction.

3.1.2 Non-orthogonal Wavelets

The non-orthogonal wavelets are defined as mother wavelets that do not have scaling functions or have scaling functions, which do not generate polynomial basis functions [63]. There have been several examples of non-orthogonal wavelets including the *Morlet* ('*morl*') wavelet, *Mexican Hat* ('*mexihat*') wavelet, *Gaussian* ('*Gaus*') wavelets, *complex Gaussian* wavelets, *complex Morlet* wavelet, *complex Shannon* wavelets, *complex frequency B-spline* wavelets [65]. The main properties of non-orthogonal wavelets are [65]: (i) the mother wavelet $\psi(t)$ and its bases are not compactly supported, (ii) perfect reconstruction is not assured, (iii) some mother wavelets do not have scaling functions $\phi(t)$ and consequently, the non-orthogonal analysis is carried out using the wavelet bases. Figures 3.4-3.5 show the non-orthogonal wavelet ('*Morlet*' and '*Mexican Hat*') functions.

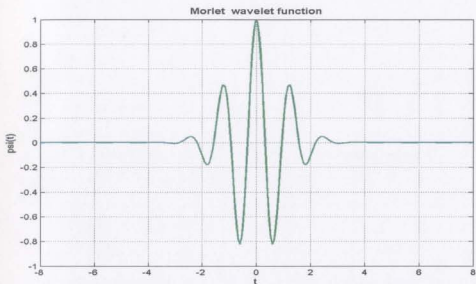


Figure 3.4: The non-orthogonal *Morlet* ('*morl*') wavelet function (does not have scale function).

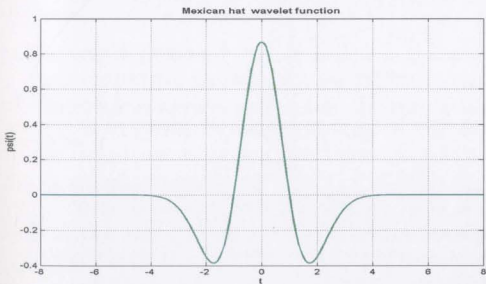


Figure 3.5: The non-orthogonal *Mexican Hat* ('*mexh*') wavelet function (does not have scale function).

3.2 Wavelet Transforms

The wavelet transform analysis uses little wavelike functions known as the wavelets. Actually, local wavelike function is the more accurate description of a wavelet. Figures 3.1-3.5 show a few examples of the wavelets and their scaling functions (if they exist). Wavelets are used to transform the signal under investigation into another representation, which presents the signal information in a more useful form. This transformation of the signal is known as the *wavelet transform*. Mathematically speaking, the wavelet transform is a convolution of the wavelet function with the signal. The wavelet can be manipulated in two ways: it can be moved to various locations on the signal and it can be stretched or squeezed. If the wavelet matches the shape of the signal well at a specific scale and location, then a large transform value is obtained. If, however, the wavelet and the signal do not correlate well, a low value of the transform is obtained [61]. The wavelet transform like any other transform can be applied to both continuous and discrete signals. In the following subsections, the different forms of wavelet transforms along with their mathematical forms are briefly presented.

3.2.1 Continuous Wavelet transform

The wavelet transform of a continuous signal $x(t)$ with respect to the wavelet function $\psi(t)$ is defined as [61]:

$$T(a,b) = w(a) \int_{-\infty}^{\infty} x(t) \psi^* \left(\frac{t-b}{a} \right) dt \quad (3.12)$$

where $w(a)$ is the weighting function, a and b are the dilation and translation parameters, respectively. The asterisk indicates that the complex conjugate of the wavelet function is used in the transformation. The wavelet transform can be thought as of the cross-correlation of a signal with a set of wavelets of various widths. Typically, $w(a)$ is set to $1/\sqrt{a}$ for the reasons of energy conservation i.e. it ensures that the wavelets at every scale have the same energy. If one sets $w(a)=1/\sqrt{a}$, then the wavelet transform of a continuous signal $x(t)$ can be written as:

$$T(a, b) = \frac{1}{\sqrt{a}} \int_{-\infty}^{\infty} x(t) \psi^* \left(\frac{t-b}{a} \right) dt \quad (3.13)$$

The equation (3.13) is known as the continuous wavelet transform (CWT) of the signal $x(t)$. It contains both the dilated and translated wavelet $\psi((t-b)/a)$ and the continuous signal $x(t)$, where $x(t)$ could be a beating heart, an audio signal, gearbox vibration, a financial index or perhaps even a spatial signal such as a crack profile or land surface heights, signal range. In mathematical terms this is called a convolution [61]. The normalized wavelet function is often written more compactly as:

$$\psi_{a,b}(t) = \frac{1}{\sqrt{a}} \psi \left(\frac{t-b}{a} \right) \quad (3.14)$$

where the normalization is in the sense of wavelet energy. Hence, the transform integral may be written as

$$T(a, b) = \int_{-\infty}^{\infty} x(t) \psi_{a,b}^*(t) dt \quad (3.15)$$

One can express the wavelet transform in even more compact form as an inner product:

$$T(a, b) = \langle x, \psi_{a,b} \rangle \quad (3.16)$$

The dilation and contraction of the mother wavelet is governed by the dilation parameter a that is the distance between the center of the wavelet function and its crossing in the time axis. The movement of the wavelet along the time axis is governed by the translation parameter b . Figure 3.6 shows the Mexican Hat wavelet stretched and squeezed to respectively double and half of its original width on the time axis. The movement of the Mexican Hat wavelet function along the time axis from b_1 via b_2 to b_3 is shown in Fig. 3.7.

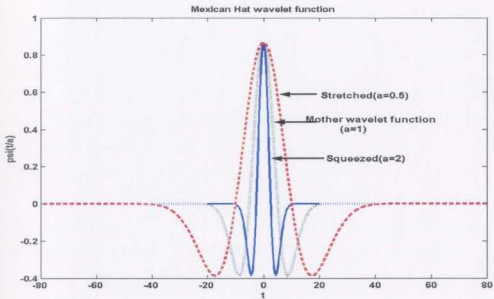


Figure 3.6: Stretching and squeezing the Mexican Hat wavelet (dilation).

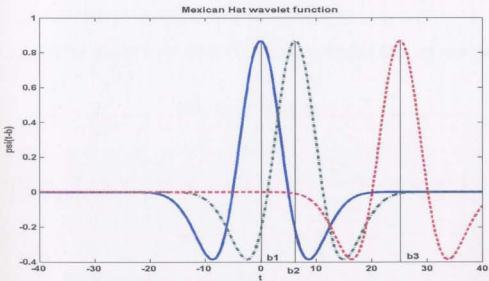


Figure 3.7: Moving the Mexican Hat wavelet (translation).

3.2.2 Discrete Wavelet transform

The continuous wavelet transform (CWT) is carried out by the dilation and translation of the mother wavelet continuously over a real continuous number system (\mathfrak{R}). As a result, it generates substantial redundant information. Therefore, instead of continuous dilation and translation, the mother wavelet can be dilated and translated discretely by selecting $a = a_0^m$ and $b = nb_0a_0^m$, where a_0 and b_0 are fixed constants with $a_0 > 1$, $b_0 > 0$, $m, n \in \mathbb{N}$, and \mathbb{N} is the set of positive integers. Then, the discretized mother wavelet becomes [71],

$$\psi_{m,n}(t) = a_0^{-m/2} \psi\left(\frac{t - nb_0a_0^m}{a_0^m}\right) \quad (3.17)$$

and the corresponding discrete wavelet transform is given by

$$DWT_{\psi} x(m, n) = \int_{-\infty}^{\infty} x(t) \psi_{m,n}^*(t) dt \quad (3.18)$$

By careful selection of a_0 and b_0 , the family of dilated mother wavelets constitute an orthonormal basis of $L^2(\mathfrak{R})$. An orthonormal basis is a basis that consists of a set of vectors S such that $u \cdot u = 1$ for all u in S . The simplest choice of a_0 and b_0 are $a_0 = 2$ and $b_0 = 1$. With this, the wavelet transform is called a dyadic-orthonormal wavelet transform. There are several implications of the orthonormal basis. The first is that there will be no information redundancy among the decomposed signals due to the orthonormal properties. The second is that with this choice of a_0 and b_0 there exists an elegant algorithm, which is known as the multiresolution signal decomposition technique, to decompose a signal into scales with different time and frequency resolution [69]. The multiresolution analysis is illustrated later in this chapter.

The resolution of the signal, which is a measure of the amount of detail information in the signal, is changed by the filtering operations, and the scale is changed by down sampling operations. The procedure starts with passing the signal $x[n]$ of length N through a half band digital low pass filter with impulse response $g[n]$ and a half band

digital high pass filter with impulse response $h[n]$. The low-pass and high-pass filters are also called scaling and wavelet filters, respectively. The output of these filters consists of N wavelet coefficients. The outputs from the low-pass filter are the approximation coefficients $a_n^1 = [a_0^1 a_1^1 a_2^1 \dots a_{N-1}^1]$ at the first level of resolution. The outputs from the high-pass filter are the detail coefficients $d_n^1 = [d_0^1 d_1^1 d_2^1 \dots d_{N-1}^1]$ at the first level of resolution. This constitutes first level of decomposition, and can mathematically be expressed as:

$$a_n^1 = \sum_{k=0}^{N-1} g[k]x[n-k] \quad (3.19)$$

$$d_n^1 = \sum_{k=0}^{N-1} h[k]x[n-k] \quad (3.20)$$

The approximation coefficients at the first level of resolution are used as inputs for another pair of wavelet filters (identical with the first pair), generating sets of approximations $a_n^2 = [a_0^2 a_1^2 a_2^2 \dots a_{N/2-1}^2]$ and details $d_n^2 = [d_0^2 d_1^2 d_2^2 \dots d_{N/2-1}^2]$ coefficients of length $N/2$ at the second level of resolution [52]. This constitutes second level of decomposition, and can mathematically be expressed as:

$$a_n^2 = \sum_{k=0}^{N/2-1} g[k]a_n^1[2n-k] \quad (3.21)$$

$$d_n^2 = \sum_{k=0}^{N/2-1} h[k]a_n^1[2n-k] \quad (3.22)$$

If the main information lies in high frequency components, then the time localization of these high frequencies will be very precise, since they are characterized by large number of samples. However, if the information lies at low frequency components, the time localization will be very poor, since small numbers of samples are used to express the signal at these frequencies [63]. The decomposition tree of the discrete wavelet transform (DWT) is shown in Fig. 3.8, which uses the half band high pass filters H and the half band low pass filters G in the decomposition process.

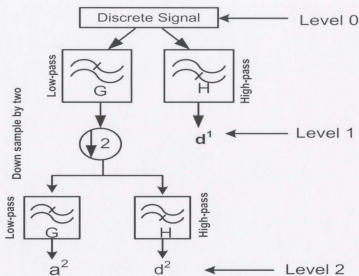


Figure 3.8: The two-level decomposition of a discrete signal by the discrete wavelet transform (DWT)

3.2.3 Wavelet Packet transform

Whereas the discrete wavelet transform (DWT) provides one with more flexible time-frequency resolution properties as described, one possible drawback is that the frequency resolution is rather poor in the high-frequency region. Therefore, it faces some difficulties for discrimination between signals having close high-frequency components. *Wavelet packets*, a generalization of the wavelet bases, are alternative bases that are formed by taking linear combinations of usual wavelet functions. These bases inherit properties such as the orthonormality and time-frequency localization from their corresponding wavelet functions. A wavelet packet function is a function with three indices: j , k and n , and is given as [43]:

$$W_{j,k}^n(t) = 2^{j/2} W^n(2^j t - k) \quad (3.23)$$

As with usual wavelets, integers j and k are the index of scale and translation operations, respectively. The index n is called the modulation parameter or oscillation parameter. The first two-wavelet packet functions are the usual scaling function and mother wavelet function, respectively

$$W_{0,0}^0(t) = \phi(t) \quad (3.24)$$

$$W_{0,0}^1(t) = \psi(t) \quad (3.25)$$

Wavelet packet functions for $n=2,3,\dots$ are then defined by the following recursive relationships [43]:

$$W_{0,0}^{2n}(t) = \sqrt{2} \sum_k h(k) W_{1,k}^n(2t - k) \quad (3.26)$$

$$W_{0,0}^{2n+1}(t) = \sqrt{2} \sum_k g(k) W_{1,k}^n(2t - k) \quad (3.27)$$

where $h(k)$ and $g(k)$ are the quadrature mirror filters (QMF) associated with the predefined scaling function and mother wavelet function. To measure specific time-frequency information in a signal, one simply takes the inner product of the signal and that particular basis function. The wavelet packet coefficients of a function are computed as:

$$w_{j,n,k} = \langle f, W_{j,k}^n \rangle = \int f(t) W_{j,k}^n(t) dt \quad (3.28)$$

Computing the full wavelet packet decomposition (WPD) of a discrete-time signal involves applying both filters to the discrete-time signal $[x_1, x_2, x_3, \dots, x_n]$ and then recursively to each intermediate signal. The procedure is illustrated in Fig. 3.9 up to the second level of resolution.

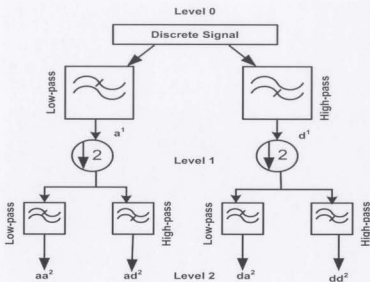


Figure 3.9: The two-level decomposition of a discrete signal by the wavelet packet transform (WPT)

The first level of decomposition of the discrete signal $x[n]$ of length N in the wavelet packet transform (WPT) generates two frequency sub-bands including the approximation coefficients $a_n^1 = [a_0^1 a_1^1 a_2^1 \dots a_{N-1}^1]$ and detail coefficients $d_n^1 = [d_0^1 d_1^1 d_2^1 \dots d_{N-1}^1]$. The second level of decomposition generates four-frequency sub-bands using same set of filters of the first level of resolution. These four sub-bands are $aa^2[N/2]$, $ad^2[N/2]$, $da^2[N/2]$ and $dd^2[N/2]$. The second level low and high frequency details and approximations can be mathematically expressed as:

$$\text{Low frequency approximations: } aa_n^2 = \sum_{k=0}^{N/2-1} g[k] a_n^1 [2n - k] \quad (3.29)$$

$$\text{Low frequency details: } ad_n^2 = \sum_{k=0}^{N/2-1} h[k] a_n^1 [2n - k] \quad (3.30)$$

$$\text{High frequency approximations: } da_n^2 = \sum_{k=0}^{N/2-1} g[k] d_n^1 [2n - k] \quad (3.31)$$

High frequency details:
$$dd_n^2 = \sum_{k=0}^{N/2-1} h[k]d_n^1[2n-k] \quad (3.32)$$

3.3 Multiresolution Analysis

The multiresolution analysis (MRA) is a tool that utilizes the discrete wavelet transform (DWT) to represent a time-varying signal in terms of its frequency components. It essentially maps a one-dimensional (1D) signal of time into a two-dimensional (2D) signal of time and frequency. The goal of MRA is to develop representations of a complicated signal $f(t)$ in terms of its orthonormal basis, which are the scaling and wavelet functions. These functions can be scaled and translated for decomposing and representing the signal $f(t)$ at different resolutions. This can be mathematically presented as [70]

$$f(t) = \sum_k c_0(k)\varphi(t-k) + \sum_k \sum_{j=0}^{J-1} d_j(k)2^{j/2}\psi(2^j t - k) \quad (3.33)$$

Using MRA, the time domain signal $f(t)$ can be mapped into the wavelet domain, and represented at different resolution levels in terms of following expansion coefficients

C_{signal}

$$C_{signal} = [c_0|d_0|d_1|\dots\dots\dots d_{J-1}] \quad (3.34)$$

where d_j presents the detail coefficients at different resolution levels, and c_0 presents the last approximate coefficients. The effective implementation of the multiresolution analysis has four requirements, which are given as [61,63]:

- The multiresolution analysis involves a decomposition of the function space into a sequence of subspaces, and each subspace must be contained in the higher subspaces. This requirement implies that a new level of resolution can be created by dilating the mother wavelet without any loss of information in the decomposed signal, and also to ensure orthogonality of basis functions at all levels of resolution.

- As the resolution gets coarser and coarser, more and more details are removed in such a way that as $j \rightarrow \infty$, only a constant frequency component remains.
- All the spaces V_j are scaled versions of the central version V_0 , i.e. if $x(t)$ does not contain any fluctuations (transient components) at scales smaller than $1/2^j$, then $x(2t)$ will not contain any fluctuations at scales smaller than $1/2^{j+1}$.
- If the signal $x(t) \in V_0$ and does its entire integer shifts $x(t-m)$, then all the subspaces V_j are shift invariance.

In case of the continuous wavelet transform, the MRA is carried out by the translation and correlation of the mother wavelet with the signal at different scales. In the discrete wavelet transform (DWT), the MRA is performed by passing the discrete signal through low pass and high pass filters. Down sampling is performed on the low pass filter outputs in order to get the better frequency resolution at each levels of resolution j . The MRA is implemented in the wavelet packet transform (WPT) in the same way as the discrete wavelet transform except the down sampling is performed here on both the low pass and high pass filters' outputs.

3.3.1 Quadrature Mirror Filter Banks

One of the simplest methods to construct the MRA is the implementation of quadrature mirror filter (QMF) banks in wavelet transforms. A selected wavelet function is used to generate the needed QMF coefficients. In general, QMF banks have stages of filters, where each stage has low pass filters (G) as well as high pass filters (H). The coefficients of G and H are not independent from each other; rather they are related by the following relation as:

$$h_k = (-1)^k g_{L-k}; k = 0, 1, 2, \dots, L-1 \quad (3.35)$$

here $\{h_k\}_{k=0,1,2,\dots,L-1}$ represents a high pass filtering function and $\{g_k\}_{k=0,1,2,\dots,L-1}$ represents a low pass filtering function. Any filter bank that satisfies the relation in equation (3.35) is known as the quadrature mirror filter (QMF) bank [40].

The QMF banks have specified minimum stop band attenuation of the composite magnitude-frequency response. In other words, they have the minimum stop band attenuation for the individual filters in QMF banks. The QMF banks have real coefficients in addition to the almost linear phase even with the asymmetric mother wavelet function [71]. They also allow the perfect reconstruction of a signal, because of the elimination of the non-ideal transition and stop band filtering in the filter banks. Again, each filter in the QMF banks is described using a minimal set of parameters, which are directly related to the zeros of the filter. This eliminates the addition of any pre-assigned set of zeros in the stop band in constructing the filter banks [68,71].

3.4 Selection of the Mother Wavelet

Choosing a wavelet function that optimally fits the signal depends on the application and the signal itself. There are several factors that should be considered in choosing the optimal wavelet function. The first two are the ability to reconstruct the signal from the wavelet decomposition and to preserve the energy of the signal under the transformation. Another factor is symmetry, which is important in avoiding the drift of the information. The length of the wavelet filter depends on the regularity of the signal to be decomposed. The higher the length of the wavelet filters the longer the calculation time of the process and decreases in the accuracy of the localization [72].

In the area of fault detection applications, selection of the mother wavelet is essential to enhance the performance of the detection technique in extracting the useful information rapidly. In order to detect the high impedance transmission line faults in the example of reference [73], two conditions are compared for the selection of optimal mother wavelet: 1) the significant magnitude of the detail coefficients of fault currents at the first level of resolution; 2) the classification ability between the faulted and healthy phases.

For a given signal, the optimum wavelet maximizes the coefficient values within the time-scale domain. In other words, the optimum wavelet should be capable of generating the highest local maxima of the signal of interest in the wavelet pattern. Also,

the optimum wavelet must best characterize the frequency content of transient signals along the levels. The optimum wavelet maximizes the cross correlation between the signal of interest and the wavelet i.e. it maximizes the value of $\gamma(X,Y)$ in equation (3.36) given as [74-75]:

$$\gamma = \frac{\sum (X - \bar{X})(Y - \bar{Y})}{\sqrt{\sum (X - \bar{X})^2 \sum (Y - \bar{Y})^2}} \quad (3.36)$$

where X represents the input data set and Y represents the wavelet data set. \bar{X} and \bar{Y} are the mean values of data sets X and Y , respectively. Thus, the optimal wavelet is the one that maximizes γ . A particular setup for the problem of selecting the mother wavelet can be defined as the selection of orthonormal discrete basis function with compact support, which helps in implementing the wavelet transform using the digital computers. Such compactness provides means of isolation and detection of signals at certain region, which has proved useful in many applications of signal processing [63,71].

3.4.1 Best-basis Selection

For choosing the optimal decomposition based on organization of the wavelet packet library, it is essential to count the decompositions issued from a given orthogonal wavelet. A signal of length $N = 2L$ can be expanded in α different ways, where α is the number of binary sub trees of a complete binary tree of depth L . As a result, the number of possible decompositions can be expressed as [76]:

$$\alpha \geq 2^{N/2} \quad (3.37)$$

As this number may be very large, and since explicit enumeration is generally unmanageable, it is interesting to find an optimal decomposition with respect to a convenient criterion, computable by an efficient algorithm. Functions verifying an additive type property are well suited for efficient searching of binary-tree structures and the fundamental splitting. Classical entropy-based criteria match these conditions and describe information- related properties for an accurate representation of a given signal [56]. Entropy is a common concept in many fields, mainly in signal processing. Many

types of entropy criterion are available. Here four different types of entropy criterion are listed. In the following expressions s is the signal and s_i are the coefficients of s in an orthonormal basis. The entropy E must be an additive cost function such that $E(0)=0$ and

$$E(s) = \sum_i E(s_i) \quad (3.38)$$

- The non-normalized Shannon entropy [56]

$$E1(s_i) = -s_i^2 \log(s_i^2) \quad (3.39)$$

so, by equation (3.38)
$$E1(s) = \sum_i -s_i^2 \log(s_i^2) \quad (3.40)$$

- The concentration in L_p norm with $p \geq 1$ [56]

$$E2(s_i) = |s_i|^p \quad (3.41)$$

so, by equation (3.38)
$$E2(s) = \sum_i |s_i|^p \quad (3.42)$$

- The logarithm of the "energy" entropy [56]

$$E3(s_i) = \log(s_i^2) \quad (3.43)$$

so, by equation (3.38),
$$E3(s) = \sum_i \log(s_i^2) \quad (3.44)$$

- The threshold entropy [56]

$$\begin{aligned} E4(s_i) &= 1 \text{ if } |s_i| > \epsilon; \quad \epsilon = \text{threshold} \\ &= 0 \quad \text{elsewhere} \end{aligned} \quad (3.45)$$

To determine the optimal number of levels of resolution, the entropy is evaluated at each level, where there is a new level j such that [52]

$$H(x)_j \geq H(x)_{j-1} \quad (3.46)$$

then level j is redundant and can be omitted. Here, $H(x)_j$ is the entropy of the signal $x[n]$ at level j . If the equation (3.46) satisfies for the signal $x[n]$, then the decomposition up to the level $j-1$ is sufficient to represent the signal $x[n]$.

3.4.2 Minimum Description Length (MDL) Criterion

The minimum description length (MDL) data criterion is an important approach for the simultaneous noise suppression and signal compression. It is free from any parameter setting such as the threshold selection, which can be particularly useful for the real data where the noise level is very difficult to estimate. The MDL selects the best wavelet filter and the best number of wavelet coefficients to be retained for the signal reconstruction. The MDL principle suggests that the best model among the given collection of models is the one giving the shortest description of the data and the model itself. For each model in the collection, the length of the description of the data is counted as the code length of encoding the data using that model in binary digits (bits). The length of description of a model is the code length of specifying that model, e.g., the number of parameters and their values, if it is a parametric model [76].

The MDL criterion has the following algorithm. A discrete model is given as $f = x + n1$; where, the vector f represents the noisy observed data, vector x is the unknown true signal to be estimated, and vector $n1$ is the noise. The MDL function of the indexes k (number of coefficients to be retained) and n (number of wavelet filters) is defined as [52]:

$$MDL(k, n) = \min \left\{ \frac{3}{2} k \log N + \frac{N}{2} \log \|\tilde{\alpha}_n - \alpha_n^{(k)}\|^2 \right\} \quad (3.47)$$

$$0 \leq k < 1; 1 \leq n \leq M$$

where $\tilde{\alpha}_n = W_n f$ denotes the vector of the decomposition coefficients of the noisy observed data vector f via the wavelet filter vectors n , and $\alpha_n^{(k)} = \Theta^k \tilde{\alpha}_n = \Theta^k (W_n f)$ denotes the vector that contains k nonzero elements, and $\Theta^{(k)}$ is a hard-thresholding operation, which keeps the k largest elements of $\tilde{\alpha}_n$ in absolute value intact and set all other elements to zero. The integers N and M denote the length of the signal and the total number of wavelet filters, respectively. The vectors $\tilde{\alpha}_n$ and $\alpha_n^{(k)}$ are normalized by $\|\tilde{\alpha}_n\|$, so that the magnitude of each coefficient in $\tilde{\alpha}_n$ and $\alpha_n^{(k)}$ is strictly less than one. The MDL function is expressed as the sum of two conflicting terms. The

first term of the equation (3.47) represents the penalty function, which is linearly increasing with the number of the retained wavelet coefficients k , whereas the second term of the equation (3.47) describes the logarithmic of residual energy between the vectors $\tilde{\alpha}_n$ and $\alpha_n^{(k)}$. Number of coefficients k , for which the MDL function reaches its minimum value, is considered as the optimal one. With this criterion, the wavelet filters can also be optimized as well. It should be noted that each wavelet filter has different characteristics. A wavelet filter, which is optimal for a given signal, is not necessarily the best for another type of signal [52].

The next chapter describes the off-line testing of the proposed wavelet packet transform based algorithm for the protection of disturbances in the three-phase interior permanent magnet motors. Shannon entropy and minimum description data length (MDL) criterion are used to determine the optimal mother wavelet and the optimal number of levels of decomposition in the implementation of the proposed algorithm. The algorithm is tested off-line using the real data from the three-phase interior permanent magnet motors acquired through the A/D converter of the DS1102 digital signal processor board.

Chapter 4

Data Acquisition and the Mother Wavelet

This chapter provides an overview of the experimental setup for the data acquisition under different faulted conditions to test the proposed wavelet packet transform based algorithm on three-phase interior permanent magnet motors. The collected data are used for the off-line testing of the proposed algorithm in the MATLAB environment using the selected mother wavelet and number of levels of resolution. The minimum description length data criterion [52], which has been described in the previous chapter, is used here for selecting the optimal mother wavelet from the set of orthogonal or nonorthogonal mother wavelets. After the selection of the mother wavelet, the optimal number of levels of resolution is determined by the Shannon non-normalized entropy based criterion [52]. The digital data are acquired through the three-channel A/D converter of the DS1102 digital signal processor board. The actual fault currents data are taken for the accurate selection of the mother wavelet and number of levels of resolution.

The experimental setup for the data acquisition through the DS1102 digital signal processor board is explained at the beginning of the chapter. Then, the procedure for calculating MDL indexes of different faulted and normal unfaulted currents is presented in order to select the optimal mother wavelet. The entropy values of each subspace of the

wavelet packet tree of normal and fault currents are compared in order to determine the optimum number of levels of resolution. Finally, the off-line test results of the proposed algorithm on three-phase interior permanent magnet motors using the selected mother wavelet and number of levels of resolution are provided.

4.1 Experimental setup for acquiring the Normal and Fault currents Data

One of the important and major tasks of this work is to setup the protected motor in order to acquire different faulted and normal unfaulted currents with all the necessary instrumentation. In this work, the collected data are to be employed for selecting the mother wavelet and for the off-line testing of the proposed algorithm. A 208 V (line-to-line), 3 A, Y-connected, 1hp laboratory prototype three-phase interior permanent magnet motor and a 220 V (line-to-line), 11.5 A, Δ -connected, 5hp laboratory prototype three-phase interior permanent magnet motor are to be protected. The data are collected from both types of interior permanent magnet motors. The experimental setup for the data acquisition is shown in Fig. 4.1. Three current transformers (CTs) are connected with stator winding terminals of the motor in order to acquire different faulted and normal unfaulted stator currents. Suitable multiplying factors are applied to get actual stator currents of the motor. The rated currents and voltages of these three CTs are 200/5 A (rms) and 15 V (max.), respectively. Therefore, faults currents of high magnitudes are transformed to a suitable level without any saturation in data acquisition instruments.

There have been many types of faults that an interior permanent magnet motor may experience. The majority of these faults are stator faults [46] such as turn-to-turn fault (later appears as the phase-to-phase or phase-to-ground faults), loss of a phase fault and rotor faults [25] including the static eccentricity, dynamic eccentricity, and flux disturbances originating from defects in buried permanent magnets and their imperfect orientations.

The faults that have been considered during the data acquisition include:

- Loss of supply (single phasing) fault.
- Line to ground (L-G) fault.
- Line-to-line (L-L) fault.

The data acquisition instrument consists of the DS1102 DSP controller board that contains a TMS320C31 floating-point digital signal processor. It is a standard PC/AT card that is plugged into the PC using the ISA bus as a backplane. The digital data are acquired through the on-board three-channel analog-to-digital (A/D) converters of the controller board. For this purpose, a program is written in the turbo C language, which used a set of initialization and input/output (I/O) functions for initializing the TMS320C31's on-chip timers and for accessing the DS1102's on board analog-to-digital (A/D) and digital-to-analog (D/A) converters. The data are collected at the sampling rate of 8 kHz, and stored in the personal computer (PC) through the dSPACE TRACE module. Then, these are converted to the ASCII format for further processing.

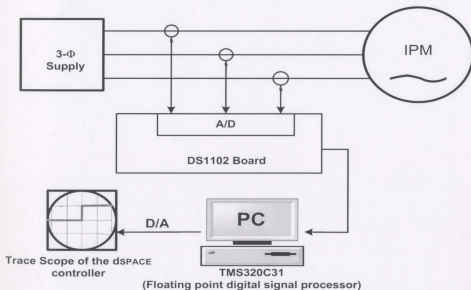


Figure 4.1: Experimental setup for the data acquisition.

In all the cases of acquiring fault currents data, the duration of the fault was insured to be less than 10 cycles to prevent the damage to the motor or other instruments. A relay switch, which is activated by the 555-timer circuit, is used for initiating a fault in the motor. The 555-timer circuit diagram is shown in figure 4.2.

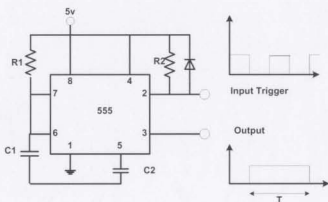


Figure 4.2: The 555-timer circuit connection ($R1=100\text{ k}\Omega$, $C1=1\text{ }\mu\text{F}$, $R2=10\text{ k}\Omega$, $C2=0.01\text{ }\mu\text{F}$, and $T=1.1R1C1=0.1\text{ sec}$)

4.2 Selection of Mother Wavelet and Number of Levels of Resolution

In this section, the collected data are used for selecting the mother wavelet and number of levels of resolution. The MDL criterion described in chapter 3 is applied here on the collected data, initially to select the mother wavelet. Once the mother wavelet is selected, the Shannon non-normalized criterion is applied to determine the optimal number of levels of resolution using the selected mother wavelet.

4.2.1 Selecting Mother Wavelet

The MDL function of equation (3.47) for selecting the optimal mother wavelet is a function of two variables: (a) number of coefficients that have to be retained for perfect reconstruction; k (b) number of wavelet filters; n . The minimum value of the MDL function using a wavelet filter determines the number of coefficients that have to be retained. There have been many known wavelets including the orthogonal wavelets (Daubechies family, Coiflet family, Meyer and Symlet family), biorthogonal wavelets (the biorthogonal spline wavelet family), and the nonorthogonal wavelets (Morlet, Gaussian, and Mexican Hat). In this work, the available orthogonal or nonorthogonal wavelets of the MATLAB wavelet toolbox are tested by the MDL criterion for the optimal mother wavelet selection. The candidate mother wavelets for this work are:

a) Orthogonal Wavelet Families

1. Daubechies (*db3*, *db4*)
2. Coiflet (*coif3*)
3. Symlet (*sym3*)
4. B-spline(*bior3.5*)
5. Meyer (*dmey*)

b) Nonorthogonal Wavelet Families

1. Mexican Hat (*mexh*)
2. Gaussian (*gaus8*)

The MDL is applied for each candidate mother wavelet on four types of collected data, which are the normal unloaded current, loss of supply (single phasing) fault current, line-to-line fault current, and normal full load current. The collected discrete data are decomposed up to the second level of resolution by each candidate mother wavelet.

Table 4.1(a) shows the evaluations of the MDL index for the normal unloaded current of the 1hp interior permanent magnet motor by each candidate mother wavelet.

Table 4.1(b) shows the evaluations of the MDL index for the line-to-line fault current of the 1hp interior permanent magnet motor by each candidate mother wavelet.

Table 4.2(a) shows the evaluations of the MDL index for the normal full load current of the 5hp interior permanent magnet motor by each candidate mother wavelet.

Table 4.2(b) shows the evaluations of the MDL index for the line-to-line fault current of the 5hp interior permanent magnet motor by the each candidate mother wavelet.

Mother Wavelet	MDL(1)	MDL(2)
<i>db3</i>	550	580
<i>db4</i>	725	650
<i>coif3</i>	585	890
<i>sym3</i>	557	950
<i>bior3.5</i>	665	820
<i>dmey</i>	375	350
<i>mexh</i>	850	800
<i>gaus8</i>	1100	590

(a)

Mother Wavelet	MDL(1)	MDL(2)
<i>db3</i>	450	550
<i>db4</i>	480	950
<i>coif3</i>	405	900
<i>sym3</i>	440	552
<i>bior3.5</i>	470	540
<i>dmey</i>	348	548
<i>mexh</i>	920	920
<i>gaus8</i>	975	560

(b)

Table 4.1: The two level MDL index evaluations of the phase-a stator current of the 1hp interior permanent magnet motor: (a) normal unfaulted condition, (b) line-to-line (L-L) fault.

Mother Wavelet	MDL(1)	MDL(2)
<i>db3</i>	630	800
<i>db4</i>	700	1200
<i>coif3</i>	515	1100
<i>sym3</i>	640	800
<i>bior3.5</i>	660	1000
<i>dmey</i>	400	700
<i>mexh</i>	1422	1422
<i>gaus8</i>	1500	1010

(a)

Mother Wavelet	MDL(1)	MDL(2)
<i>db3</i>	550	590
<i>db4</i>	750	1200
<i>coif3</i>	375	1000
<i>sym3</i>	550	590
<i>bior3.5</i>	752	900
<i>dmey</i>	320	600
<i>mexh</i>	600	600
<i>gaus8</i>	620	598

(b)

Table 4.2: The two level MDL index evaluations of the phase-a stator current of the 5hp interior permanent magnet motor: (a) normal unfaulted condition, (b) line-to-line (L-L) fault.

The evaluation of the MDL indices shows that the discrete Meyer wavelet [65] has the smallest MDL indices among all the candidate mother wavelets in both levels of resolution. The discrete Meyer wavelet is the FIR based approximations of the Meyer wavelet, which is an infinitely regular orthogonal wavelet. However, it does not have the characteristic of compactness, which is very important for the wavelet packet transform based analysis of the high frequency signals [65]. The mother wavelet 'db3' of the *Daubechies* family has the second smallest MDL indices among all the candidate mother wavelets in both levels of resolution for both normal and fault currents data. As a result, the mother wavelet 'db3' can be employed to carry out a MRA with the highest degree of similarity between the approximations and the original signal [77]. In this work, the selected mother wavelet 'db3' is used for both the off-line and on-line testing of the wavelet packet transform based algorithm on the three-phase IPM motors.

4.2.2 Selecting number of Levels of resolution

The levels of resolution of the wavelet packet transform determine the resolution of a signal in terms of its time and frequency. Depending upon the type of application, a signal may have high frequency and low time resolution or low frequency and high time resolution. Therefore, a signal can be decomposed into many different ways. But due to the constraint of memory requirements and the computational complexity in real-time implementation, it is sometimes necessary to find the optimal decomposition of a signal. The optimum number of levels of resolution is the minimum number of levels, where the decomposed signal can be reconstructed to the original form without any loss of information.

In this work, the non-normalized Shannon entropy based criterion is used to determine the optimal number of levels of resolution using the selected mother wavelet 'db3'. The entropy-based criterion as described in chapter 3 calculates the entropy of each subspace of the wavelet packet tree. It compares the entropy of a parent subspace with those of its children subspaces in order to find out the optimal levels of resolution.

The procedure is illustrated in the following Figs. 4.3-4.4 for the case of normal unfaulted and faulted currents of the 1hp interior permanent magnet motor.

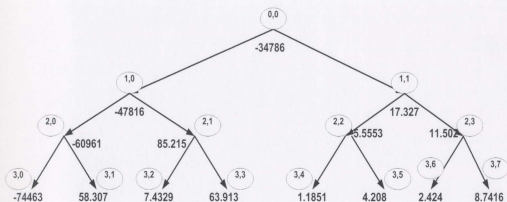


Figure 4.3: The entropy values of each subspace of the wavelet packet tree up to the third level of resolution for the case of normal full load current of the 1hp IPM motor.

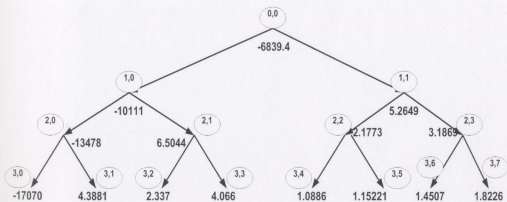


Figure 4.4: The entropy values of each subspace of the wavelet packet tree up to the third level of resolution for the case of loss of supply fault (single phasing) current of the 1hp IPM motor.

Figure 4.3 shows the entropy values of each subspace of the wavelet packet tree up to the third level of resolution in case of normal full load current of the 1hp IPM motor. Here, the entropy values of each parent subspace are higher than those of its combined children subspaces. As a result, according to equation (3.46) the children subspaces can be kept in the tree, and decomposition of the signal up to the third level of resolution is not enough to represent its properties. The entropy values of each subspace of the wavelet packet tree up to the third level of resolution for the case of loss of supply fault are shown in figure 4.4. Here, the entropy value of the first level high frequency details is lower than those of its combined children subspaces. Therefore, according to equation (3.46) its two children could be omitted from the tree, which would result into the single level wavelet packet transform for the fault current. However, disturbances in IPM motors often manifest themselves as short transient superimposed on the fundamental frequency. In order to detect these short transients, one needs more detail representation of the signal. As a result, the second level of resolution is selected as the optimal level of resolution for the wavelet packet transform based algorithm, which is based on the protection requirement of fault current disturbances in IPM motors.

4.3 Proposed Disturbance Detector and Classifier

The modern approaches for the IPM motor protection are mainly based on the mathematical modeling of the motor according to the disturbances. These approaches monitor currents, voltages, or torque waveforms of the faulted motor in order to detect and diagnose faults in IPM motors. There have been some post-fault control strategies for the protection of the IPM motor drive. As the demagnetization effect (armature reaction) of the external magnetic field increase with disturbances in an IPM motor, so it is necessary to develop a complete protection technique for preventing the fault induced damages in the motor. The harmonic analysis based detection techniques employed various algorithms to calculate the fundamental and sometimes, the third harmonic of fault currents. Most of these algorithms are based on the Fourier analysis of fault

currents, which requires the signal to have periodicity and stationarity. In addition, it uses the linear non-localized frequency subdivision [54].

The disturbances that are most likely to occur in three-phase interior permanent magnet motors are with transient components that decay quickly, and the desired features are located in high frequencies present in the fault current. The sub-band frequency structures of the wavelet packet transform that are extracted using the multiresolution analysis (MRA) can provide the needed features to detect and classify any disturbance an IPM motor may experience. These features can be extracted through the analysis of fault current signatures of the sub-band frequency components resulting from different transient disturbances.

In the proposed case, the signature analysis method is used for the feature extraction. The signal is decomposed up to the second level of resolution of the wavelet packet tree using the selected mother wavelet 'db3'. Figs. 4.5-4.10 show the time location color diagrams of the WPT coefficients (d^1 , dd^2) of line currents of different faulted and normal conditions. When a disturbance occurred as in Figs. 4.6, 4.9, and 4.10, the details (dd^2) showed high density of color strips between the faulted region as compared to those of normal currents (loaded or unloaded) of Figs. 4.5, 4.7, and 4.8. As a result, the significant features for faults detection are extracted based on the density of color strips of the WPT coefficients (dd^2) of fault currents of Figs. 4.5-4.10, which are also able to provide accurate and reliable diagnosis of fault currents. So, the proposed wavelet packet transform based algorithm is dependent upon the identification of high frequency components or coefficients (dd^2) of line currents of the second level of resolution of the wavelet packet tree.

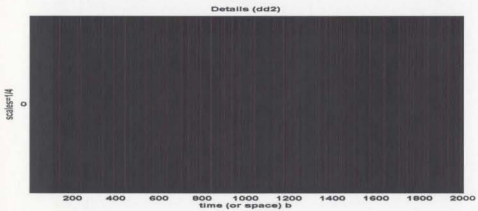
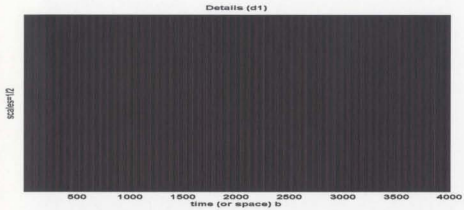


Figure 4.5: The time location diagram of the wavelet packet coefficients for the case of normal unloaded current of the 1hp IPM motor: (a) first level high frequency details (d^1), (b) second level high frequency details (dd^2).

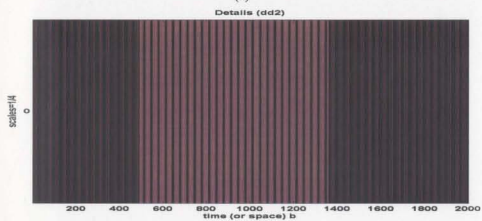
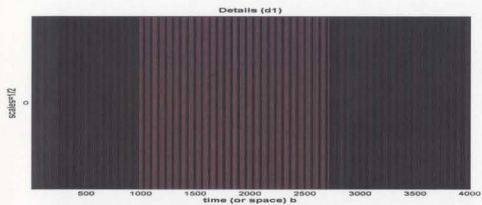


Figure 4.6: The time location diagram of the wavelet packet coefficients for the case of line-to-line (L-L) fault current of the 1hp IPM motor: (a) first level high frequency details (d^1), (b) second level high frequency details (dd^2).

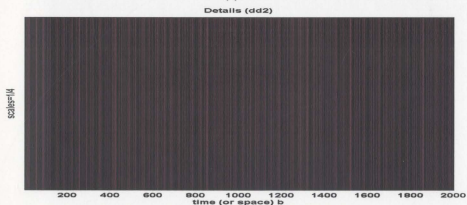
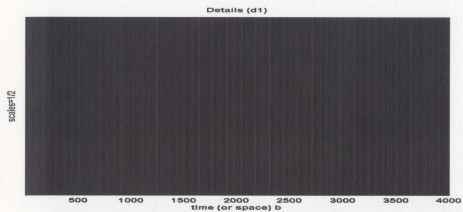


Figure 4.7: The time location diagram of the wavelet packet coefficients for the case of normal (unfaulted) full load current of the 1hp IPM motor: (a) first level high frequency details (d^1), (b) second level high frequency details (dd^2).

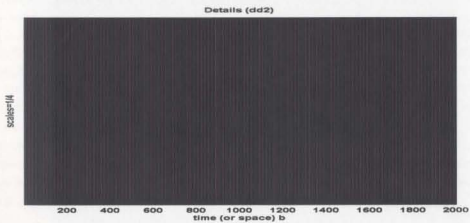
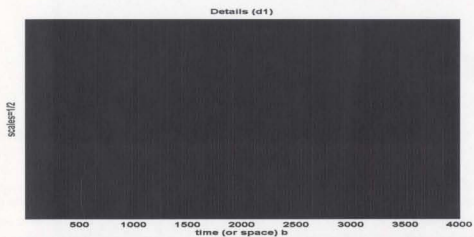


Figure 4.8: The time location diagram of the wavelet packet coefficients for the case of normal unloaded current of the 5hp IPM motor: (a) first level high frequency details (d^1), (b) second level high frequency details (dd^2).

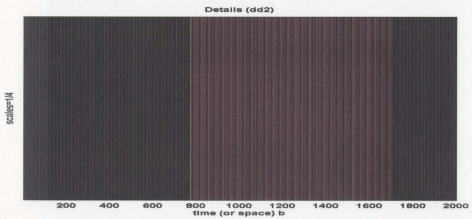
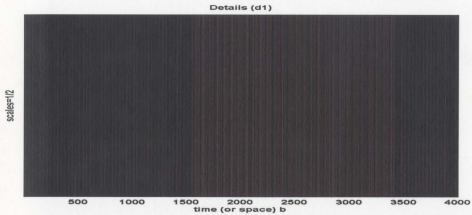


Figure 4.9: The time location diagram of the wavelet packet coefficients for the case of line to ground (L-G) fault current of the 5hp IPM motor: (a) first level high frequency details (d^1), (b) second level high frequency details (dd^2).

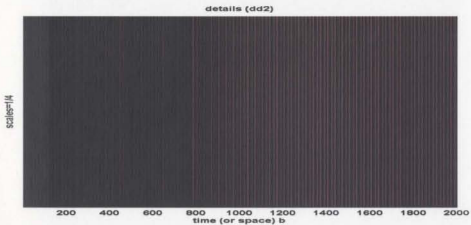
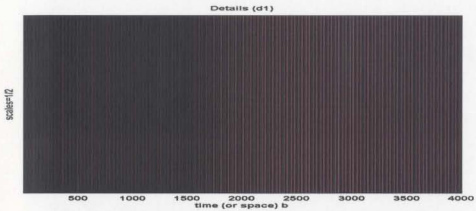


Figure 4.10: The time location diagram of the wavelet packet coefficients for the case of loss of supply (single phasing) fault current of the 5hp IPM motor: (a) first level high frequency details (d^1), (b) second level high frequency details (dd^2).

The proposed WPT algorithm is shown in the flow chart of Fig. 4.11 for the protection of three-phase interior permanent magnet motors. The algorithm checks the values of the highest frequency sub-band in the second level of resolution of the WPT, and determines whether it is greater than the threshold or not. In this work, the threshold is set by the maximum of absolute values of WPT-coefficients (dd^2) of the highest frequency sub-band determined during the healthy condition of the motor. It is to be noted that because of the leakage of energy between the high pass and low pass filters magnitude response and the influence of machine parameters on the magnetic saturation, some highest frequency sub-band components are present at the second level high frequency details (dd^2) for the case of healthy operating condition of the motor.

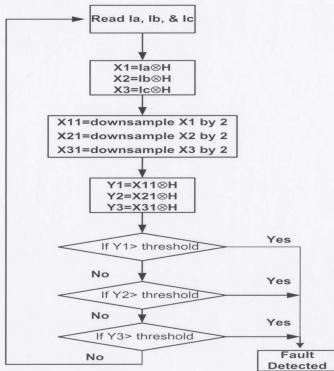


Figure 4.11: The flow chart of the proposed WPT algorithm.

4.4 Off-line Testing of the WPT-based Algorithm

At this stage, the algorithm is ready to be tested on the data collected from three-phase 1hp and 5hp interior permanent magnet motors. The selected mother wavelet 'db3' of the Daubechies family is used in the flow chart of the WPT algorithm to generate high pass filter coefficients and low pass filter coefficients [65]. The filter coefficients are given as:

$$\{g_6\}=\{0.0352 \quad -0.0854 \quad -0.135 \quad 0.4599 \quad 0.8069 \quad 0.3327\} \quad (4.1)$$

$$\{h_6\}=\{-0.3327 \quad 0.8069 \quad -0.4599 \quad -0.135 \quad 0.0854 \quad 0.0352\} \quad (4.2)$$

The desired off-line testing will include different fault currents and normal operating currents. Figure 4.12 shows the off-line test results for the case of normal (unfaulted) unloaded condition of the 1hp interior permanent magnet motor. It is clear that the WPT algorithm has responded accurately by keeping the status of the trip signal unchanged. Figure 4.13 shows the off-line test results for the case of normal (unfaulted) loaded condition of the 1hp IPM motor, and again the WPT algorithm has responded accurately by keeping the status of the trip signal unchanged. Figure 4.14 shows the off-line test results for the case of line to ground (L-G) fault of the 1hp IPM motor, and it is clear that the WPT algorithm has identified the disturbance properly and changed the status of the trip signal almost at the instant of the fault occurrence. Figure 4.15 shows the case of line-to-line fault (L-L) in the 1hp IPM motor, and the WPT has responded by changing the status of the trip signal almost at the instant of the fault occurrence. Figure 4.16 shows the off-line test results for the case of loss of supply (single phasing) fault in the 1hp IPM motor, and the WPT algorithm changed the status of the trip signal within one cycle of the fault occurrence. Figures 4.17-4.20 show the off-line test results of different fault currents and normal operating currents of the 5hp interior permanent magnet motor. Here, the WPT algorithm has responded in the same way as for the case of 1hp interior permanent magnet motor. In other words, the WPT algorithm has changed the status of

the trip signal only for the case of fault currents data, and it occurred almost at the instant or within one cycle of the fault occurrence based on a 60 Hz system.

The off-line testing of the proposed algorithm has demonstrated quite encouraging results, where different fault currents were identified within one cycle of the fault occurrence. The response of the WPT algorithm was very fast. In addition, it has provided high accuracy, small computational burden and powerful capability of identifying the type of current signatures. The next chapter will provide the on-line test results of the proposed algorithm including the experimental setup for the on-line testings, the realization of the WPT algorithm and all cases of normal and fault currents of the experimental interior permanent magnet motor.

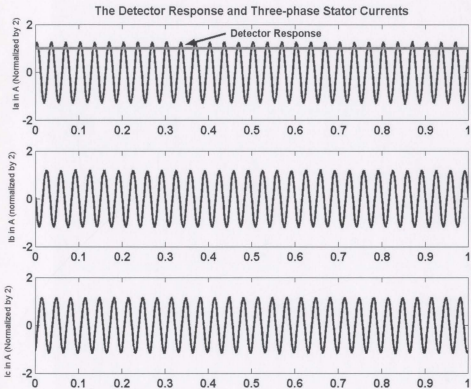


Figure 4.12: The WPT based detector response and the three-phase stator currents for the case of normal (unfaulted) unloaded condition of the 1hp interior permanent magnet motor.

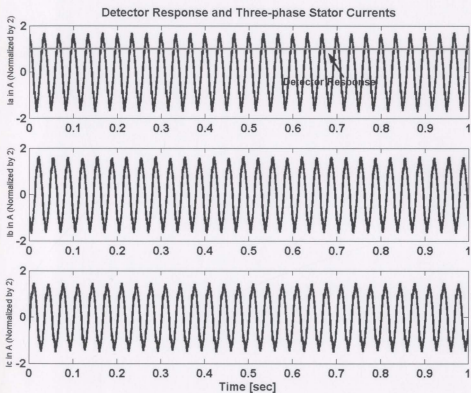


Figure 4.13: The WPT based detector response and the three-phase stator currents for the case of normal (unfaulted) loaded condition of the 1hp interior permanent magnet motor.

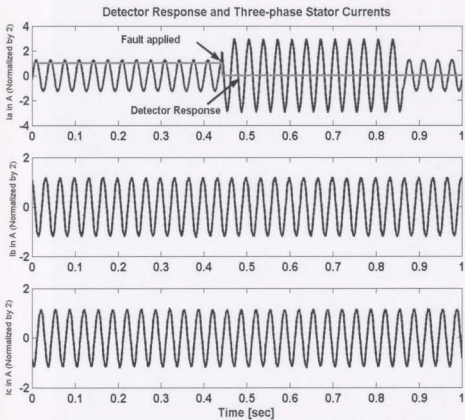


Figure 4.14: The WPT based detector response and the three-phase stator currents for the case of line to ground (L-G) fault of the 1hp interior permanent magnet motor.

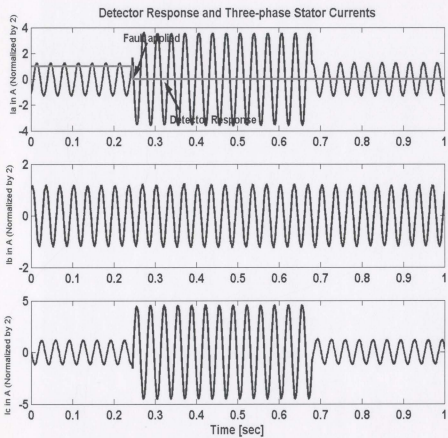


Figure 4.15: The WPT based detector response and the three-phase stator currents for the case of line-to-line (L-L) fault of the 1hp interior permanent magnet motor.

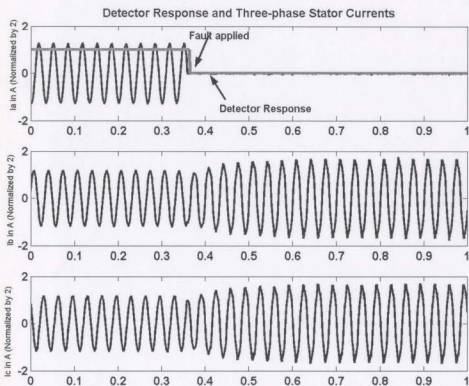


Figure 4.16: The WPT based detector response and the three-phase stator currents for the case of loss of supply (single phasing) fault of the 1hp interior permanent magnet motor.

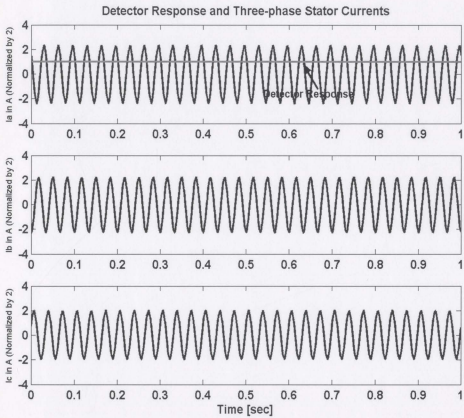


Figure 4.17: The WPT based detector response and the three-phase stator currents for the case of normal (unfaulted) unloaded current of the 5hp interior permanent magnet motor.

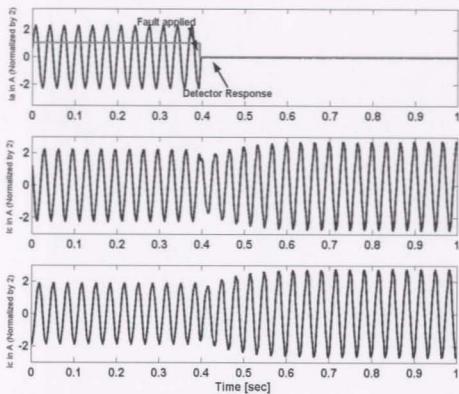


Figure 4.18: The WPT based detector response and the three-phase stator currents for the case of loss of supply (single phasing) fault of the 5hp interior permanent magnet motor.

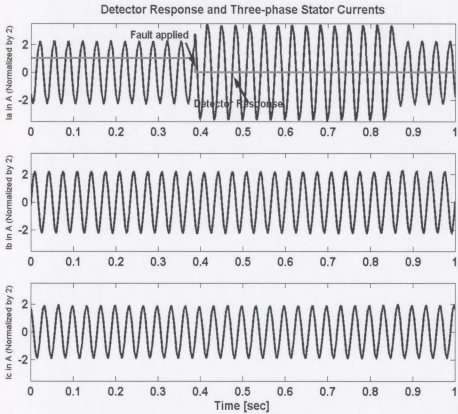


Figure 4.19: The WPT based detector response and the three-phase stator currents for the case of line to ground (L-G) fault of the 5hp interior permanent magnet motor.

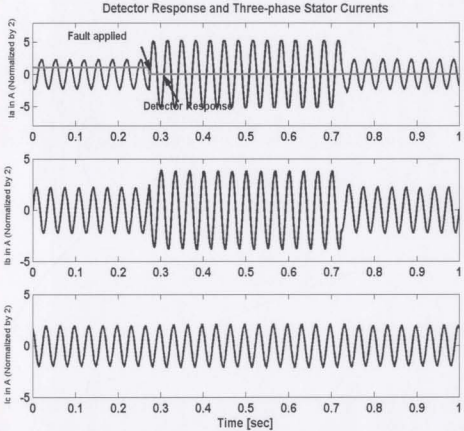


Figure 4.20: The WPT based detector response and the three-phase stator currents for the case of line-to-line (L-L) fault of the 5hp interior permanent magnet motor.

Chapter 5

On-line Testing of the WPT based Algorithm

The off-line testing of the proposed algorithm for the normal unfaulted and faulted conditions in chapter 4 shows encouraging results for the on-line implementation of the proposed protection technique. The on-line implementation of the proposed technique involves the development of the experimental setup that includes both the hardware and software components. The hardware includes the dSPACE digital signal processor board model DS1102 with the 32-bit floating-point processor TMS320C31. The protection technique utilizes the on board analog to digital (A/D) and digital to analog (D/A) converters of the DS1102 digital signal processor board for acquiring fault currents and initiating the trip signal, respectively. The processor TMS320C31 executes the proposed WPT based algorithm on the samples of fault currents in order to make a decision on the status of the trip signal. The hardware also includes the three-triac switches, which are implemented in order to disconnect the motor from the supply in case of faults. Finally, the software part consists of the WPT based algorithm for the protection of three-phase interior permanent magnet (IPM) motors. The complete experimental setup for the on-line testing of the proposed algorithm as well as the on-line test results of different faulted and normal unfaulted conditions are provided in the following sections.

5.1 Experimental setup for On-line Testings

For the case of on-line testings, the interior permanent magnet (IPM) motors are fed from the balanced three-phase supply through three-triac switches. These switches are used for the protection of disturbances in IPM motors. The current transformers (CTs) are used with the terminals of the motor to acquire different normal and fault currents. The DS1102 digital signal processor board is used for acquiring three-phase line currents and making a decision on the status of the trip signal for the case of normal unfaulted and faulted conditions. A relay switch, which is energized by the use of 555-timer circuit, is used in initiating various disturbances. Figure 5.1 shows the complete experimental setup for the on-line testings of the proposed WPT based algorithm on IPM motors.

5.2 Real-time Implementation of the Proposed Algorithm

The wavelet packet transform (WPT) based algorithm is tested on a 3-phase, Y-connected, 1hp laboratory prototype interior permanent magnet motor and on a 3-phase, Δ -connected, 5hp laboratory prototype interior permanent magnet motor. The on-line test results for both types of IPM motors are provided in this chapter. The complete protection technique includes both the hardware and software. Samples of different normal and fault currents are processed by the WPT based algorithm in the 32-bit floating-point processor TMS320C31. For this purpose, a programme written in Turbo C language is developed, where the wavelet packet transform (WPT) is applied to the samples of line currents using the selected mother wavelet '*db3*'. This constitutes the first level of decomposition. Then, the details of the first level of resolution are down sampled by two and the WPT is applied again. The details of the second level of resolution are checked whether it is greater than the threshold or not in order to identify a disturbance. Figure 5.2 shows the flow chart of on-line implementation of the proposed WPT algorithm using the DS1102 digital signal processor board.

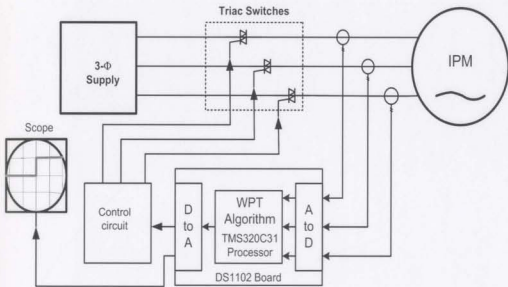


Figure 5.1: Experimental setup for on-line testings on the three-phase interior permanent magnet motor.

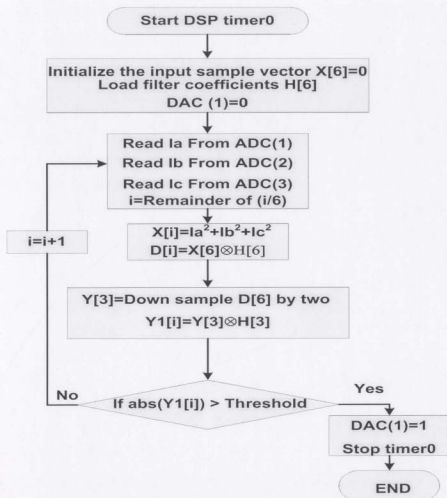


Figure 5.2: Flowchart of on-line implementation of the wavelet packet transform (WPT) based algorithm using the DS1102 digital signal processor board.

The proposed algorithm, written in the Turbo C language, used a set of initialization and input/output (I/O) functions in order to initialize the TMS320C31's on-chip timers and to access the DS1102's on board analog to digital (A/D) and digital to analog (D/A) converters. When a timer is started, A/D converters of the DS1102 digital signal processor board continuously sample three-phase line currents at the rate of 8 kHz. The samples of three-phase line currents are sent to the memory of the DSP by the host PC, where they are squared and summed into one sample, and this sample is placed into a circular buffer of size 6. A vector of length 6 is used to store these sample values. Each time a sample is placed in the circular buffer, the previous 6th sample is automatically dropped off the buffer and the vector is updated. Another vector of length 6 is used to store the high pass filter coefficients of the selected mother wavelet 'db3' described in chapter 4. These high pass filter coefficients are convolved circularly with the elements of the input sample vector. It results into the first level details of the original signal, and then the first level details are down sampled by two to get better frequency resolution. Finally, a discrete 3-sample circular convolution is applied on the first level details with the same filter coefficients. The circular convolution produces the second level details. The second level details are checked whether it is higher than the threshold or not in order to identify fault currents. If the absolute values of the second level details exceed the threshold, then a fault is detected by initiating a trip signal through the digital to analog converter of the DS1102 digital signal processor board.

5.3 On-line Test Results

The wavelet transforms are found to be very effective in reducing the computational burden of the power systems faults detection [77-78]. However, in order to achieve more reduction in computational burden for the protection of IPM motors, the samples of three-phase line currents are squared and summed into one sample before applying the WPT algorithm to it. This method is found to be very effective and is known as the unbiased method [58,79]. However, other method such as applying the WPT algorithm to three vectors separately representing three-phase line currents samples could have used for

further reduction in computational burden. But the technique could affect the response of the proposed algorithm.

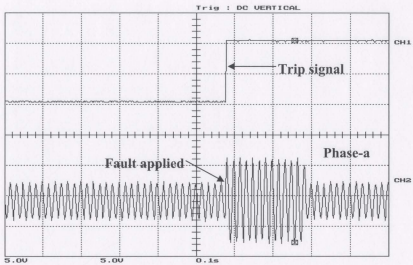
5.3.1 Fault currents

The WPT-based algorithm response for different faults under conditions of with and without loading is tested on-line using the DS1102 digital signal processor board. Three different asymmetrical faults are investigated in this work to test the WPT-based algorithm response: (i) line to ground (L-G) fault, (ii) line to line (L-L) fault, and (iii) loss of supply (single phasing) fault. These fault conditions were tested for each phase of the three-phase interior permanent magnet motor. A relay switch, which was activated by the 555-timer circuit, was used in all the testings for connecting the two points involved in the fault. The on-line test results showed that the fault is detected and the trip signal is initiated within one cycle of the fault occurrence based on 60 Hz system in all cases.

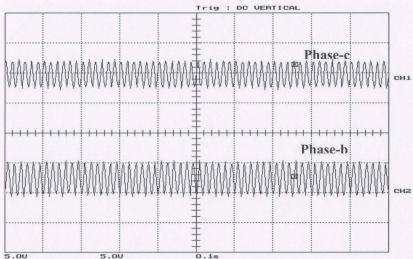
5.3.1.1 Line to ground (L-G) fault

The test for the line to ground (L-G) fault was carried out by connecting a phase to the ground through a resistance under conditions of with and without loading. It is to be noted that in all cases of loading of the 5hp IPM motor, a balanced resistive load of 35 Ω /phase is used with the synchronous generator that has been coupled to the IPM motor. However, in case of the 1hp IPM motor, an electro-dynamometer is used for the loading of the motor. Figures 5.3-5.6 show the test results of the line to ground (L-G) fault took place on phase-a of both types of three-phase interior permanent magnet motors. The test results for phase-b and phase-c are given in Appendix A. The three-phase line currents as well as the WPT trip signal of the proposed algorithm are shown in these figures. For all the tests carried out, the disturbance was identified promptly and properly, and the trip signal was initiated at the instant of the fault occurrence. Figures 5.3-5.4 show the three-phase line currents and the WPT trip signal for the case of line to ground (L-G) fault occurring on phase 'a' in the 1hp IPM motor with and without load, respectively. The

results of the same type of L-G faults for the case of 5hp IPM motor are shown in Figs. 5.5-5.6.

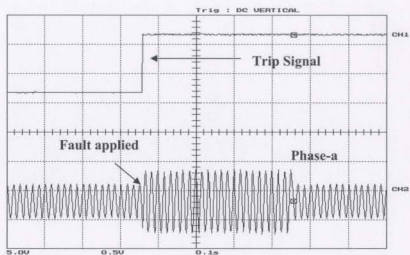


(a)

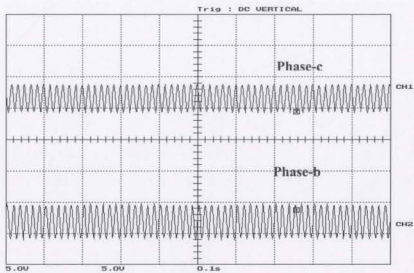


(b)

Figure 5.3: Loaded line to ground (L-G) fault on phase-a of the 1hp IPM motor: (a) the WPT response and phase-a stator current, (b) phase-c and phase-b stator currents. (Scales: time: 0.1s/div., trip signal: 5v/div., phase-a: 4.172 A/div., phase-b: 4.66 A/div., and phase-c: 4.82 A/div.)

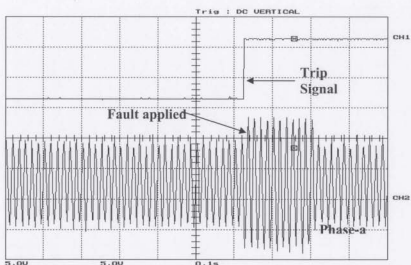


(a)

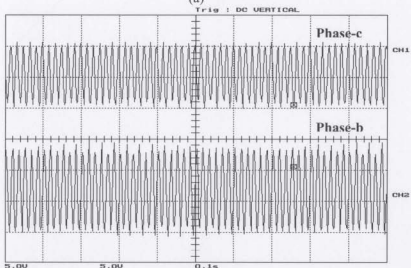


(b)

Figure 5.4: Unloaded line to ground (L-G) fault on phase-a of the 1hp IPM motor: (a) the WPT response and phase-a stator current, (b) phase-c and phase-b stator currents. (Scales: time: 0.1s/div., Trip signal: 5v/div., phase-a: 4.172 A/div., phase-b: 4.66 A/div., and phase-c: 4.82 A/div.)

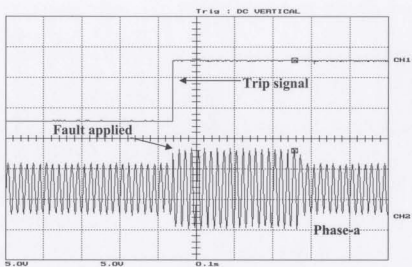


(a)

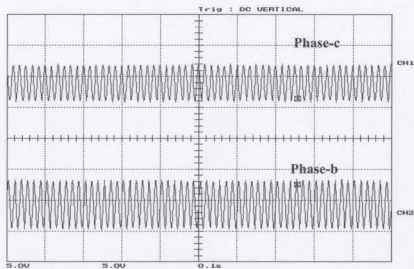


(b)

Figure 5.5: Loaded line to ground (L-G) fault on phase-a of the 5hp IPM motor: (a) the WPT response and phase-a stator current, (b) phase-c and phase-b stator currents. (Scales: time: 0.1s/div., trip signal: 5v/div., phase-a: 4.172 A/div., phase-b: 4.66 A/div., and phase-c: 4.82 A/div.)



(a)



(b)

Figure 5.6: Unloaded line to ground (L-G) fault on phase-a of the 5hp IPM motor: (a) the WPT response and phase-a stator current, (b) phase-c and phase-b stator currents. (Scales: time: 0.1s/div., trip signal: 5v/div., phase-a: 4.172 A/div., phase-b: 4.66 A/div., and phase-c: 4.82 A/div.)

5.3.1.2 Line-to-line (L-L) fault

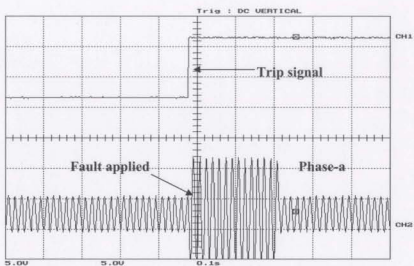
The test for the line-to-line (L-L) fault was carried out by connecting two phases through a resistance under the conditions of with and without loading. Figures 5.7-5.10 show the test results of the line-to-line (L-L) fault that took place between phase-a and phase-b in both types of three-phase interior permanent magnet motors. However, the remaining results for the line-to-line fault between phases a & c and phases b & c are shown in Appendix B. For all the tests carried out, the disturbance was identified properly and the trip signal was initiated at the instant of the fault occurrence.

5.3.1.3 Loss of supply (single phasing) fault

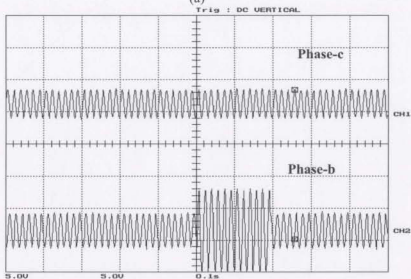
This type of fault can be caused by the mechanical/electrical failure of a machine terminal connector, an internal winding rupture, or by an electrical failure in one of the inverter legs of the interior permanent magnet motor drives [5]. In this work, the test for the single phasing fault was carried out by connecting a single pole single through switch between the power supply and machine terminal. Opening of the switch for few seconds created the fault momentarily. The results of the loss of supply fault that took place on phase-a in both types of interior permanent magnet motors are shown in Figs. 5.11-5.14. The on-line test results of the loss of supply fault that took place on phase-b and phase-c are given in Appendix C. The proposed WPT algorithm identified the disturbance properly, and generated a trip signal within one cycle of the fault occurrence.

5.3.2 Normal (unfaulted) conditions

The proposed WPT algorithm was tested for normal (unfaulted) currents under the conditions of with and without loading. The WPT algorithm identified it as a normal condition and did not generate any trip signal. Three-phase line currents and the associated no trip signal for the case of normal (unfaulted) current of both types of interior permanent magnet motors are shown in Figs. 5.15-5.18.

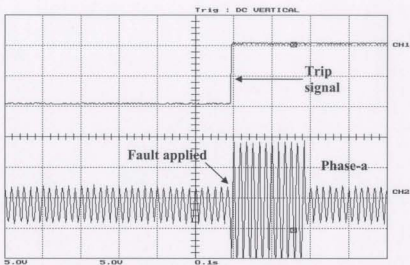


(a)

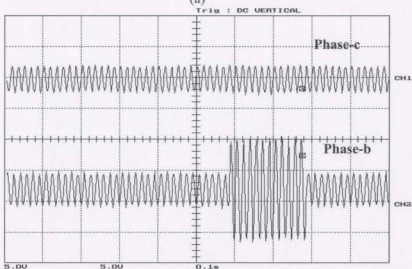


(b)

Figure 5.7: Unloaded line-to-line fault (L-L) between phase-a and phase-b of the 1hp IPM motor: (a) the WPT response and phase-a stator current, (b) phase-c and phase-b stator currents. (Scales: time: 0.1s/div., trip signal: 5v/div., phase-a: 4.172 A/div., phase-b: 4.66 A/div., and phase-c: 4.82 A/div.)

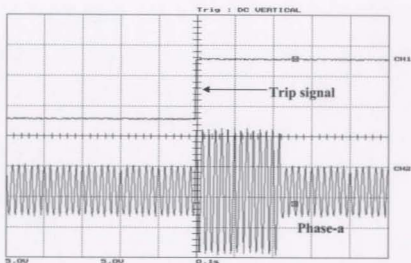


(a)

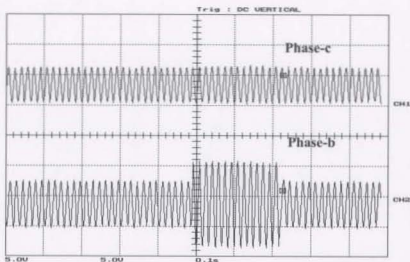


(b)

Figure 5.8: Loaded line-to-line (L-L) fault between phase-a and phase-b of the 1hp IPM motor: (a) the WPT response and phase-a stator current, (b) phase-c and phase-b stator currents. (Scales: time: 0.1s/div., trip signal: 5v/div., phase-a: 4.172 A/div., phase-b: 4.66 A/div., and phase-c: 4.82 A/div.)

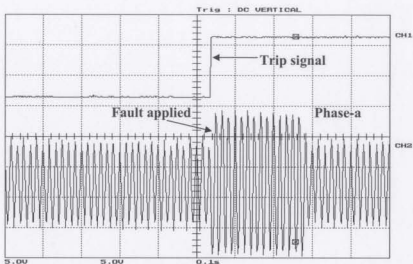


(a)

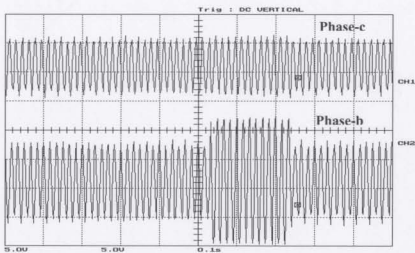


(b)

Figure 5.9: Unloaded line-to-line (L-L) fault between phase-a and phase-b of the 5hp IPM motor: (a) the WPT response and phase-a stator current, (b) phase-c and phase-b stator currents. (Scales: time: 0.1s/div., trip signal: 5v/div., phase-a: 4.172 A/div., phase-b: 4.66 A/div., and phase-c: 4.82 A/div.)

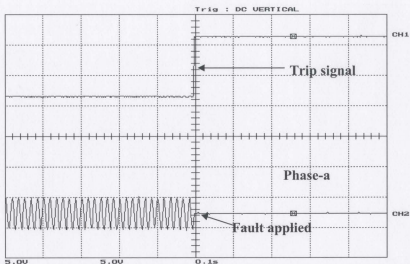


(a)

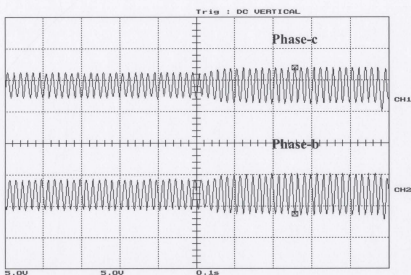


(b)

Figure 5.10: Loaded line-to-line (L-L) fault between phase-a and phase-b of the 5hp IPM motor: (a) the WPT response and phase-a stator current, (b) phase-c and phase-b stator currents. (Scales: time: 0.1s/div., trip signal: 5v/div., phase-a: 4.172 A/div., phase-b: 4.66 A/div., and phase-c: 4.82 A/div.)

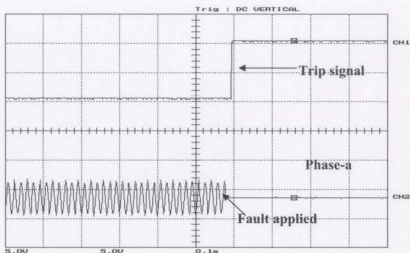


(a)

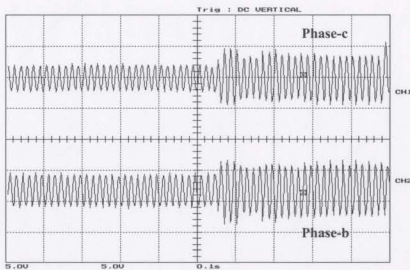


(b)

Figure 5.11: Unloaded loss of supply fault in phase-a of the 1hp IPM motor: (a) the WPT response and phase-a stator current, (b) phase-c and phase-b stator currents. (Scales: time: 0.1s/div., trip signal: 5v/div., phase-a: 4.172 A/div., phase-b: 4.66 A/div., and phase-c: 4.82 A/div.)

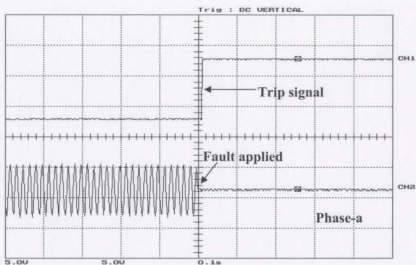


(a)

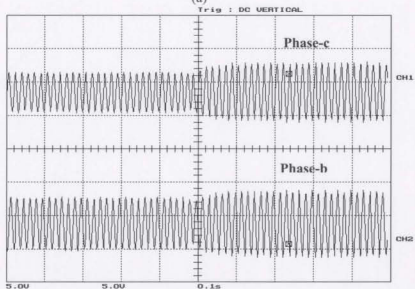


(b)

Figure 5.12: Loaded loss of supply fault in phase-a of the 1hp IPM motor: (a) the WPT response and phase-a stator current, (b) phase-c and phase-b stator currents. (Scales: time: 0.1sec/div., Trip signal: 5v/div., phase-a: 4.172 A/div., phase-b: 4.66 A/div., and phase-c: 4.82 A/div.)

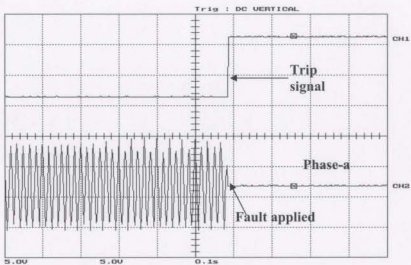


(a)

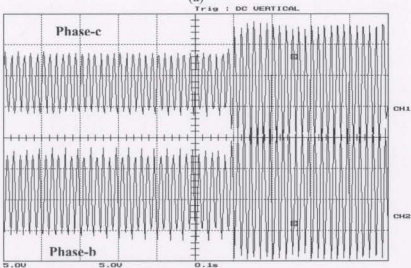


(b)

Figure 5.13: Unloaded loss of supply fault in phase-a of the 5hp IPM motor: (a) the WPT response and phase-a stator current, (b) phase-c and phase-b stator currents. (Scales: time 0.1s/div., trip signal: 5v/div., phase-a: 4.172 A/div., phase-b: 4.66 A/div., and phase-c: 4.82 A/div.)

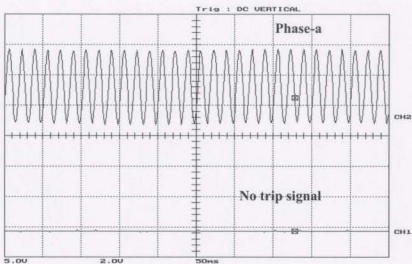


(a)

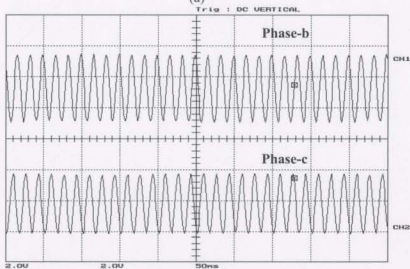


(b)

Figure 5.14: Loaded loss of supply fault in phase-a of the 5hp IPM motor: (a) the WPT response and phase-a stator current, (b) phase-c and phase-b stator currents. (Scales: time 0.1s/div., trip signal: 5v/div., phase-a: 4.172 A/div., phase-b: 4.66 A/div., and phase-c: 4.82 A/div.)

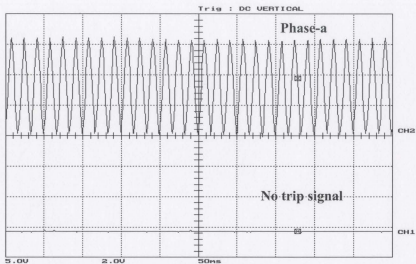


(a)

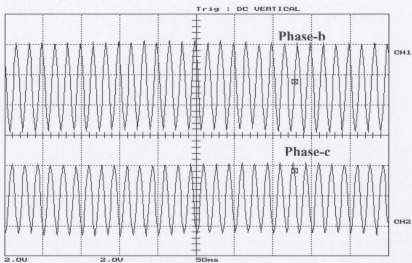


(b)

Figure 5.15: Unloaded normal (unfaulted) current condition of the 1hp IPM motor: (a) the phase-a stator current and WPT response of no trip signal, (b) phase-b and phase-c stator currents. (Scales: time: 50ms/div., trip signal: 5v/div., phase-a: 1.93 A/div., phase-b: 1.87 A/div., and phase-c: 1.67 A/div.)

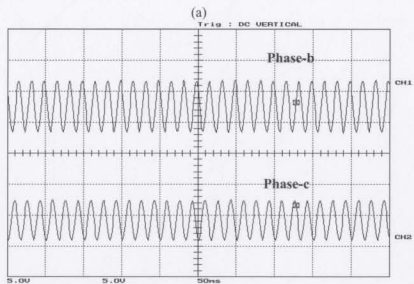
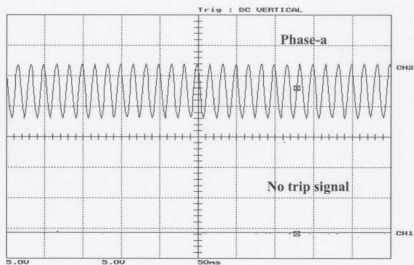


(a)



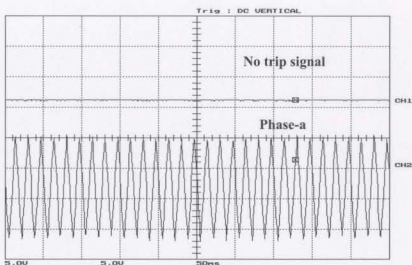
(b)

Figure 5.16: Loaded normal (unfaulted) current condition of the 1hp IPM motor: (a) the phase-a stator current and WPT response of no trip signal, (b) phase-b and phase-c stator currents. (Scales: time: 50ms/div., trip signal: 5v/div., phase-a: 1.93 A/div., phase-b: 1.87 A/div., and phase-c: 1.67 A/div.)

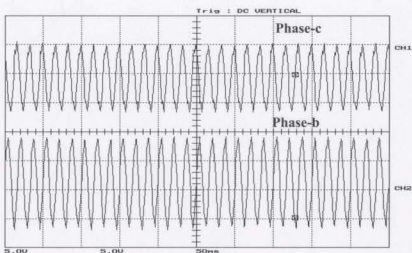


(b)

Figure 5.17: Unloaded normal (unfaulted) current condition of the 5hp IPM motor: (a) the phase-a stator current and WPT response of no trip signal, (b) phase-b and phase-c stator currents. (Scales: time: 50ms/div., trip signal: 5v/div., phase-a: 4.172 A/div., phase-b: 4.66 A/div., and phase-c: 4.82 A/div.)



(a)



(b)

Figure 5.18: Loaded normal (unfaulted) current condition of the 5hp IPM motor: the phase-a stator current and WPT response of no trip signal, (b) phase-b and phase-c stator currents. (Scales: time: 50ms/div., trip signal: 5v/div., phase-a: 4.172 A/div., phase-b: 4.66 A/div., and phase-c: 4.82 A/div.)

5.4 Extending the Real-time Testing

The on-line test results of the wavelet packet transform based algorithm in section 5.3 have shown an effective and fast response in distinguishing between normal and fault currents under different operating conditions. The algorithm was tested successfully and effectively on both types of line-fed three-phase interior permanent magnet motors. This section extends the real-time testing of the proposed wavelet packet transform based algorithm on the inverter-fed three-phase interior permanent magnet motor. The real-time testing is extended mainly to demonstrate the universality of the proposed WPT-based protection algorithm for either the line-fed or inverter-fed three-phase interior permanent magnet motors. The inverter-fed three-phase interior permanent magnet motor is to be tested using the same algorithm developed previously along with the modified experimental setup used for line-fed IPM motors. The experimental setup for the on-line testing of the proposed algorithm on the inverter-fed IPM motor is described in the next subsection. Then the on-line test results are presented. Finally, a comparison between the on-line test results obtained from the line-fed and inverter-fed IPM motor is given.

5.4.1 Experimental Setup for the Inverter-fed IPM Motor

In this case, the three-phase interior permanent magnet motor is fed from the sinusoidal pulse width modulated voltage source inverter. The insulated gate bipolar transistor (IGBT) inverter with the three-phase rectifier is implemented for on-line testing of the inverter-fed IPM motor. An open loop control technique based on the pulse width modulation is used in the IPM drive system, where base transistors of the inverter are activated and controlled by the PWM (pulse width modulated) pulses, and these are generated through the on-board digital input/output (I/O) pins of the DS1102 digital signal processor board. The processing of normal or fault currents are done in the same way as for the line-fed IPM motor. Three triac switches are also used with the supply for isolating the dc links to the inverter for the protection and thereby preventing any fault induced damages to the motor or the inverter. The complete experimental setup for the on-line protection of the inverter-fed IPM motor is shown in Fig. 5.19.

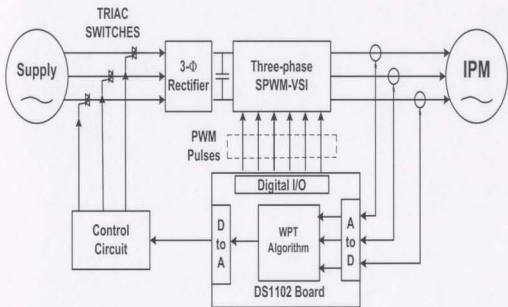


Figure 5.19: Experimental setup for on-line testing of the WPT-algorithm on the inverter-fed interior permanent magnet motor.

5.4.2 On-line Test Results of the Inverter-fed IPM Motor

The on-line testing of the proposed algorithm in section 5.3 was performed on the line-fed IPM motors of different stator configurations. The 1hp and 5hp IPM motors used has the wye (Y) and delta (Δ) configuration in the stator, respectively. However, the results of the proposed algorithm of these two types of IPM motors showed an excellent and unique ability to identify and respond to the different types of fault currents flowing through the line-fed IPM motors with different configurations in the stator. This motivates the application of the proposed algorithm with the modified experimental setup to the inverter-fed IPM motor in order to show the universal capability of the WPT algorithm in diagnosing the line-fed or inverter-fed IPM motor.

5.4.2.1 Fault currents

Three different fault currents are investigated in order to test the WPT-based algorithm on the inverter-fed IPM motor: (a) loss of supply (single phasing) fault, (b) line to ground (L-G) fault, and (c) line to line (L-L) fault. These fault conditions were tested on phase-a of the three-phase interior permanent magnet motor. Each fault condition was performed by connecting the two points involved in the fault. The on-line test results showed that the proposed algorithm identified the disturbance properly and initiated a trip signal to open the circuit breaker almost at the instant or within one cycle of the fault occurrence based on the 60 Hz system in all cases.

Line to ground (L-G) fault: The test for the line to ground (L-G) fault was carried out by connecting a phase to the ground through a resistance under condition of no load. Figure 5.20 shows the test results of the line to ground (L-G) fault tested on phase-a of the 1hp interior permanent magnet motor. The three-phase line currents as well as the WPT trip signal of the proposed algorithm are shown in this figure. In the test carried out, the disturbance was identified properly and the trip signal was initiated to open the circuit breaker almost at the instant of the fault occurrence.

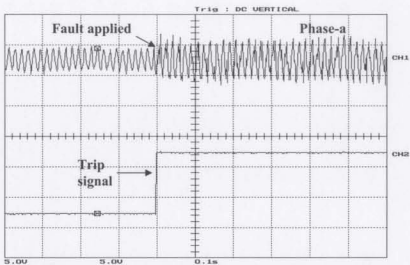
Line to line (L-L) fault: Connecting two phases through a resistance without any load carried out the real-time testing of the line-to-line (L-L) fault on the inverter-fed

IPM motor. Figure 5.21 shows the test results of the line-to-line (L-L) fault took place between phase-b and phase-c of the 1hp interior permanent magnet motor. In the test carried out, the fault was detected and the trip signal was initiated almost at the instant of the fault occurrence.

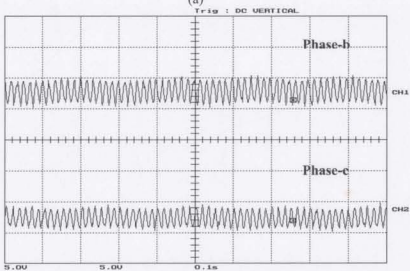
Loss of supply (single phasing) fault: The real-time testing of the loss of supply fault can be carried out by the mechanical/electrical failure of a machine terminal connector, an internal winding rupture, or by an electrical failure in one of the inverter legs of the interior permanent magnet motor drives [5]. In this work, the test for this fault was carried out by connecting a single pole single through switch between the power supply and machine terminal. Opening of the switch for few seconds created the fault momentarily. The on-line test results of the single phasing fault that took place on phase-a of the inverter-fed 1hp IPM motor is shown in Fig. 5.22. The proposed WPT algorithm identified the disturbance properly and generated a trip signal within one cycle of the fault occurrence.

5.4.2.2 Normal (unfaulted) condition

The proposed WPT algorithm was tested on the inverter-fed IPM motor for the normal (unfaulted) current under the condition of without loading. The WPT algorithm identified it as a normal condition and did not generate any trip signal. Three-phase line currents and the associated no trip signal for the case of normal (unfaulted) current condition are shown in Fig. 5.23.

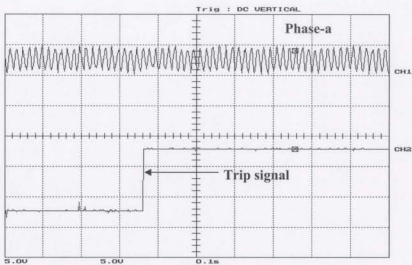


(a)

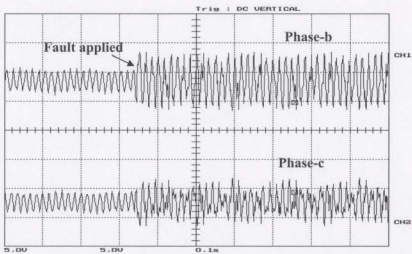


(b)

Figure 5.20: Unloaded line to ground fault (L-G) on phase-a of the inverter-fed 1hp IPM motor: (a) the phase-a stator current and WPT response, (b) phase-b and phase-c stator currents. (Scales: time: 0.1s/div., trip signal: 5v/div., phase-a: 4.172 A/div., phase-b: 4.66 A/div., and phase-c: 4.82 A/div.)

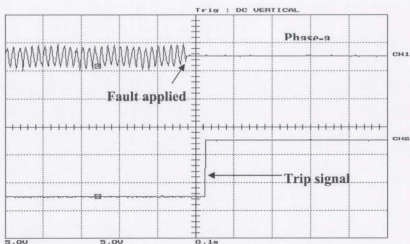


(a)

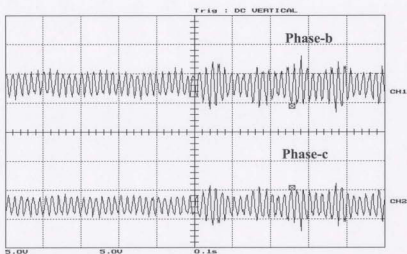


(b)

Figure 5.21: Unloaded line-to-line (L-L) fault between phase-b and phase-c of the inverter-fed 1hp IPM motor: (a) the phase-a stator current and WPT response, (b) phase-b and phase-c stator currents. (Scales: time: 0.1s/div., trip signal: 5v/div., phase-a: 4.172 A/div., phase-b: 4.66 A/div., and phase-c: 4.82 A/div.)

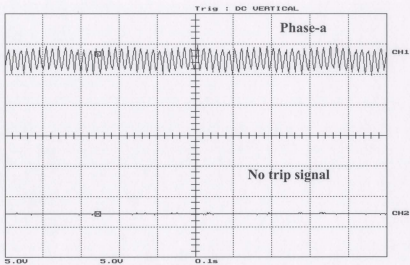


(a)

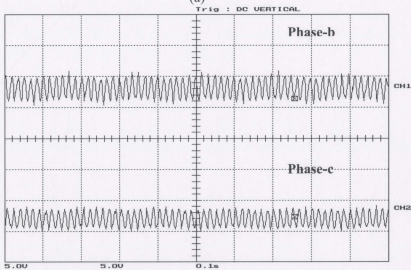


(b)

Figure 5.22: Unloaded single phasing fault on phase-a of the inverter-fed 1hp IPM motor: (a) the phase-a stator current and WPT response, (b) phase-b and phase-c stator currents. (Scales: time: 0.1s/div., trip signal: 5v/div., phase-a: 4.172 A/div., phase-b: 4.66 A/div., and phase-c: 4.82 A/div.)



(a)



(b)

Figure 5.23: Unloaded normal (unfaulted) current condition of the inverter-fed 1hp IPM motor: (a) the phase-a stator current and WPT response of no trip signal, (b) phase-b and phase-c stator currents. (Scales: time: 0.1s/div., trip signal: 5v/div., phase-a: 4.172 A/div., phase-b: 4.66 A/div., and phase-c: 4.82 A/div.)

The results obtained from both the line-fed and inverter-fed interior permanent magnet motors show that the WPT based algorithm is able to distinguish accurately between the faulted and normal (unfaulted) currents. In addition, the WPT based algorithm is also able to distinguish the fault currents of the wye (Y) or delta (Δ) connected IPM motors. Moreover, the trip signal was initiated almost at the instant or within one cycle of the fault occurrence in all the tests carried out on both types of line-fed and inverter-fed interior permanent magnet motors. It is worth mentioning that the proposed algorithm was also able to differentiate successfully between the normal unfaulted and faulted conditions even with the presence of large harmonics in stator currents produced by the converter for the case of inverter-fed interior permanent magnet motor. It is also to be noted that two separate oscilloscopes have been used during the experimental works in order to capture three-phase line currents and the status of the trip signal. The wave shapes are captured at the same time using the "hold" options of the two scopes. As the scopes are not synchronized with each other, so the captured currents are also slightly unsynchronized in few cases. Due to this phenomenon, the trip signal seems to occur before the inception of faults in some cases.

The next chapter provides a brief summary of this work along with the major contributions. Finally, the thesis is concluded by the future scopes of work.

Chapter 6

Conclusions and Future Work

6.1 Summary

Interior permanent magnet (IPM) synchronous motors are attractive for a variety of applications because of their high electromagnetic torque per permanent-magnet volume, high efficiency, high power factor, low noise and relatively low cost. The protection of the interior permanent magnet motor against the disturbances represents a critical task to maintain both the stability and reliability of the systems connected to the motor. This also results in minimum downtime and optimum maintenance schedules of the motor. The frequency domain analysis of the fault currents is one of the most common techniques used for the detection and diagnosis of faults in the interior permanent magnet motors. This technique is based on evaluating the discrete Fourier transform (DFT) of the fault currents to extract the fundamental, third and sometimes, the fifth harmonic as well. The basic assumption behind this technique is that the fault currents contain significant amount of fundamental and third harmonics than the normal unfaulted currents. However, loaded unfaulted currents can have a significant amount of the fundamental and third harmonics. As a result, this technique can be responsible for the occurrence of mal-functioning of the relay or circuit breakers implemented for the protection of the IPM motors. In addition, the output signals of the running machine often contain non-stationary components due to the presence of faults. But the frequency domain analysis

based technique is suitable only for the stationary or quasi-stationary signals and is not able to reveal the inherent information of non-stationary signals.

There have been some latest techniques for the three-phase interior permanent magnet motor protection. Among these new approaches are the fuzzy logic systems (FLS), artificial neural networks (ANN), genetic algorithm (GA), short time Fourier transform (STFT), higher order spectrum (HOS) analysis such as: bi-spectrum, tri-spectrum, etc. These approaches are fast in terms of response and ability to diagnose the type of fault currents. However, these are highly dependent on the machine parameters and/or loading conditions. Furthermore, they cannot localize a fault in time domain and have poor time resolution. In addition, they have some practical limitations because of the large computational burden and complex interpretations.

It is clear from the preceding discussion that an alternative method is needed due to the limitations of common approaches of protecting the interior permanent magnet motors. In this work, the proposed method is the wavelet packet transform based detection of fault currents. Wavelets and wavelet transforms have been applied with success in a wide variety of research areas such as signal analysis, image processing, data compression, de-noising and numerical solution of differential equations. Recently it has been used in transient detection, localization and classification. The problem of protecting the interior permanent magnet motor against disturbances can be formulated as the discrimination between the normal unfaulted and faulted currents. The wavelet packet transform based detection of fault currents is implemented in this work and tested off-line and on-line successfully on two different types of three-phase interior permanent magnet motors.

An extensive literature review on techniques used for the prognosis of failures in induction and permanent magnet motors has been conducted in chapter 1. Based on the reviews, the problem involving the interior permanent magnet motor protection is stated and consequently a solution using the wavelet packet transform is proposed.

Chapter 2 provides an overview of the application of the commonly used techniques for detecting and diagnosing various disturbances in three-phase interior permanent

magnet motors. There have been many techniques to detect and diagnose faults in the IPM motors. Four of them have been illustrated and implemented in chapter 2 and these are: (a) fast Fourier transform (FFT), (b) power spectral density (PSD), (c) short time Fourier transform (STFT), and (d) artificial neural network (ANN). Each of the above mentioned approaches are explained first with its basics and principal of operations and then they are implemented off-line to discriminate the normal (unfaulted) currents from the fault currents.

In chapter 3, the concept of the wavelet and wavelet transforms in addition to the definition of wavelet and scaling functions, and their characteristics are illustrated. A brief description of different wavelet families including the orthogonal and nonorthogonal wavelets, and their characteristics are given at the beginning of the chapter. The different wavelet transforms and their mathematical expressions for the case of continuous and discrete signal have been explained. In addition, the concept of the quadrature mirror filter (QMF) banks essential for carrying out the multiresolution analysis (MRA) has also been briefly discussed. The MRA is performed by dilating and shifting the mother wavelet over different levels of resolution. The dilating process generates the daughter wavelet with the same nature and characteristics of the mother wavelet, while the shifting process is the transformation from one level of resolution to a higher one. Finally, chapter 3 describes the Shannon entropy based criterion and minimum description length data criterion for selecting the optimal mother wavelet and optimal number of levels of resolution, respectively.

An experimental setup is developed and described in chapter 4 for collecting the digital data, where line currents of different faulted and normal (unfaulted) conditions are acquired through the on-board A/D converters of the DS1102 digital signal processor board. The collected data are used for selecting the optimal mother wavelet and optimal number of levels of resolution according to the criterions mentioned in chapter 3. The application of these criteria has resulted in selecting the mother wavelet '*db3*' of the *daubeuchies* family and the second level of resolution as the optimal number of resolution. The collected data are also used for extracting the features of different fault

currents, and an algorithm is developed based on the analysis of these fault current signatures. Finally, the proposed disturbance detector based on the WPT-algorithm is tested off-line in the MATLAB environment by these collected data on two types of interior permanent magnet motors.

The real time implementation and testing of the proposed WPT based protection algorithm using the DS1102 digital signal processor board is given in chapter 5. The on-line testings are carried out on both types of IPM motors with the help of modified experimental setup used for data acquisition. The results are also consistent with the off-line test results in terms of speed of response and ability to diagnose the type of fault currents. The on-line responses of the WPT based algorithm are found to be fast, prompt and reliable. In all the tests carried out, the fault is detected and the trip signal is initiated almost at the instant or within one cycle of the fault occurrence based on a 60 Hz system.

In order to demonstrate the universality of the proposed WPT based protection algorithm for three-phase interior permanent magnet motors, the real time testing has been extended to the inverter-fed interior permanent magnet motor. The results of the on-line testing of the WPT based algorithm on the inverter-fed IPM motor using the modified experimental setup are given in chapter 5. The results are also consistent with the on-line test results of the line-fed interior permanent magnet motors and found to be fast, accurate, and reliable. It is to be noted that the WPT algorithm is insensitive to loading conditions as well as motor parameters. The detector identified every disturbance properly and initiated the trip signal almost at the instant or within one cycle of the fault occurrence even with the presence of large harmonics produced by the converter in stator currents of the inverter-fed IPM motor.

6.2 Contributions

The major contributions of this work are:

- A novel algorithm based on the wavelet packet transform of line currents for the protection of interior permanent magnet motors is developed.
- An innovative disturbance detection and classification technique is successfully implemented in real-time and tested on-line using the DS-1102 digital signal processor board.
- The minimum description length (MDL) data criterion and the Shannon entropy based criterion have been successfully implemented for selecting the optimal mother wavelet and optimal number of levels of resolution respectively for the protection of interior permanent magnet motors.
- The proposed WPT-based detection algorithm also has been successfully implemented in real-time for the protection of inverter-fed interior permanent magnet motor. This has confirmed the applicability of the proposed algorithm for the protection of any type of interior permanent magnet motors.

6.3 Conclusions

- The wavelet packet transform is a relatively new tool for the detection, localization, and classification of different power system transients. In this work, an innovative application of the wavelet packet transform for the protection of three-phase interior permanent magnet motors is successfully implemented on-line for the first time.
- Unlike any other fault diagnosis and condition monitoring techniques of the IPM motors, the WPT-based protection technique used in this work did not require any harmonic contents analysis or off-line training of faulted or normal (unfaulted) currents. As a result, the unpredictable characteristics of fault currents did not prevent the proposed algorithm from initiating the trip signal. It is also to be noted that the proposed algorithm is insensitive of CT saturation, machine

parameters, or different loading characteristics. The proposed algorithm successfully distinguished the normal unfaulted current and did not change the status of the trip signal for all the investigated normal operating conditions.

- The minimum description length (MDL) data criterion and the Shannon entropy based criterion are implemented first time for the protection of IPM motors in selecting the optimum mother wavelet and optimum number of levels of resolution.
- The proposed algorithm is tested on-line on both the line-fed and inverter-fed interior permanent magnet motors. The consistent results obtained from line-fed and inverter-fed IPM motors demonstrate the universal applicability of the proposed algorithm for IPM motors protection.
- The proposed technique is quite fast and easy to implement. It requires less computational memory for the on-line implementation. Thus the proposed technique can be installed in the supervisory control system for the on-line diagnosis and protection of disturbances including faults in three-phase interior permanent magnet motor drives.

6.4 Future Works

The encouraging results of testing the proposed algorithm on IPM motors have made a significant contribution in the area of the fault diagnosis of the PM motors and opened a new area of research. Therefore, the proposed algorithm can be applied to other applications, where the needed protection can be implemented with some modifications in hardware equipments. Such applications may include:

- Protection of high voltage motors in power plants. The partial discharge (PD) method is normally used for the protection of high voltage motors and generators in the power plant. Although in this work the proposed algorithm has been tested successfully on the low voltage IPM motors, it can be applied to high voltage motors with less cost and minimum efforts.

- Protection of permanent magnet generators in wind turbines. Recently, wind turbines are extensively used as an alternative source of energy. Most of the wind turbines are recently using permanent magnet generator because of its high efficiency, high power factor and relatively low cost. As a result, the proposed algorithm can be implemented for the protection of PM generators, which in turn can improve the reliability of the wind turbine.
- Other types of applications, which may include the power quality assessment and improvement, power system relaying, transmission line high impedance faults (HIFs) detection, monitoring the high voltage direct current (HVDC) transmission system, etc.

Appendix A

A. Line to Ground Fault

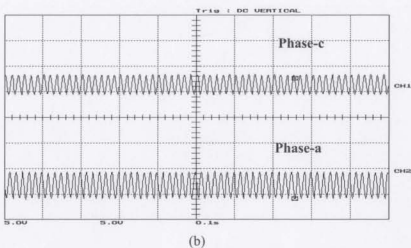
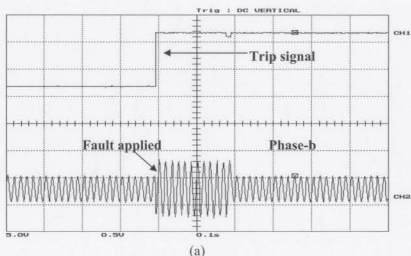
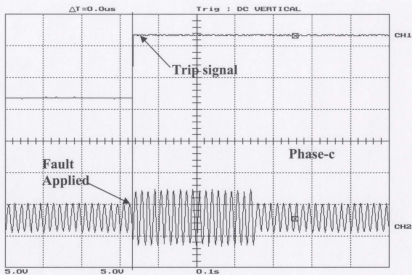
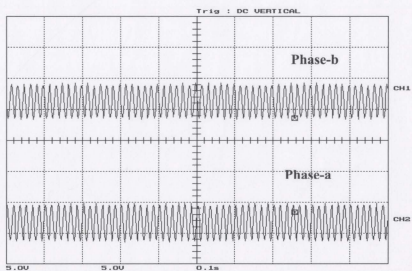


Figure A.1: Unloaded line to ground (L-G) fault on phase-b of the 1hp IPM motor: (a) the WPT response and phase-b stator current, (b) phase-c and phase-a stator currents. (Scales: time: 0.1s/div., trip signal: 5v/div., phase-a: 4.172 A/div., phase-b: 4.66 A/div., and phase-c: 4.82 A/div.)

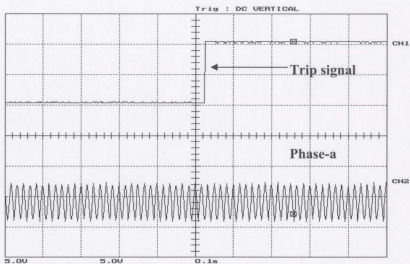


(a)

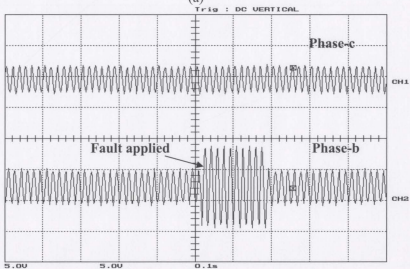


(b)

Figure A.2: Unloaded line to ground (L-G) fault on phase-c of the 1hp IPM motor: (a) the WPT response and phase-c stator current, (b) phase-b and phase-a stator currents. (Scales: time: 0.1s/div., trip signal: 5v/div., phase-a: 4.172 A/div., phase-b: 4.66 A/div., and phase-c: 4.82 A/div.)

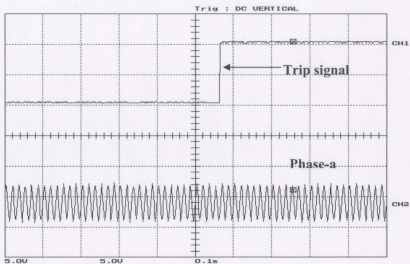


(a)

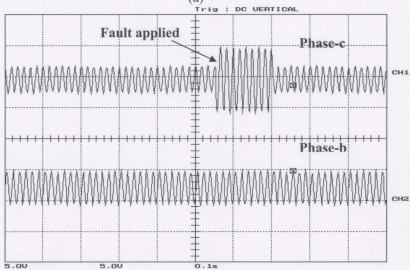


(b)

Figure A.3: Loaded line to ground (L-G) fault on phase-b of the 1hp IPM motor: (a) the WPT response and phase-a stator current, (b) phase-c and phase-b stator currents. (Scales: time: 0.1s/div., trip signal: 5v/div., phase-a: 4.172 A/div., phase-b: 4.66 A/div., and phase-c: 4.82 A/div.)

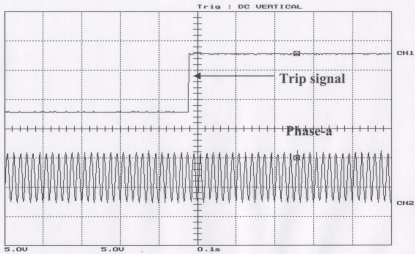


(a)

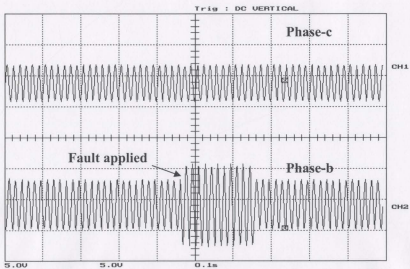


(b)

Figure A.4: Loaded line to ground (L-G) fault on phase-c of the 1hp IPM motor: (a) the WPT response and phase-a stator current, (b) phase-c and phase-b stator currents. (Scales: time: 0.1s/div., trip signal: 5v/div., phase-a: 4.172 A/div., phase-b: 4.66 A/div., and phase-c: 4.82 A/div.)

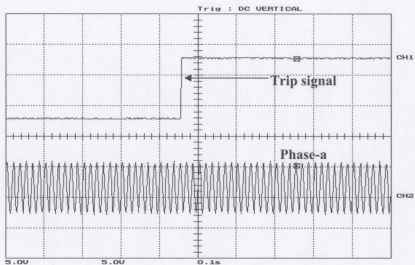


(a)

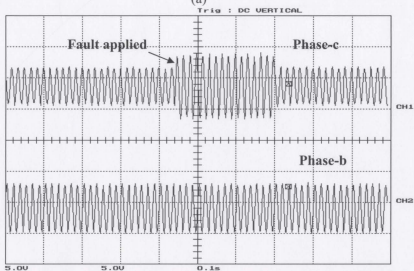


(b)

Figure A.5: Unloaded line to ground (L-G) fault on phase-b of the 5hp IPM motor: (a) the WPT response and phase-a stator current, (b) phase-c and phase-b stator currents. (Scales: time: 0.1s/div., trip signal: 5v/div., phase-a: 4.172 A/div., phase-b: 4.66 A/div., and phase-c: 4.82 A/div.)

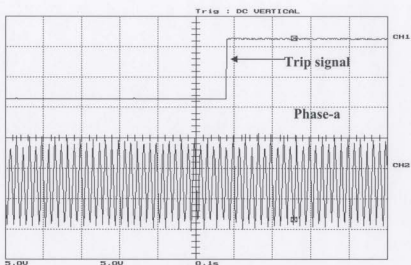


(a)

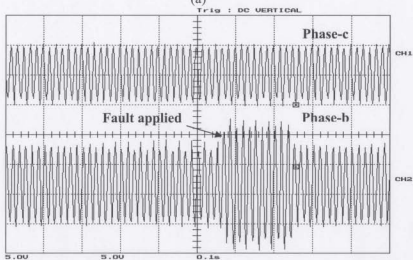


(b)

Figure A.6: Unloaded line to ground (L-G) fault on phase-c of the 5hp IPM motor: (a) the WPT response and phase-a stator current, (b) phase-c and phase-b stator currents. (Scales: time: 0.1s/div., trip signal: 5v/div., phase-a: 4.172 A/div., phase-b: 4.66 A/div., and phase-c: 4.82 A/div.)

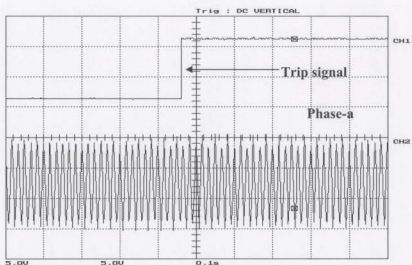


(a)

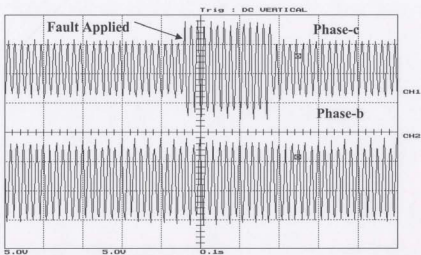


(b)

Figure A.7: Loaded line to ground (L-G) fault on phase-b of the 5hp IPM motor: (a) the WPT response and phase-a stator current, (b) phase-c and phase-b stator currents. (Scales: time: 0.1s/div., trip signal: 5v/div., phase-a: 4.172 A/div., phase-b: 4.66 A/div., and phase-c: 4.82 A/div.)



(a)



(b)

Figure A.8: Loaded line to ground (L-G) fault on phase-c of the 5hp IPM motor: (a) the WPT response and phase-a stator current, (b) phase-c and phase-b stator currents. (Scales: time: 0.1s/div., trip signal: 5v/div., phase-a: 4.172 A/div., and phase-c: 4.82 A/div.)

Appendix B

B. Line-to-Line Fault

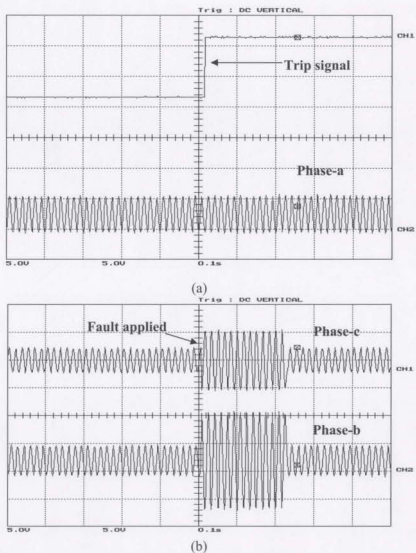
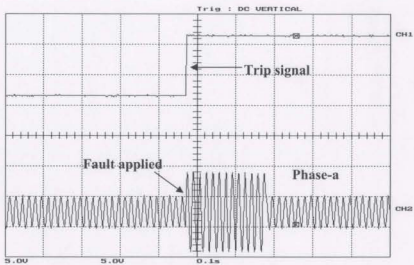
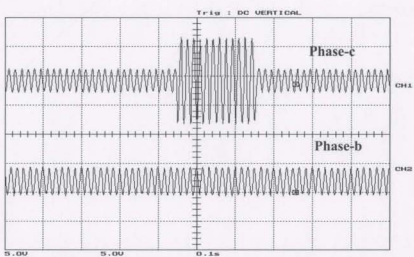


Figure B.1: Unloaded line-to-line (L-L) fault between phase-b and phase-c of the 1hp IPM motor: (a) the WPT response and phase-a stator current, (b) phase-c and phase-b stator currents. (Scales: time: 0.1s/div., trip signal: 5v/div., phase-a: 4.172 A/div., phase-b: 4.66 A/div., and phase-c: 4.82 A/div.)

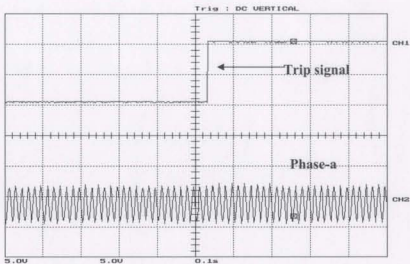


(a)

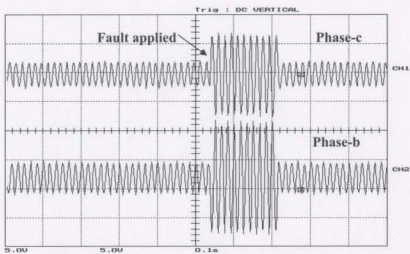


(b)

Figure B.2: Unloaded line-to-line (L-L) fault between phase-a and phase-c of the 1hp IPM motor: (a) the WPT response and phase-a stator current, (b) phase-c and phase-b stator currents. (Scales: time: 0.1s/div., trip signal: 5v/div., phase-a: 4.172 A/div., phase-b: 4.66 A/div., and phase-c: 4.82 A/div.)

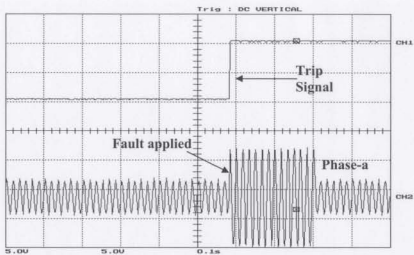


(a)

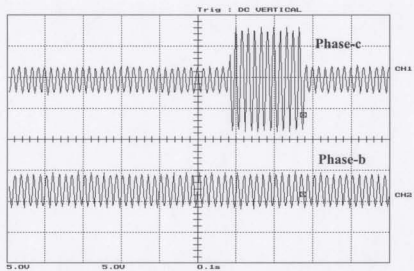


(b)

Figure B.3: Loaded line-to-line (L-L) fault between phase-b and phase-c of the 1hp IPM motor: (a) the WPT response and phase-a stator current, (b) phase-c and phase-b stator currents. (Scales: time: 0.1s/div., trip signal: 5v/div., phase-a: 4.172 A/div., phase-b: 4.66 A/div., and phase-c: 4.82 A/div.)

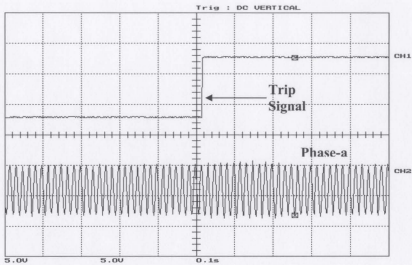


(a)

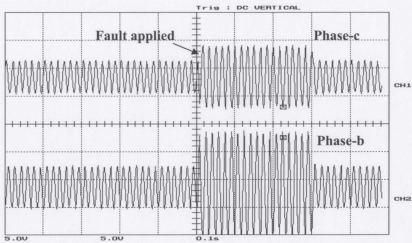


(b)

Figure B.4: Loaded line-to-line (L-L) fault between phase-a and phase-c of the 1hp IPM motor: (a) the WPT response and phase-a stator current, (b) phase-c and phase-b stator currents. (Scales: time: 0.1s/div., trip signal: 5v/div., phase-a: 4.172 A/div., phase-b: 4.66 A/div., and phase-c: 4.82 A/div.)

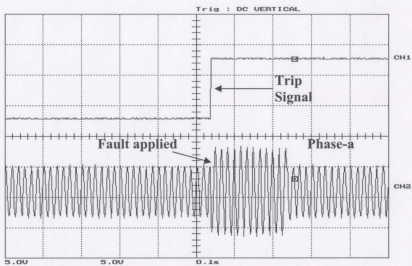


(a)

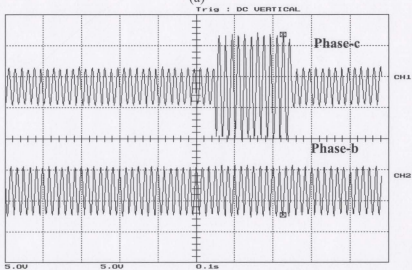


(b)

Figure B.5: Unloaded line-to-line (L-L) fault between phase-b and phase-c of the 5hp IPM motor: (a) the WPT response and phase-a stator current, (b) phase-c and phase-b stator currents. (Scales: time: 0.1s/div., trip signal: 5v/div., phase-a: 4.172 A/div., phase-b: 4.66 A/div., and phase-c: 4.82 A/div.)

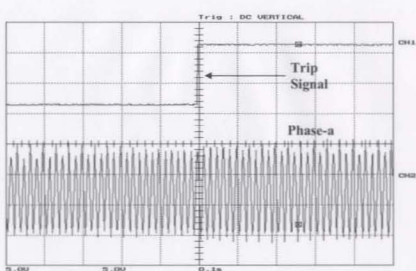


(a)

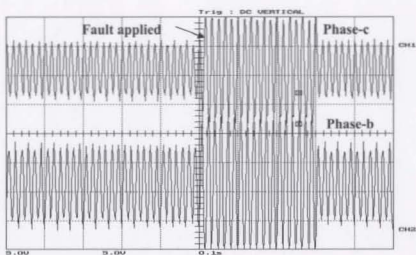


(b)

Figure B.6: Unloaded line-to-line (L-L) fault between phase-a and phase-c of the 5hp IPM motor: (a) the WPT response and phase-a stator current, (b) phase-c and phase-b stator currents. (Scales: time: 0.1s/div., trip signal: 5v/div., phase-a: 4.172 A/div., phase-b: 4.66 A/div., and phase-c: 4.82 A/div.)

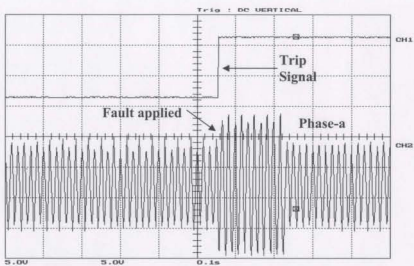


(a)

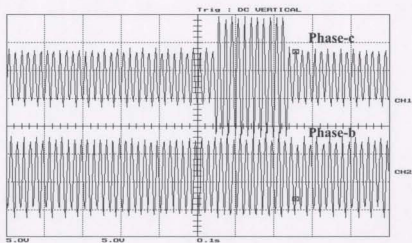


(b)

Figure B.7: Loaded line-to-line (L-L) fault between phase-b and phase-c of the 5hp IPM motor: (a) the WPT response and phase-a stator current, (b) phase-c and phase-b stator currents. (Scales: time: 0.1s/div., trip signal: 5v/div., phase-a: 4.172 A/div., phase-b: 4.66 A/div., and phase-c: 4.82 A/div.)



(a)



(b)

Figure B.8: Loaded line-to-line (L-L) fault between phase-a and phase-c of the 5hp IPM motor: (a) the WPT response and phase-a stator current, (b) phase-c and phase-b stator currents. (Scales: time: 0.1s/div., trip signal: 5v/div., phase-a: 4.172 A/div., phase-b: 4.66 A/div., and phase-c: 4.82 A/div.)

Appendix C

C. Loss of Supply (Single phasing) fault

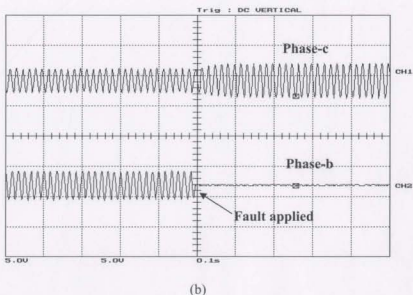
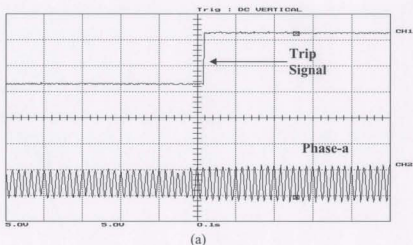
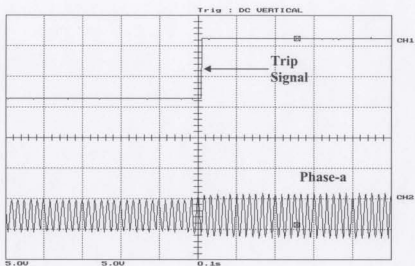
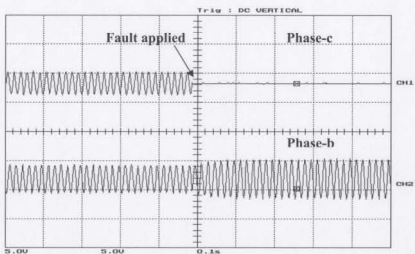


Figure C.1: Unloaded single phasing fault on phase-b of the 1hp IPM motor: (a) the WPT response and phase-a stator current, (b) phase-c and phase-b stator currents. (Scales: time: 0.1s/div., trip signal: 5v/div., phase-a: 4.172 A/div., phase-b: 4.66 A/div., and phase-c: 4.82 A/div.)

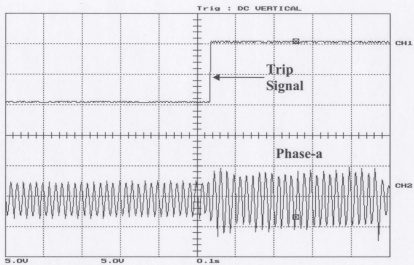


(a)

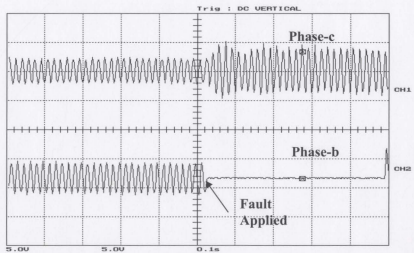


(b)

Figure C.2: Unloaded single phasing fault on phase-c of the 1hp IPM motor: (a) the WPT response and phase-a stator current, (b) phase-c and phase-b stator currents. (Scales: time: 0.1s/div., trip signal: 5v/div., phase-a: 4.172 A/div., phase-b: 4.66 A/div., and phase-c: 4.82 A/div.)

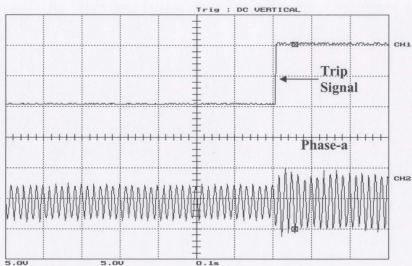


(a)

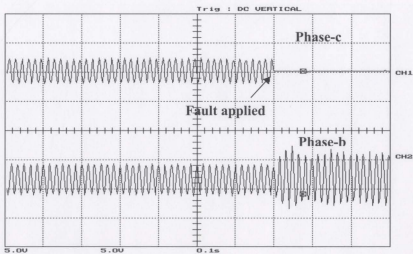


(b)

Figure C.3: Loaded single phasing fault on phase-b of the 1hp IPM motor: (a) the WPT response and phase-a stator current, (b) phase-c and phase-b stator currents. (Scales: time: 0.1s/div., trip signal: 5v/div., phase-a: 4.172 A/div., phase-b: 4.66 A/div., and phase-c: 4.82 A/div.)

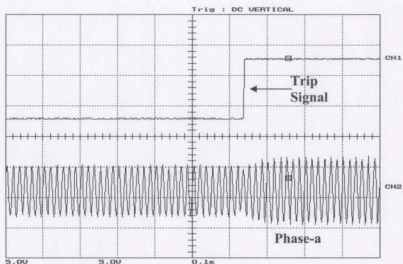


(a)

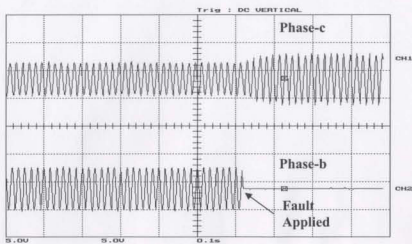


(b)

Figure C.4: Loaded single phasing fault on phase-c of the 1hp IPM motor: (a) the WPT response and phase-a stator current, (b) phase-c and phase-b stator currents. (Scales: time: 0.1s/div., trip signal: 5v/div., phase-a: 4.172 A/div., phase-b: 4.66 A/div., and phase-c: 4.82 A/div.)

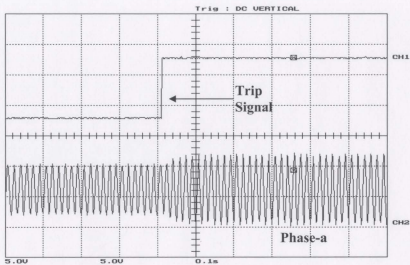


(a)

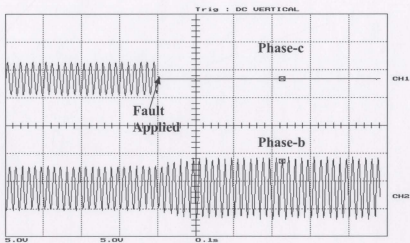


(b)

Figure C.5: Unloaded single phasing fault on phase-b of the 5hp IPM motor: (a) the WPT response and phase-a stator current, (b) phase-c and phase-b stator currents. (Scales: time: 0.1s/div., trip signal: 5v/div., phase-a: 4.172 A/div., phase-b: 4.66 A/div., and phase-c: 4.82 A/div.)

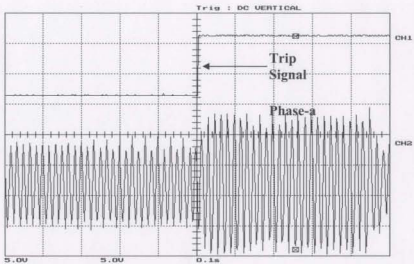


(a)

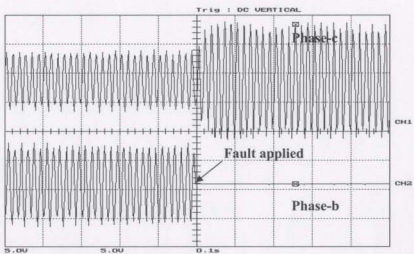


(b)

Figure C.6: Unloaded single phasing fault on phase-c of the 5hp IPM motor: (a) the WPT response and phase-a stator current, (b) phase-c and phase-b stator currents. (Scales: time: 0.1s/div., trip signal: 5v/div., phase-a: 4.172 A/div., phase-b: 4.66 A/div., and phase-c: 4.82 A/div.)

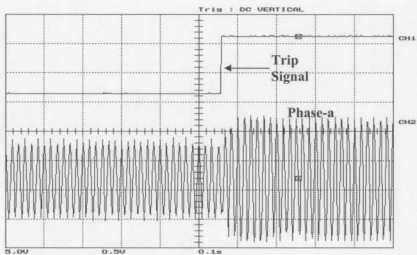


(a)

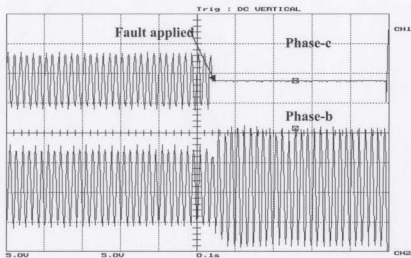


(b)

Figure C.7: Loaded single phasing fault on phase-b of the 5hp IPM motor: (a) the WPT response and phase-a stator current, (b) phase-c and phase-b stator currents. (Scales: time: 0.1s/div., trip signal: 5v/div., phase-a: 4.172 A/div., phase-b: 4.66 A/div., and phase-c: 4.82 A/div.)



(a)



(b)

Figure C.8: Loaded single phasing fault on phase-c of the 5hp IPM motor: (a) the WPT response and phase-a stator current, (b) phase-c and phase-b stator currents. (Scales: time: 0.1s/div., trip signal: 5v/div., phase-a: 4.172 A/div., phase-b: 4.66 A/div., and phase-c: 4.82 A/div.)

Bibliography

- [1] J.F. Gieras and M. Wing, *Permanent Magnet Motor Technology (Design and application)*. Marcel. Dekker, Inc, second edition, revised and expanded edition, 2002.
- [2] M.A. Rahman, "Recent Advances of IPM Motor Drives- Power Electronics World", *Plenary Lecture, IEEE Power Electronics and Drive Systems Conference*, Kuala Lumpur, November30-December02, 2005, CD ROM.
- [3] M.N. Uddin, "*Intelligent Control of An Interior Permanent Magnet Synchronous Motor Drive*". PhD Thesis, Memorial University of Newfoundland, St. John's, NF, Canada, October 2000.
- [4] M.A. Rahman, "Permanent Magnet Synchronous Motors- A Review of the State of Design Art", *Proceedings Conference Record International Electrical Machine Conference (ICEM'80)*, Athens, 1980, pp. 312-319.
- [5] B.A. Welchko, T.M. Jahns, and S. Hiti, "IPM Synchronous Machine Drive Response to a Single-Phase Open Circuit Fault", *IEEE Transactions on Power Electronics*, Vol. 17, No. 5, pp.764-771, Sept. 2002.
- [6] P. Vas, *Parameter Estimation, Condition Monitoring, and Diagnosis of Electrical Machines*. Calrendon Press, Oxford, 1993.
- [7] A. Siddique, G.S. Yadava, and B. Singh, "Applications of Artificial Intelligence Techniques for Induction Machine Stator Fault Diagnostics: Review", *Proceedings Conference Record IEEE Diagnostics for Electrical Machines, Power Electronics and Drives Symposium (SDEMPED'03)*, Atlanta, GA, 24-26 August 2003, pp. 29-34.
- [8] F. Filippetti, G. Franceschini, M. Martelli, and C. Tassoni, "An Approach to a Knowledge Representation about Induction Machine Diagnostics in Expert Systems", *Proceedings Conference Record International Electrical Machine Conference (ICEM'88)*, Pisa, Italy, September 1988, Vol. 3, pp. 289-296.

- [9] D. Leith, N.D. Deans, and L.I.D Stewart, "Condition Monitoring of Electrical Machine Using Real-time Expert Systems", *Proceedings Conference Record International Electrical Machine Conference (ICEM'88)*, Pisa, Italy, September 1988, Vol. 3, pp.297-302.
- [10] M. Chow, P.M. Mangum, and S.O. Yee, "A Neural Network Approach to Real-Time Condition Monitoring of Induction Motors", *IEEE Transactions on Industrial Electronics*, Vol. 38, No. 6, pp.448-453, Dec.1991.
- [11] R.R. Schoen, B.K. Lin, T.G. Habetler, J.H. Schlag, and S. Farag, "An Unsupervised, On-Line System for Induction Motor Fault Detection Using Stator Current Monitoring", *IEEE Transactions on Industry Applications*, Vol. 31, No. 6, pp.1280-1286, Nov./Dec.1995.
- [12] M. Chow, R.N. Sharpe, and J.C. Hung, "On the Application and Design of Artificial Neural Networks for Motor Fault Detection- Part I", *IEEE Transactions Industrial Electronics*, Vol. 40, No. 2, pp.181-188, Apr.1993.
- [13] M. Chow, R.N. Sharpe, and J.C. Hung, "On the Application and Design of Artificial Neural Networks for Motor Fault Detection- Part II", *IEEE Transactions Industrial Electronics*, Vol. 40, No. 2, pp.189-196, Apr.1993.
- [14] I. Lasurt, A.F. Stronach, and J. Penman, "A Fuzzy Logic Approach to the Interpretation of Higher Order Spectra Applied to Fault Diagnosis in Electrical Machines", *Conference Record International North American Fuzzy Information Processing Society Conference (NAFIPS)*, Atlanta, GA, 13-15 July 2000, pp.158-162.
- [15] M.E.H Benbouzid and H. Nejjari, "A Simple Fuzzy Logic Approach for Induction Motors Stator Condition Monitoring", *Conference Record IEEE International Electrical Machines and Drives Conference (IEMDC'01)*, Cambridge, MA, 17-20 June 2001, pp.634-639.

- [16] P.V. Goode and M.Y. Chow, "A Hybrid Fuzzy/Neural System Used to Extract Heuristic Knowledge from a Fault Detection Problem", *Proceedings Conference Record IEEE 3rd Fuzzy Systems Conference*, Orlando, FL, 26-29 June 1994, Vol. 3, pp.1731-1736.
- [17] P.V. Goode and M.Y. Chow, "Using a Neural/Fuzzy System to Extract Knowledge of Incipient Fault in Induction Motors. Part I- Methodology", *IEEE Transactions on Industrial Electronics*, Vol. 42, pp.131-138, Apr.1995.
- [18] P.V. Goode and M.Y. Chow, "Using a Neural/Fuzzy System to Extract Knowledge of Incipient Fault in Induction Motors. Part II- Application", *IEEE Transactions on Industrial Electronics*, Vol. 42, pp.139-146, Apr. 1995.
- [19] Y. Zhongming, W. Bin, and A.R. Sadeghian, "Electrical Machine Fault Detection Using Adaptive Neuro-Fuzzy Inference", *Proceedings International North American Fuzzy Information Processing Society (NAFIPS) Conference*, Vancouver, BC, 25-28 July 2001, Vol. 1, pp.390-394.
- [20] J. Park, D. Kim, S. Kim, D. Lee, and M. Chum, "C-ANFIS Based Fault Diagnosis for Voltage-Fed PWM Motor Drive Systems", *Proceedings IEEE North American Fuzzy Information Processing Society (NAFIPS) Annual Meeting*, 27-30 June 2004, Vol. 1, pp.379-383.
- [21] S. Pöyhönen, M. Negrea, A. Arkkio, H. Hyötyniemi, and H. Koivo, "Support Vector Classification for Fault Diagnostics of an Electrical Machine", *Proceedings Conference Record International 6th Signal Processing (ICSP'02) Conference*, Beijing, China, August 2002, Vol. 2, pp. 1719-1722.
- [22] V.N. Vapnik, "Statistical Learning Theory", John Wiley & Sons, 1998.
- [23] S. Pöyhönen, M. Negrea, A. Arkkio, H. Hyötyniemi, and H. Koivo, "Fault Diagnostics of an Electrical Machine with Multiple Support Vector Classifiers", *Proceedings IEEE International Intelligent Control Symposium (ISIC'02)*, Vancouver, BC, 27-30 October, 2002, Vol. 1, pp.373-378.

- [24] D.M. Yang, A.F. Stronach, and P. Macconnell, "The Application of Advanced Signal Processing Techniques to Induction Motor Bearing Condition Diagnosis", *Italian Association International Journal on Theoretical and Applied Mechanics*, Vol. 38, No. 2, pp.297-308, Mar. 2003.
- [25] W.L. Roux, R.G. Harley, and T.G. Habetler, "Detecting Rotor Faults in Permanent Magnet Synchronous Machines", *Proceedings Conference Record IEEE Diagnostics for Electrical Machines, Power Electronics and Drives Symposium (SDEMPED'03)*, Atlanta, GA, 24-26 August 2003, pp.198-203.
- [26] S. Pöyhönen, M. Negrea, P. Jover, A. Arkkio, and H. Hyötyniemi, "Numerical Magnetic Field Analysis and Signal Processing for Fault Diagnostics of Electrical Machines", *International Journal on Computation and Mathematics in Electrical and Electronic Engineering*, No. 4, pp.969-981, 2003.
- [27] G. Dalpiaz and A. Rivola, "Condition Monitoring and Diagnostics in Automatic Machines: Comparison of Vibration Analysis Techniques", *Journal on Mechanical Systems and Signal Processing*, Vol. 11, No. 1, pp.53-73, 1997.
- [28] W.L. Roux, R.G. Harley, and T.G. Habetler, "Converter Control Effects on Condition Monitoring of Rotor Faults in Permanent Magnet Synchronous Machine", *Proceedings Conference Record IEEE Industry Applications Society Annual Meeting*, 12-16 Oct. 2003, Vol. 2, pp.1389 – 1396.
- [29] W.G. Zanardelli and E.G. Strangas, "Failure Prognosis for Permanent Magnet AC Machines Based on Time-Frequency Analysis", *Proceedings Conference Record International Electrical Machine Conference (ICEM'04)*, Cracow, Poland, 5-8 September 2004, CD-ROM.
- [30] N. Arthur and J. Penman, "Induction Machine Condition Monitoring with Higher Order Spectra", *IEEE Transactions on Industrial Electronics*, Vol. 47, No. 5, pp.1031-1041, Oct. 2000.
- [31] M.E.H. Benbouzid, M. Vieira, and C. Theys, " Induction Motors' Faults Detection and Localization Using Stator Current Advanced Signal Processing Techniques", *IEEE Transactions on Power Electronics*, Vol. 14, No. 1, pp.14–22, Jan. 1999.

- [32] R.R. Schoen, T.G. Habetler, F. Kamran, and R.G. Bartheld, "Motor Bearing Damage Detection Using Stator Current Monitoring", *IEEE Transactions on Industry Applications*, Vol. 31, No. 6, pp.1274-1279, Nov./Dec. 1995.
- [33] B. Yazici and G. Kliman, "An Adaptive Statistical Time-Frequency Method for Detection of Broken Bars and Bearing Faults in Motors Using Stator Current", *IEEE Transactions on Industry Applications*, Vol. 35, No. 2, pp.442-452, Mar./Apr. 1999.
- [34] T. Lindh, J. Ahola, J.K. Kamarainen, V. Kyrki, and J. Partanen, "Bearing Damage Detection Based on Statistical Discrimination of Stator Current", *Proceedings Conference Record IEEE Diagnostics for Electrical Machines, Power Electronics and Drives Symposium (SDEMPED'03)*, Atlanta, GA, 2003, pp.177-181.
- [35] W.G. Zanardelli, E.G. Strangas, and S. Aviyente, "Failure Prognosis for Permanent Magnet AC Drives Based on Wavelet Analysis", *Proceedings IEEE International Electrical Machines and Drives Conference (IEMDC'05)*, San Antonio, Texas, 15-18 May 2005, CD-ROM.
- [36] W.G. Zanardelli, E.G. Strangas, H.K. Khalil, and J.M. Miller, "Comparison of Wavelet-Based Methods for the Prognosis of Failures in Electric Motors", *Proceedings Conference Record IEEE Power Electronics in Transportation Workshop*, Auburn Hills, Michigan, 24-25 October 2002, pp.61-67.
- [37] K. Kim and A.G. Parlos, "Induction Motor Fault Diagnosis Based on Neuropredictors and Wavelet Signal Processing", *IEEE/ASME Transactions on Mechatronics*, Vol. 7, No. 2, pp.201-219, Jun. 2002.
- [38] T.W.S Chow and S. Hai, "Induction Machine Fault Diagnostic Analysis with Wavelet Technique", *IEEE Transactions on Industrial Electronics*, Vol. 51, No. 3, pp.558-565, Jun. 2004.
- [39] G.Y. Luo, D. Osypiw, and M. Irle, "On-Line Vibration Analysis with Fast Continuous Wavelet Algorithm for Condition Monitoring of Bearing", *Journal of Vibration and Control*, Vol. 9, No. 8, pp.931-947, 2003.

- [40] S.A. Saleh, M.A. Khan, and M.A. Rahman, "Application of a Wavelet-Based MRA for Diagnosing Disturbances in a Three-Phase Induction Motor", *Proceedings IEEE Diagnostics for Electrical Machines, Power Electronics and Drives Symposium (SDEMPED'05)*, Vienna, Austria, September 7-9, 2005, CD-ROM.
- [41] H. Douglas, P. Pillay, and A.K. Ziarani, "A New Algorithm for Transient Motor Current Signature Analysis Using Wavelets", *IEEE Transactions on Industry Applications*, Vol. 40, No. 5, pp.1361-1368, Sept./Oct. 2004.
- [42] H. Toliyat, K. Abbaszadeh, M. Rahimian, and L. Olson, "Rail Defect Diagnosis Using Wavelet Packet Decomposition", *IEEE Transactions on Industry Applications*, Vol. 39, No. 5, pp.1454-1461, Sept./Oct. 2003.
- [43] G.G. Yen and K-C. Lin, "Wavelet Packet Feature Extraction for Vibration Monitoring", *IEEE Transactions on Industrial Electronics*, Vol. 47, No. 3, pp.650-667, Jun. 2000.
- [44] H. Zhengjia, Z. Ji Yuan, H. Yibin, and M. Qingfeng, "Wavelet Transform and Multiresolution Signal Decomposition for Machinery Monitoring and Diagnosis", *Proceedings Conference Record IEEE Industrial Technology Conference (ICIT'96)*, Shanghai, China, 2-6 December 1996, pp.724-727.
- [45] A.M. Gaouda, S.H. Kanoun, M.M.A. Salama, and A.Y. Chikhani, "Wavelet Based Signal Processing for Disturbance Classification and Measurement", *Proceedings IEE Generation, Transmission, and Distribution*, May 2002, Vol.149, No. 3, pp. 310-318.
- [46] B.A. Welchko, T.M. Jahns, W.L. Soong, and J.M. Nagashima, "IPM Synchronous Machine Drive Response to Symmetrical and Asymmetrical Short Circuit Faults", *IEEE Transactions on Energy Conversion*, Vol. 18, No. 2, pp.291-298, Jun. 2003.
- [47] Y-S. Jeong, S-K. Sul, S.E. Schulz, and N.R. Patel, "Fault Detection and Fault-Tolerant Control of Interior Permanent-Magnet Motor Drive System for Electric Vehicle", *IEEE Transactions on Industry Applications*, Vol. 41, No. 1, pp.46-51, Jan./Feb. 2005.

- [48] A.G. Jack, B.C. Mecrow, and J.A. Haylock, "A Comparative Study of Permanent Magnet and Switched Reluctance Motors for High-Performance Fault Tolerant Applications", *IEEE Transactions on Industry Applications*, Vol. 32, No. 4, pp.889-895, Jul./Aug. 1996.
- [49] C.F. Trutt, J. Sottile, and J.L. Kohler, "Online Condition Monitoring of Induction Motors", *IEEE Transactions on Industry Applications*, Vol. 38, No. 6, pp.1627-1632, Nov./Dec. 2002.
- [50] M. Arkan and P.J. Unsworth, "Stator Fault Diagnosis in Induction Motors using Power Decomposition", *Proceedings Conference Record IEEE Industry Applications Society Annual Meeting*, Phoenix, AZ, 3-7 October 1999, Vol. 3, pp.1908-1912.
- [51] M. Rosu, J. Saitz, and A. Arkkio, "Hysteresis Model for Finite-Element Analysis of Permanent-Magnet Demagnetization in a Large Synchronous Motor Under a Fault Condition", *IEEE Transactions on Magnetics*, Vol. 41, No. 6, pp.2118-2123, Jun. 2005.
- [52] E.Y. Hamid and Z.I. Kawasaki, "Wavelet-Based Data Compression for Power Disturbances Using Minimum Description Length Data", *IEEE Transactions on Power Delivery*, Vol. 17, No. 2, pp.460-466, Apr. 2002.
- [53] A.V. Oppenheim, R.W. Schaffer, and J.R. Buck, *Discrete-Time Signal Processing*. Prentice-Hall, Inc, Second Edition, 1999.
- [54] S.A.M. Saleh, *A Wavelet Packet Transform-Based Technique For Three Phase Power Transformer Protection*. Master's Thesis, Memorial University of Newfoundland, St. John's, NF, Canada, July 2003.
- [55] W.L. Roux, R.G. Harley, and T.G. Habetler, "Rotor Fault Analysis of a Permanent Magnet Synchronous Machine", *Proceedings Conference Record International Electrical Machine Conference (ICEM'02)*, Brugge, Belgium, 25-28 August 2002, CD-ROM.
- [56] Mathworks, *Matlab: Signal Processing Tool Box*, 2002. Ver. 6.5.0.1
- [57] S.L. Marple, *Digital Spectral Analysis*. Englewood Cliffs, NJ: Prentice Hall, 1987.

- [58] M.R. Zaman and M.A. Rahman, "Experimental Testing of the Artificial Neural Network Based Protection of Power Transformers", *IEEE Transactions on Power Delivery*, Vol. 13, No. 2, pp.510-517, Apr.1998.
- [59] M.C. Pan and P. Sas, "Transient Analysis on Machinery Condition Monitoring", *Proceedings Conference Record International Signal Processing Conference (ICSP'96)*, 1996, Vol. 2, pp.1723-1726.
- [60] Z.K. Peng and F.L. Chu, "Application of the Wavelet Transform in Machine Condition Monitoring and Fault Diagnostics: A Review with Bibliography", *Journal on Mechanical Systems and Signal Processing*, Vol. 18, No. 2, pp.199-221, 2004.
- [61] P.S. Addison, *The Illustrated Wavelet Transform Handbook (Introductory Theory and Applications in Science, Engineering, Medicine, and Finance)*. Institute of Physics Publishing Ltd, first edition, 2002.
- [62] C.H. Kim and R. Aggarwal, "Wavelet Transform in Power Systems: Part I", *IEE Journal on Power Engineering*, Vol. 14, No. 2, pp. 81-87, Apr. 2000.
- [63] G. Stang and T. Nguyen, *Wavelets and Wavelet Filter Banks*. Wellesly-Cambridge Press, 1996.
- [64] O.A.S. Youssef, "A Wavelet-Based Technique for Discrimination between Faults and Inrush Currents in Transformers", *IEEE Transactions on Power Delivery*, Vol. 18, No. 1, pp. 170-176, Jan. 2003.
- [65] Mathworks, *Matlab:Wavelet Tool Box*, 2002. Ver. 6.5.0.1
- [66] S.A. Saleh and M.A. Rahman, "A Wavelet-Controlled Dynamic Voltage Restorer for Power Quality Applications", *Proceedings IEEE Newfoundland Electrical and Computer Engineering Conference (NECEC)*, St. John's, NL, Canada, 2002, CD-ROM.
- [67] J.A. Orr, M. Negenevitsky, and T. Nguyen, "A Neural-Fuzzy Classifier for Recognition of Power Quality Disturbances", *IEEE Transactions on Power Delivery*, Vol. 17, No. 2, pp.609-616, Apr. 2002.

- [68] T. Dogaru and L. Carin, "Multiresolution Time-Domain Algorithm using CDF Biorthogonal Wavelets", *IEEE Transactions on Microwave Theory and Techniques*, Vol. 49, No. 5, pp. 902-912, May 2001.
- [69] S. Santoso, E.J. Powers, W.M. Grady, and P. Hofmann, "Power Quality Assessment via Wavelet Transform Analysis", *IEEE Transactions on Power Delivery*, Vol. 11, No. 2, pp. 924-930, Apr.1996.
- [70] A.M. Gaouda, E.F. El-Saadany, M.M.A. Salama, V.K. Sood, and A.Y. Chikhani, "Monitoring HVDC Systems using Wavelet MultiResolution Analysis," *IEEE Transactions on Power Systems*, Vol. 16, No. 4, pp.662-670, Nov. 2001.
- [71] Y. Zhuang and J.S. Baras, "Optimal Wavelet Basis Selection for Signal Representation", CSHCN T.R. 94-7, Center for Satellite and Hybrid Communication Networks, 1994.
- [72] B. Castro, D. Kogan, and A.B. Geva, "ECG Feature Extraction using Optimal Mother Wavelet", *Proceedings IEEE 21st Electrical and Electronic Engineers Convention*, Tel-Aviv, Israel, 11-12 April 2000, pp. 346-350.
- [73] C.H. Kim, H. Kim, Y.H. Ko, S.H. Byun, R.K. Aggarwal, and A.T. Johns, "A Novel Fault-Detection Technique of High-Impedance Arcing Faults in Transmission Lines using the Wavelet Transform", *IEEE Transactions on Power Delivery*, Vol. 17, No. 4, pp. 921-929, Oct. 2002.
- [74] X. Zhou, C. Zhou, and I.J. Kemp, "An Improved Methodology for Application of Wavelet Transform to Partial Discharge Measurement and De-noising", *IEEE Transactions on Dielectrics and Electrical Insulation*, Vol. 12, No. 3, pp.586-594, Jun. 2005.
- [75] X. Ma, C. Zhou, and I.J. Kemp, "Automated Wavelet Selection and Thresholding for PD Detection", *IEEE Magazine on Electrical Insulation*, Vol. 18, No. 2, pp.37-45, Mar. 2002.
- [76] N. Satio, "Simultaneous Noise Suppression and Signal Compression using a Library of Orthonormal Bases and the Minimum Description Length Criterion", *Proceedings Wavelets in Geophysics*, San Diego, CA, 1994, pp. 299-324.

- [77] S.K. Pandey and L. Satish, "Multiresolution Signal Decomposition: A new Tool for Fault Detection in Power Transformers during Impulse Tests", *IEEE Transactions on Power Delivery*, Vol. 13, No. 4, pp.1194-1200, Oct.1998.
- [78] R.A. Devore and B.J. Lucier, *Introduction to Wavelets*, 1992.
- [79] M.R. Zaman, "Artificial Neural Network Based Protection of Power Transformer". PhD thesis, Memorial University of Newfoundland, St. John's, NF, Canada, 1996.
- [80] M.A. Rahman and M.A. Hoque, "On-line Self-Tuning ANN-Based Speed Control of a PM DC Motor", *IEEE/ASME Transactions on Mechatronics*, Vol. 2, No. 3, pp. 169-178, September 1997.
- [81] Mathworks, *Matlab:Neural Network Tool Box*, 2002. Ver. 6.5.0.1

